Gesellschaft für Anlagen-
und Reaktorsicherheit
(GRS) mbH

The TSS Project: Thermal Simulation of Drift Emplacement

Final Report Phase 2
1993 - 1995

GRS - 127

Gesellschaft für Anlagen-
und Reaktorsicherheit
(GRS) mbH

The TSS Project: Thermal Simulation of Drift Emplacement

Final Report Phase 2

J. Droste, H.-K. Feddersen
T. Rothfuchs, U. Zimmer

Braunschweig
März 1996

GSF-Forschungszentrum
für Umwelt und Gesundheit
GmbH

Institut für Tieflagerung

Die diesem Bericht zugrundeliegenden Arbeiten wurden mit Mitteln des Bundesministeriums für Bildung, Wissenschaft, Forschung und Technologie (BMBF) unter dem Förderkennzeichen 02 E 8211 A2 gefördert. Im Zeitraum bis Juni 1995 wurden die Arbeiten vom GSF-Forschungszentrum am Institut für Tieflagerung in Braunschweig durchgeführt, ab Juli 1995 von der Gesellschaft für Anlagen- und Reaktorsicherheit (GRS) mbH im neugegründeten Fachbereich Endlagersicherheitsforschung. Die Verantwortung für den Inhalt dieser Veröffentlichung liegt allein bei den Autoren.

Foreword

The reference concept for spent fuel management of nuclear power plants in the Federal Republic of Germany comprises both the reprocessing of spent fuel assemblies by recycling the uranium and plutonium and disposing the waste in boreholes in a salt dome and the direct disposal of the spent fuel elements. The direct disposal provides the packaging of the fuel rods in self shielding Pollux casks and their emplacement in the drifts of a repository mine in rock salt. The remaining volume of the drifts is backfilled with crushed salt immediately after the emplacement of the casks.

The "Thermal Simulation of Drift Emplacement" (TSS) large scale test is being performed in the Asse salt mine to demonstrate the emplacement technology and to study the thermomechanical effects with this way of disposal. The test is carried out by the Forschungszentrum Karlsruhe GmbH (FZK), the GRS - Repository Safety Research Division (until June 30, 1995 GSF - Institut für Tieflagerung (IfT)), the Bundesanstalt für Geowissenschaften und Rohstoffe (BGR) and the Deutsche Gesellschaft zum Bau und Betrieb von Endlagern für Abfallstoffe (DBE) and is sponsored by the Bundesministerium für Bildung, Wissenschaft, Forschung und Technologie (BMBF) of the Federal Republic of Germany.

Within the framework of the project the GRS is responsible for all technical measures necessary for conducting the in situ test and for the geomechanical and geophysical measurements.

This report presents the results obtained by the GRS until December 1995.

Table of Contents

1 Introduction

The "Thermal Simulation of Drift Emplacement (TSS)" is one of several demonstration tests which were performed within the framework of the R&D-programme "Direct Disposal of LWR-Fuel Elements".

The programme consisted of the following points:

- Works Regarding the Direct Disposal of LWR-Fuel Elements

- Conditioning and Development of Storage Casks
  - Cask Development
  - Conditioning Plant
  - Component Development

- Demonstration Tests for the Direct Disposal of LWR-FE
  - Thermal Simulation of Drift Emplacement
  - Handling Tests for the Drift Disposal
  - Simulation of Shaft Transport
  - Active Handling Experiment with Neutron Sources (AHE)

- Planning Works for a Repository Concept
  - System Analysis Dual Purpose Repository
  - Detailed Planning of two Repository Concepts

- Experimental Research
  - Corrosion Investigation of Cask Materials
  - Retention of Fission Gases in Backfill Materials
  - Leaching Behaviour of LWR-Fuel Elements
  - Combined Leaching Experiments Glass/Fuel/Corrosion Products

The utilities were responsible for the part "Conditioning and Cask Development" and the Federal Government was responsible for the remaining points. Coordination of the project was performed by the "Projektgruppe Andere Entsorgungstechniken (PAE)" of the Forschungszentrum Karlsruhe (FZK). The GSF-IfT was participating in the "Thermal Simulation of Drift Emplacement", in the "Active Handling Experiment" and in the "System

Analysis of Repository Concepts". On July 1, 1995 the GSF-IfT was transferred to the GRS. Within the framework of the TSS project the GRS (GSF-IfT, respectively) was responsible for all technical measures for conducting the test in the Asse mine and for most of the geomechanical and geophysical measurements.

2 Objectives and Test Design

2.1 Objectives

The "Thermal Simulation of Drift Emplacement" demonstration test is a contribution to prove the safety of drift emplacement by studying the properties and behaviour of the backfill material and the surrounding rock salt under the influence of heat and pressure. In the drifts of a repository high temperatures will arise immediately after the emplacement of the casks with spent fuel elements. In a licensing procedure for this kind of storage these effects are to be assessed by thermomechanical model calculations. The computer codes and constitutive models have to be validated in advance by appropriate experiments.

The thermomechanical effects of heat generation are of primary importance for the long term safety of a repository. In the beginning the sealing effectiveness of the backfill is low even if it contributes to the retention of radionuclides. Apart from the geosphere the isolation of the biosphere is guaranteed at that time by technical barriers like canisters, seals or dams which, however, work only over a limited period of time. As an indispensable requirement in the safety assessment of a repository the backfill has to turn into a barrier before the failure of the technical barriers and to take over their mechanical and hydraulic function. The required compaction of the backfill to a solid rock is achieved by the gradual closure of the backfilled drifts due to convergence. As a result of the heat input from the casks the creep deformations of the rock salt and thus the compaction of the backfill are accelerated terminating in a complete sealing of the waste canisters in the rock salt.

Although backfilled voids in various salt mines and laboratory experiments proved the reduction in permeability and increasing rigidity and load bearing capacity of backfill material at increasing compaction, little data are available about the development of the parameters in time. The constitutive models currently used are all based on laboratory experiments and have to be validated by in situ measurement results.

Another fundamental subject in the safety assessment of the direct disposal of spent fuel are the small amounts of gas and water contained in rock salt which can be released due to the heat-up of the salt. Miscellaneous gases may be produced by radiolytic impact of gamma radiation. The most important gas component is hydrogen generated by the corrosive reaction of water with the steel casks.

Gas production and release can result in a significant increase in gas pressure in the repository after sealing. Increasing compaction of the backfill may lead to a further rise in gas pressure. In the same way the possible generation of inflammable gas mixtures in the repository has to be taken into account.

From these considerations the following objectives were formulated for the TSS test:

- Study of the thermomechanical interactions of heated dummy casks, backfill and surrounding rock salt

- Validation of thermal and thermomechanical computer models

- Selection of a technique for the backfilling of emplacement drifts

- Development and testing of suitable measuring techniques for the safety monitoring of a salt repository

- Study of water and gas release from the backfill material due to heating

- Study of the corrosion of various packaging materials under standard repository conditions.

2.2 Test Design

The TSS demonstration test is carried out at the 800 m level of the Asse salt mine inside the Staßfurt Halite (Na2ß) of the Zechstein Series in the anticlinal core of the salt dome. The test field has been designed as similar as possible to a real repository. A general view of the entire test field is given in Figure 2-1.

Two parallel test drifts have been excavated with a length of 70 m each. The drifts are 3.5 m high and 4.5 m wide with a pillar of 10 m width between. In each test drift three dummy casks were deposited. The dimensions, weight and heat output of the casks correspond to real Pollux casks. The canisters are 5.5 m in length with a diameter of 1.5 m and a weight of 65 t. The distance between the casks is 3 m. They are equipped with electrical heaters with a thermal power output of 6.4 kW each.

After the installation of the heaters and the measuring equipment the test drifts were backfilled in slinger technique with crushed salt material using a slinger truck.

Actually, in addition to the two test drifts, the test field includes several observation and access drifts on the 800 m level and on the 750 m level (Fig. 2-1). From the observation drifts a large number of boreholes extend into the vicinity of the test drifts, as do boreholes from the test drifts into the ambient rock salt.

The total length of the more than 200 boreholes amounts to approximately 2700 m. The boreholes are equipped with various measuring gauges to determine the thermomechanical reactions of the rock. Other devices have been installed in the backfill and at the surface of the dummy casks as well. Measuring chambers along the observation and access drifts contain the power supply and the data acquisition systems.

The whole measuring system has been installed in certain monitoring cross sections which are arranged in the middle, between and distant from the casks (Fig. 2-2). The cross sections A, B, C, D, F, G, H, I, J and K are located in the heated zone, whereas the sections E1, E2 and L1 are lying in non-heated areas. Additional indices like $D1^{-1}$ or $E1^{+1}$ are introduced to specify the distance of a measuring point from the respective cross section. The index numbers indicate the distance in metres with a plus sign in western direction and a minus sign for the eastern direction.

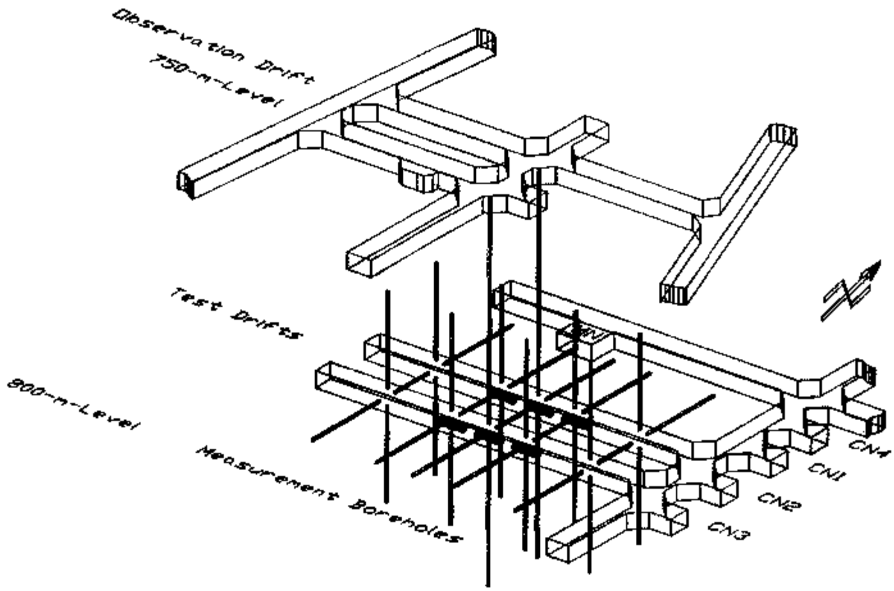

Fig. 2-1 General view of the TSS test field

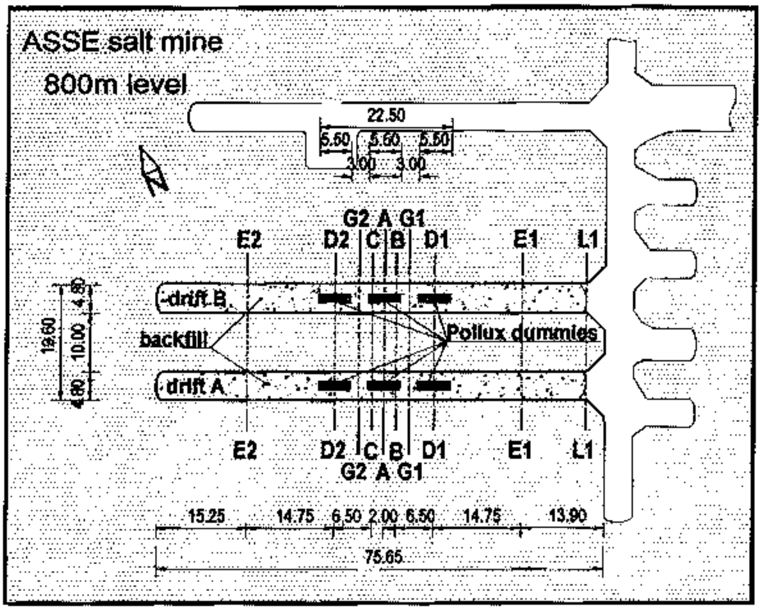

Fig. 2-2 Test drifts on the 800 m level with monitoring cross sections

3 Project Development

Planning and preliminary work for the TSS demonstration test started in 1985 and were not finished until 1989.

The excavation of the observation drifts on the 750 m level was done in 1987, followed by drilling and instrumentation of the measuring boreholes in 1988.

Mining of the test drifts on the 800 m level was carried out in spring of 1989, the effects of which on the surrounding rock salt were already recorded by the measuring devices installed on the 750 m level. After that, the drilling of the required boreholes and the instrumentation of drifts and boreholes took place as well as the emplacement of the dummy casks, step by step walking along with the backfilling of the drifts. With the whole measuring equipment being connected to the data acquisition, the test field was ready for operation in August 1990.

Heating finally started on September 25, 1990. Since then every heater cask is operated with a thermal power output of 6.4 kW. The total power output in each drift amounts up to about 19.2 kW (Fig. 3-1). Apart from several short breakdowns with no significant impact on the thermomechanical behaviour of the rock the electrical heaters operated quite well until the end of 1993. The higher thermal power output in the southern drift A from August 1991 until August 1992 was caused by a malfunction of the power regulator of the heater in section D2 which was repaired in 1992.

Different kinds of problems at the heater control system led to a higher thermal power output in 1994, resulting in increasing temperatures both at the surface and around the heater casks (Fig. 4.1-1). After the replacement of several electronic components temperatures are decreasing again in 1995. In 1995, a test phase was running with a changed power control which gave the basis for a further improvement of the whole system. By the end of November 1995, the renovation of the whole heater control system took place. The heaters are now operating faultlessly again with a higher precision.

In March 1993, a continuous registration of the total sum of the thermal power output was installed by which a continuous monitoring of the power output was possible.

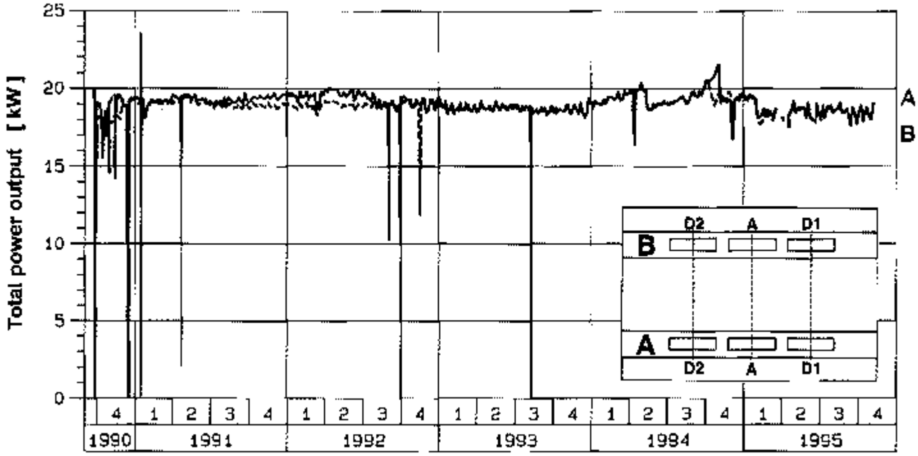

Fig. 3-1 Thermal power output in each test drift

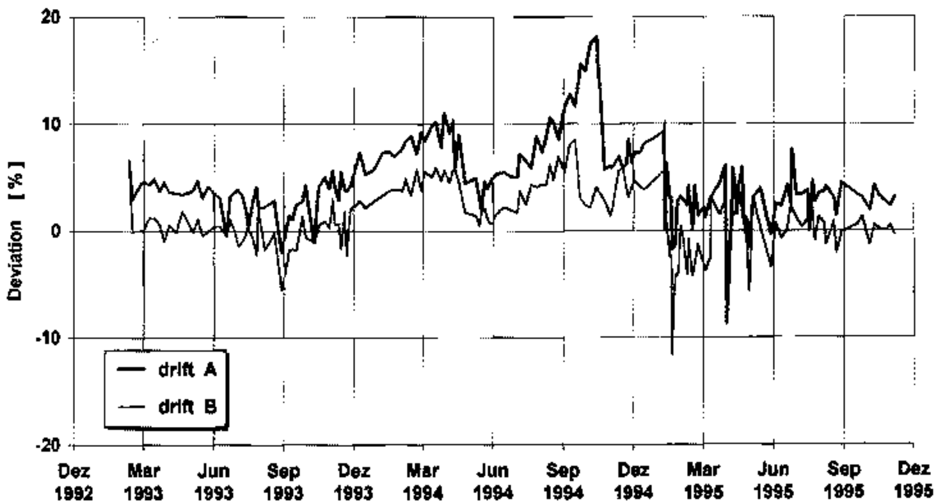

Fig. 3-2 Percentage of deviation of the thermal power output in each test drift

The percentage of deviation of the recorded power output from the design value of 19.2 kW for each drift is shown in Fig. 3-2. In 1994, the deviation especially in the southern drift reached up to 18 %. In 1995, the deviation of the power output is within the limits again.

4 Thermomechanical Effects

In drift emplacement the backfill is an important barrier and contributes to the stability of the repository. Because of the initially high permeability, however, the backfilled drifts are transient migration paths for gas and brine. Regarding the long term integrity of a repository the reduction in permeability due to the compaction of the backfill is of primary importance.

In the TSS test the crushed salt used for the backfilling of the test drifts originates from the excavation by means of a continuous miner. After cutting and sieving of the oversized grain fraction the broken salt having a grain size of less than 45 mm was re-emplaced in the test drifts by a slinger truck. After backfilling the crushed salt material had an initial density of 1400 kg/m^3, corresponding to a porosity of about 35 %.

Gradual closure of the drifts is giving rise to an increasing compaction of the backfill resulting in higher densities and lower porosities. This process is accelerated considerably due to heating.

The geotechnical investigation programme which is carried out by the GRS involves temperature, deformation and stress measurements. The temperatures are recorded by numerous resistance thermometers at the surface of the heater casks, in the backfill and in the surrounding rock salt. For determination of backfill compaction both the closure of the test drifts and the settling of the backfill are measured by means of stationary measuring equipments which had specially been designed for the TSS demonstration test. The rock deformations around the test drifts are recorded by extensometers which are registrating the axial borehole deformations. Hydraulic Glötzl pressure cells are used to observe the rising pressure in the backfill and the rock pressure around the heated drifts /SNE 93/.

4.1 Temperature

4.1.1 Backfill Temperature

Prior to heating the ambient temperature in the test drifts on the 800 m level is about 36 °C. Immediately after the heaters are switched on on September 25, 1990, the temperatures in the surrounding area are rising rapidly. At the surface of the casks the maximum temperature of approximately 210 °C is reached after five months (Fig. 4.1-1). This value corresponds adequately to the design temperature of 200 °C in a repository in rock salt.

Since the thermal conductivity of the backfill increases with its compaction the temperature at the surface of the casks decreases to about 175 °C until the end of 1993. Several short drops in temperature are due to short heater breakdowns after which the temperatures increase again immediately. The higher temperature at the surface of the heater cask in section D2 in the southern drift from August 1991 until August 1992 is a result of the already mentioned problem at the power control system. In 1994, the temperatures rise again caused by the troubles at the heater control system. After the repair measures in 1995, the temperatures at the heater surface are decreasing again as expected, reaching between 165 °C and 175 °C at the moment (Fig. 4.1-1).

For a validation of thermal model calculations the measured temperatures have to be compared with predicted values. In Fig. 4.1-2 the calculated temperatures at the heater surface are shown /KOR 91/. They correspond quite well with the measurements in the test drifts. A maximum temperature of 215 °C has been predicted after the beginning of heating. Five years after the start of heating the calculated values of 175 °C to 185 °C differ only about 10 °C from the measured temperatures. The differences are mainly a result of uncertainties in the thermal conductivity of the porous backfill material in the beginning /KOR 91/.

In the backfill around the heater casks the temperatures are also rising rapidly in the beginning. After a few months the rates are decreasing more and more until the temperatures approach steady state conditions with nearly constant values at the end of 1993.

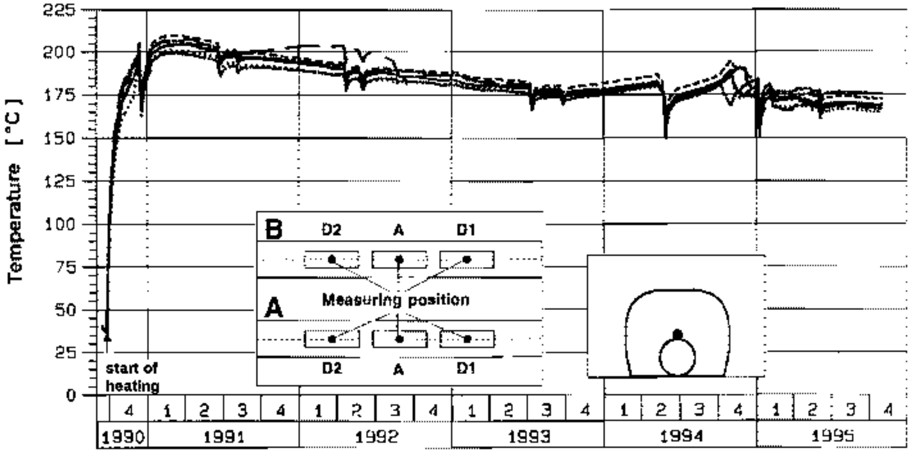

Fig. 4.1-1 Temperatures at the heater surface

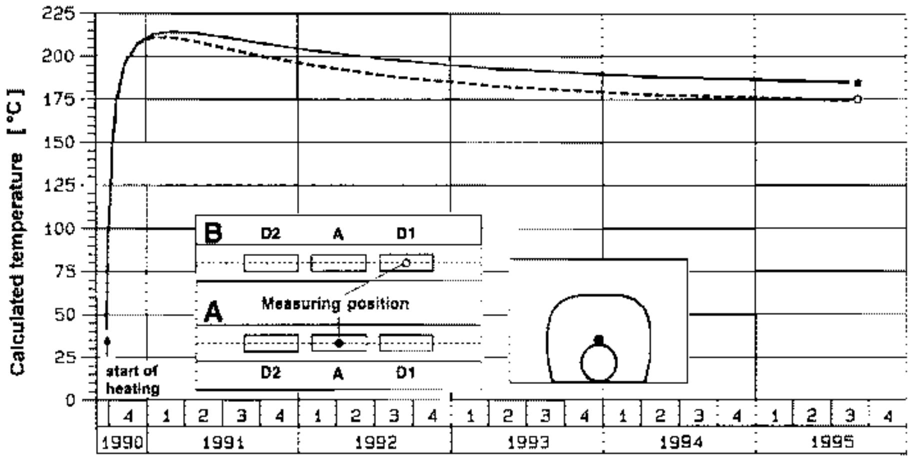

Fig. 4.1-2 Calculated temperatures at the heater surface

The highest temperatures are measured in sections around the central heaters. At that time the temperatures in different sections at the drift floor range between 115 °C and 125 °C next to the heaters and between 85 °C to 95 °C near the walls (Fig. 4.1-3). The temperatures recorded at the walls are 85 °C to 95 °C at the pillar and 80 °C to 85 °C at the opposite wall. In comparison with the opposite wall, temperatures at the pillar are generally about 5°C to 10 °C higher, as the pillar is being heated on either side. At the roof above the casks temperatures between 80 °C and 85 °C are observed. The temperatures inside the backfill range between 105 °C in the upper part of the backfill to 135 °C on the level of the casks (Fig. 4.1-4).

In 1994, the previously steady course of temperature development is disturbed by the higher thermal power output of the faulty heater control system, leading to a new temperature increase in the test drifts.

After the repair measures at the control system the temperatures in the backfill approach steady state conditions again in 1995. At the drift floor next to the heaters temperatures range between 115 °C and 125 °C at the moment. These are the same values as in 1993, when steady state conditions are already reached next to the heaters (Fig. 4.1-3). The actual temperatures inside the backfill are also in the same range again as in 1993 (Fig. 4.1-4). Towards the walls and the roof the present temperatures are about 5 °C higher than the values stated for 1993, implying that steady state conditions are still approached (Fig. 4.1-3).

Warming up of areas further away from the heaters starts with some delay. In the sections E1 and E2 at a distance of 12 m to the next heater cask temperatures begin to rise about three months after the heaters have been switched on. Up to now, temperatures in these sections reach values between 45 °C and 48 °C (Fig. 4.1-5).

Far away from the heaters in section L1 located at a distance of 23 m to the next cask, measurements show a temperature rise up to 40 °C until the end of 1995. The increase starts about half a year after the beginning of heating and takes a seasonal course with stagnating temperatures in winter time (Fig. 4.1-5). This phenomenon is related to the position of cross section L1 very close to the exit of the test drifts where the influence of the mine ventilation cannot be ignored.

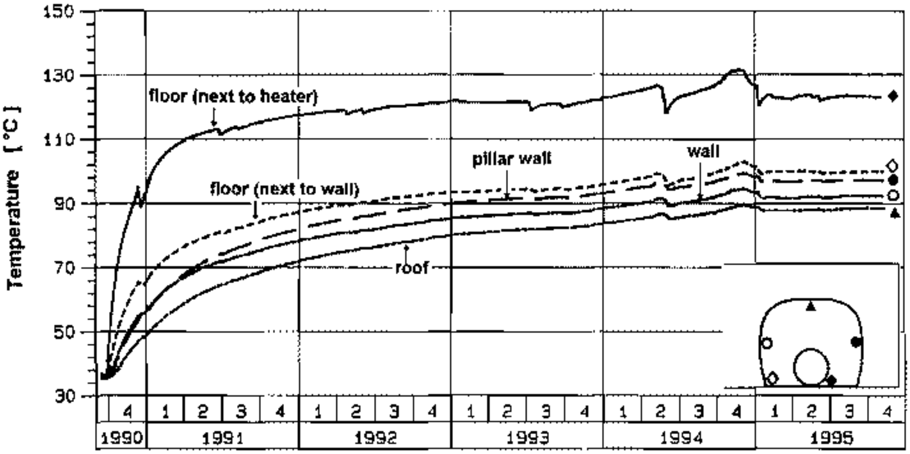

Fig. 4.1-3 Drift temperatures around a central heater (section B)

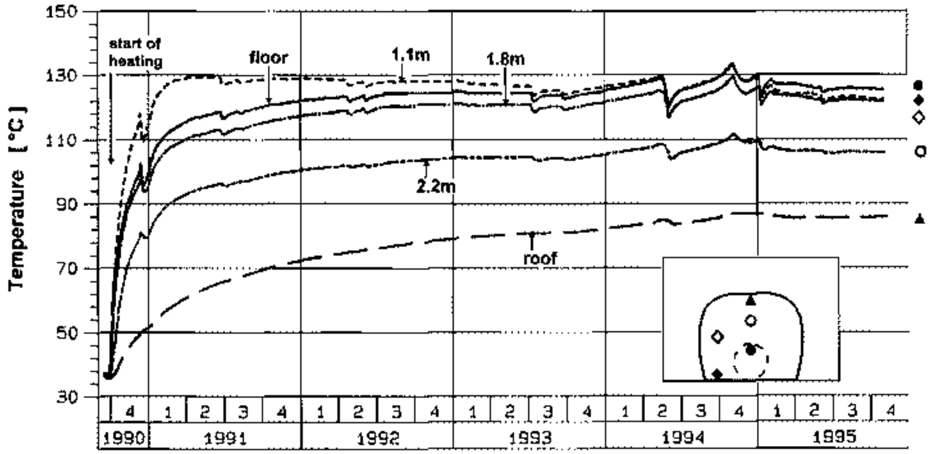

Fig. 4.1-4 Backfill temperatures around a central heater (sections B*' and G2*)

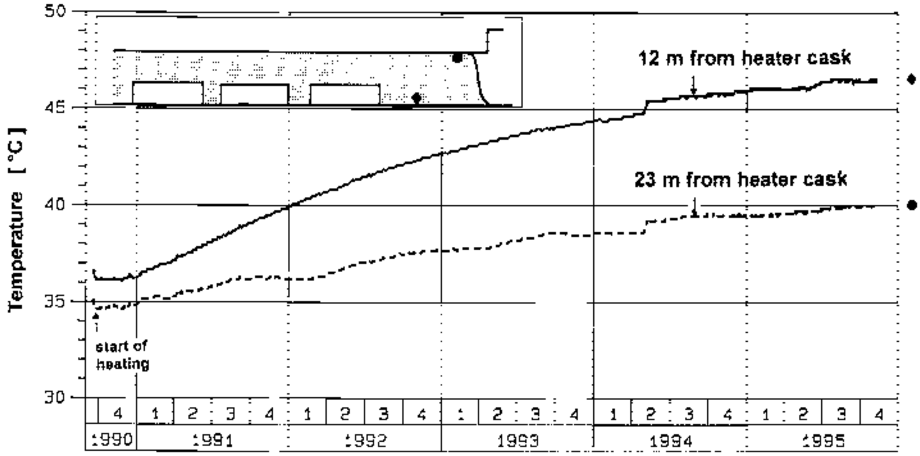

Fig. 4.1-5 Backfill temperatures in the cold area (sections E2[-1] and L1)

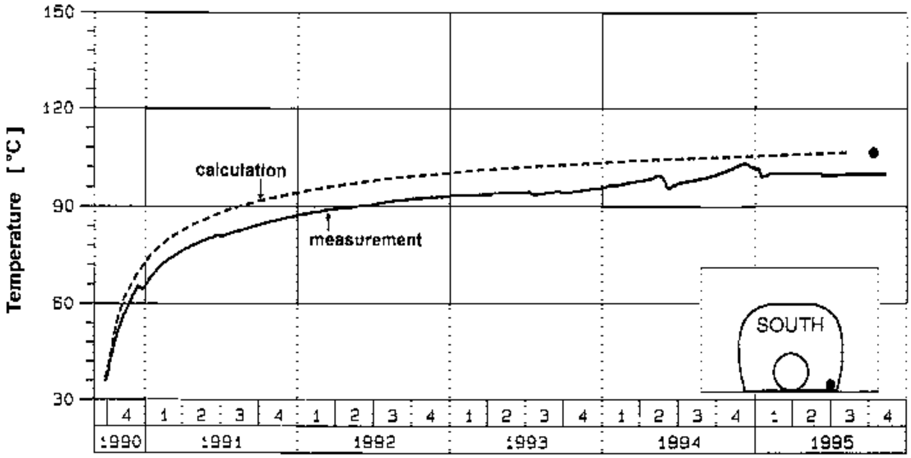

Fig. 4.1-6 Comparison of calculated and measured backfill temperatures in the heated area (section D1)

The temperatures in the cold sections of the backfill have not reached a steady state yet and will continue to rise for the next time. Steady state conditions with constant temperatures will only be reached when the thermal conductivity of the backfill does not change any more.

The temperature values predicted by numerical calculations /KOR 91/ correspond quite well to the temperatures measured in the test drifts (Fig. 4.1-6). A better fitting is still required in the initial stage of heating. The differences are mainly caused by uncertainties in the behaviour of the backfill material, in particular its thermal conductivity and its compaction at low compaction rates /KOR 91/. The impact of these parameters on heat transfer is especially pronounced in the initial stage of heating.

4.1.2 Rock Temperature

The heat transfer from the heater casks to the surrounding rock salt is taking place both via the backfill and directly over the drift floor on which the casks are set. The direct transfer of heat into the floor of the heated drifts is leading to a steep temperature gradient beneath the drifts and lower temperatures on the bottom of the heater casks as the heat input is conducted away rapidly. The high temperatures in the rock salt are restricted to a small area below the heater casks. In 0.3 m the temperatures are already 30 °C lower than at the cask surface reaching approximately 145 °C at the moment (Fig. 4.1-7). In a depth of 1.2 m temperatures of about 107 °C are measured at present.

At the end of 1993, the rock temperatures in depths less than 2.5 m below the heater casks already approach steady state conditions with nearly constant values (Fig. 4.1-7). After the disturbed temperature development in 1994 due to the faulty heater control system the temperatures approach steady state conditions again in 1995. Accordingly, the development of the rock temperatures in this area is similar to the behaviour of the backfill temperatures in the test drifts.

In greater depths, however, the temperature increase is much lower and starts with a delay. Moreover, the areas further away from the heaters are hardly affected by the higher thermal power output in 1994. The temperatures are still increasing, currently reaching about 75 °C in 5 m and 60 °C in 10 m depth. At the lowest measuring points 30 m beneath the heated drifts the initial temperature of 37 °C remains almost constant during the first year of heating. Since 1991, a gradual temperature increase is recorded up to 42 °C at the moment.

Towards the roof the heat transfer is taking place over a distance of 2 m via the backfill which has a low thermal conductivity in the beginning. Therefore, the temperatures above the heated drifts increase a little bit later than beneath the drift floor and reach lower values. Currently, temperatures at the roof amount to approximately 90 °C and decrease to 78 °C in 2 m depth (Fig. 4.1-8). Steady state conditions up to a distance of 2 m from the heated drifts are not approached until 1995. Further away the temperatures are still increasing reaching about 70 °C in 4 m and 58 °C in 8 m depth. At a distance of 32 m from the test drifts the initial temperature of 34.5 °C remains unchanged until 1993. Two and a half years after the beginning of heating the temperatures start to rise gradually up to 38 °C at present.

The rock temperatures in the walls beside the heated drifts are showing the same development and similar values as the area above the drifts. In horizontal direction the heat is transferred over a distance of 1.5 m through the backfill. After five years of heating temperatures of approximately 90 °C are measured at the drift walls (Fig. 4.1-9). The temperatures are decreasing with increasing depth just as in the area above the heated drifts.

In the pillar between the heated drifts, however, rock temperatures are higher than in the opposite walls as the pillar is heated on both sides. At the drift walls temperatures of up to 97 °C are recorded at the moment (Fig. 4.1-10). The temperature gradient inside the pillar is much lower as in the other areas. In 1.2 m temperatures still amount to 90 °C. The rock temperatures in the inner part of the pillar are almost identical. They decrease only from 83 °C at depths of 2.5 m to 80 °C at 5 m in the centre of the pillar. In the opposite walls, however, rock temperatures of approximately 72 °C and 63 °C are recorded in the corresponding depths respectively (Fig. 4.1-9).

In the end of 1993, temperatures in the outer part of the pillar are approaching steady state conditions. After the disturbed temperature development in 1994 due to the faulty heater control system the temperatures reach steady state conditions in 1995 all over the pillar (Fig. 4.1-10).

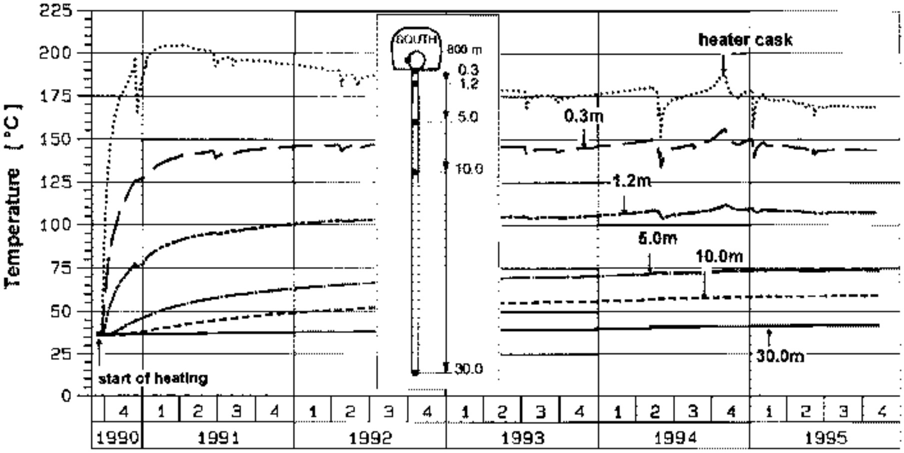

Fig. 4.1-7 Rock temperatures beneath the heated drifts (section A)

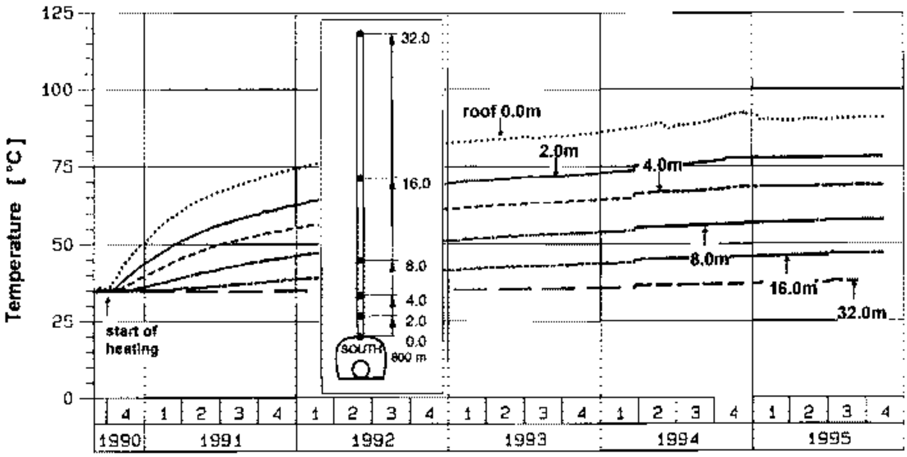

Fig. 4.1-8 Rock temperatures above the heated drifts (section A)

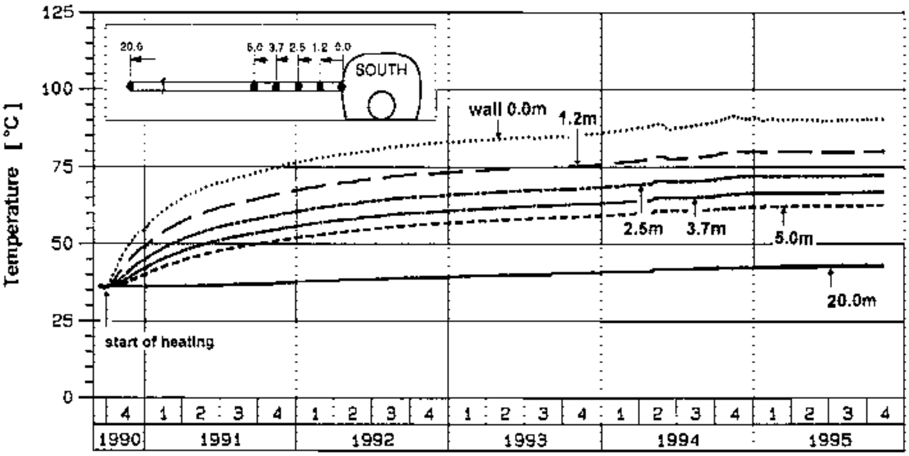

Fig. 4.1-9 Rock temperatures beside the heated drifts (section A)

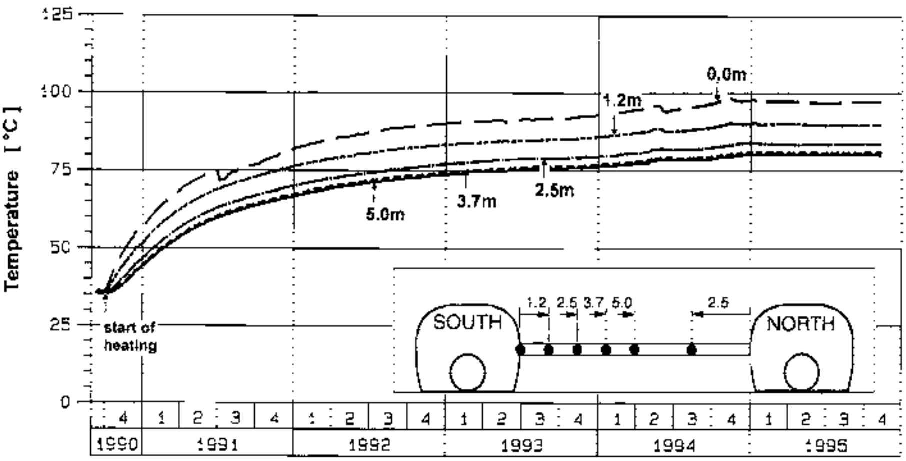

Fig. 4.1-10 Rock temperatures between the heated drifts (section A)

In the non-heated area the rock temperatures are recorded around the test drifts in the sections E1 and E2. Next to the drifts the temperatures show the same development in all directions (Fig. 4.1-11 to 4.1-14). The temperatures begin to rise about three months after the heaters have been switched on. Up to now the temperatures are still increasing, currently reaching between 45 °C to 46 °C. The temperatures are almost the same up to a distance of 5 m from the test drifts. Generally, the temperatures below the drifts are about 0.5 °C to 1 °C higher than in the walls and above the drifts. The highest values are recorded in the pillar where an identical temperature increase is taking place all over the pillar up to 47 °C at the moment (Fig. 4.1-14).

Farther away from the test drifts the temperature increase starts delayed. At a depth of 10 m below the drifts the rock temperatures begin to rise three months after the heaters have been switched on and amount to 45 °C at present (Fig. 4.1-11). At the same distance beside and above the drifts the temperatures increase not until half a year after the start of heating reaching values of approximately 43 °C at the moment (Fig. 4.1-12 and 4.1-13).

In 20 m below the non-heated drifts the first effects of heating are recorded after half a year. Up to now the temperature increases to 42 °C (Fig. 4.1-11). At the same distance beside and above the drifts the temperatures begin to rise one year after the start of heating. The actual values amount to approximately 40 °C (Fig. 4.1-12 and 4.1-13).

In Fig. 4.1-15 and Fig. 4.1-16 the measured rock temperatures below the heated drifts and in the pillar are exemplary compared with the predicted values of numerical calculations /KOR 91/. Obviously, the coincidence is satisfactory. Like the temperatures in the backfill a better fitting is still required in the initial stage of heating.

With increasing distance of the measuring points from the heated drifts the deviation between measured and calculated temperatures diminishes. The differences are mainly a result of the constitutive law of rock salt which does not fit well enough.

In summary the rock temperatures in the heated area increase continuously after the heaters have been switched on. After five years of heating the temperatures in the area next to the heated drifts and all over the heated pillar approach steady state conditions. Farther away the rock temperatures are still increasing as well as the rock temperatures in the cold sections.

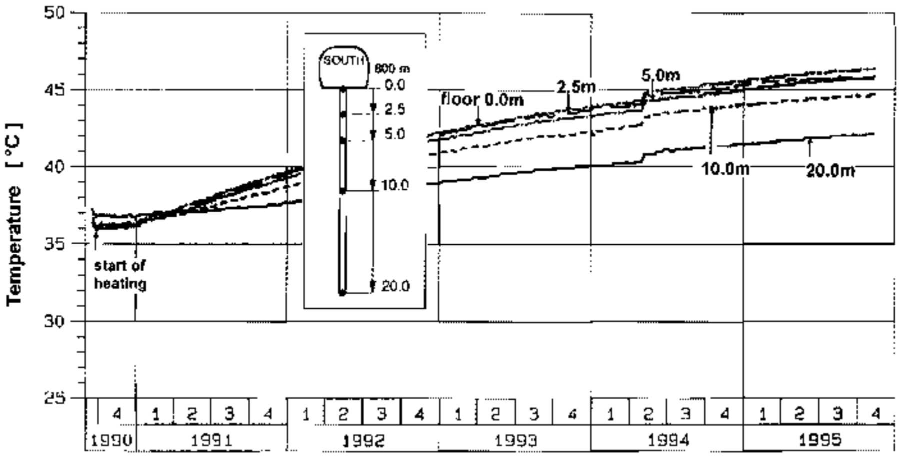

Fig. 4.1-11 Rock temperatures beneath the cold drifts (section E2)

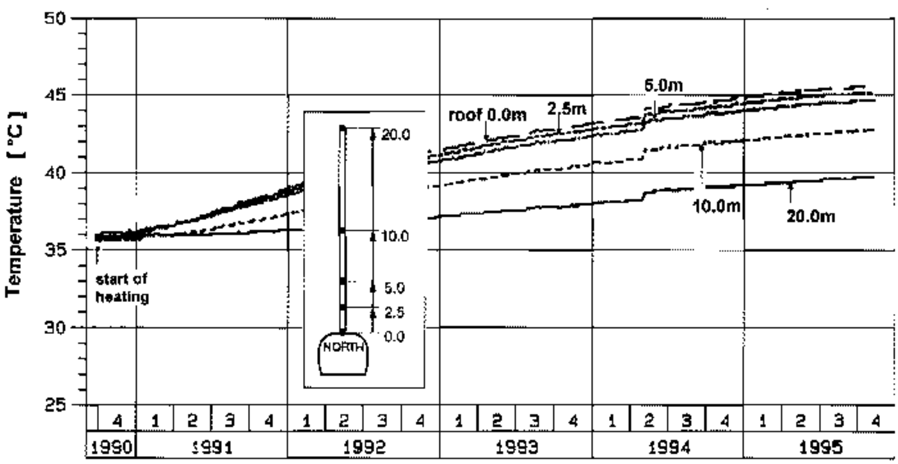

Fig. 4.1-12 Rock temperatures above the cold drifts (section E2)

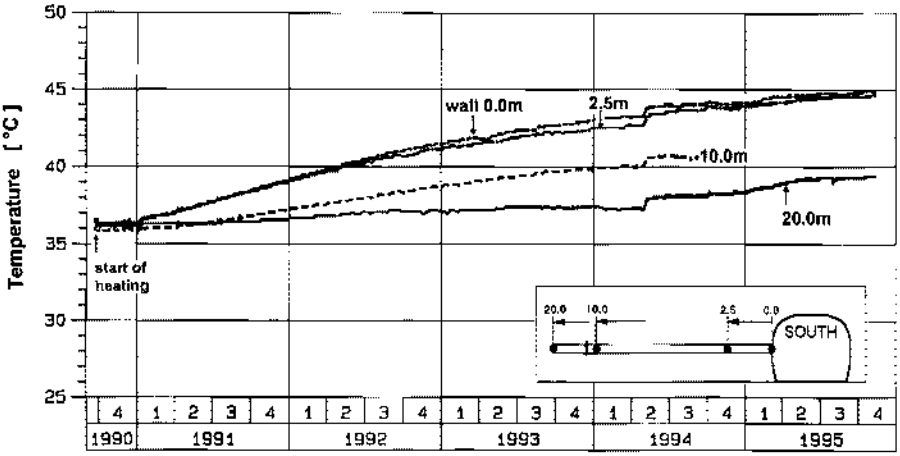

Fig. 4.1-13 Rock temperatures beside the cold drifts (section E2)

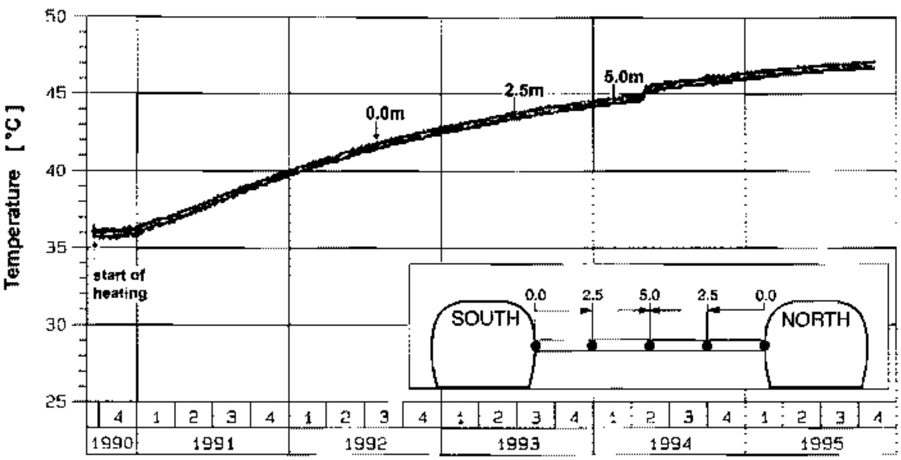

Fig. 4.1-14 Rock temperatures between the cold drifts (section E2)

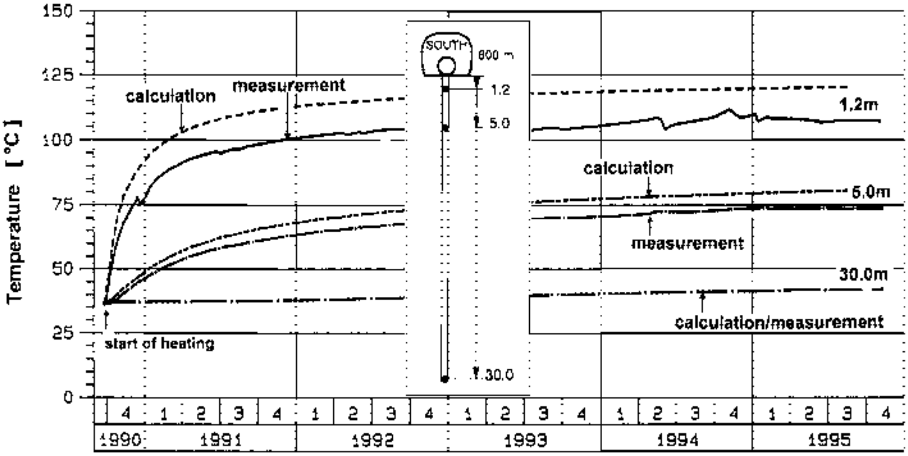

Fig. 4.1-15 Comparison of calculated and measured rock temperatures beneath the heated drifts (section A)

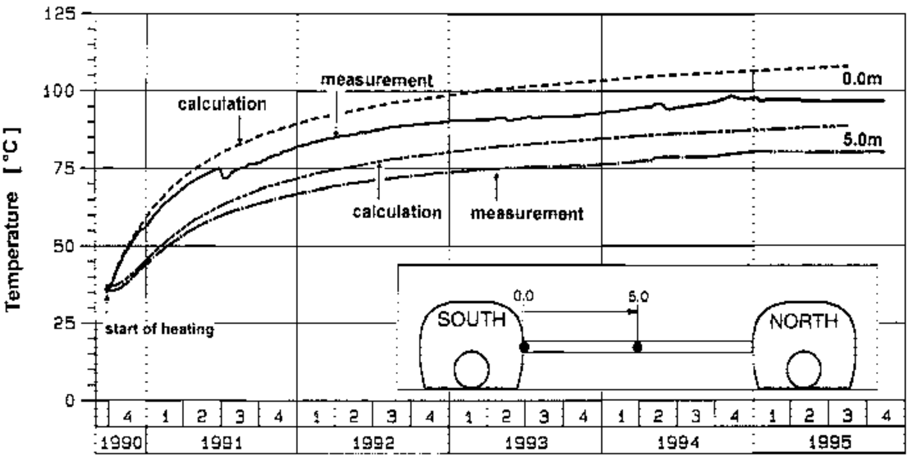

Fig. 4.1-16 Comparison of calculated and measured rock temperatures between the heated drifts (section A)

4.2 Deformation

4.2.1 Drift Convergence

Convergence measurements in the observation drifts on the 750 m level

Since 1987, the drift convergence is recorded in the observation drifts on the 750 m level in the sections D1 and D2. The measurements are carried out manually. Additionally, permanent convergence measuring gauges are installed in the sections D1 in the southern drift and D2 in the northern drift which are registrating the deformations automatically.

In the beginning after the excavation of the observation drifts the convergence rates are increasing at first. After one month the rates get already decreasing. About two years after the excavation of the drifts the convergence rates are nearly constant indicating steady state creep. The horizontal convergence rates from that time onwards amount to 0.075 - 0.09 %/a. Some higher values of 0.115 %/a are measured in section D2 of the southern drift due to the existence of the measuring chamber close by (Fig. 4.2-1). The convergences in vertical direction are a little higher reaching between 0.095 %/a to 0.13 %/a. The maximum values of 0.15 %/a are again registered next to the measuring chamber (Fig. 4.2-2).

From March to April 1989, the excavation of the test drifts on the 800 m level induces a short-term decrease of the convergence rates on the 750 m level until the end of May 1989. The heating of the test drifts since September 1990, however, does not affect the convergence rates in the observation drifts during the first years.

Not until four years after the beginning of heating the convergence rates on the 750 m level are accelerated. The horizontal convergence rates then rise about 40 % reaching 0.115 - 0.12 %/a at the moment. In section D2 next to the measuring chamber even 0.16 %/a are measured. The rates in vertical direction increase about 25 %. The actual rates amount to 0.12 - 0.165 %/a up to 0.19 %/a next to the measuring chamber.

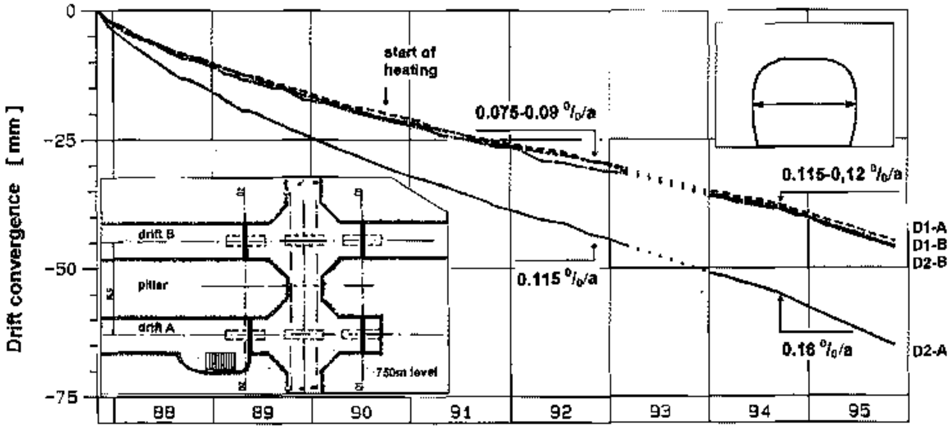

Fig. 4.2-1 Horizontal drift convergence in the observation drifts on the 750 m level (sections D1 and D2)

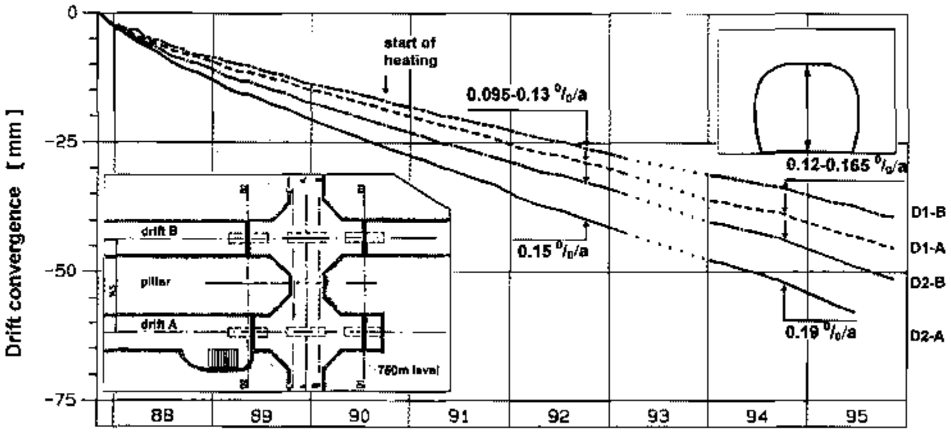

Fig. 4.2-2 Vertical drift convergence in the observation drifts on the 750 m level (sections D1 and D2)

Convergence measurements in the test drifts on the 800 m level

Horizontal and vertical convergence measurements are carried out both in the heated zone (monitoring cross sections B^{+1}, $D1^{-1}$, G1 and G2) and in the non-heated area (cross sections $E1^{-1}$ and E2) of the test drifts. The measurements started immediately after the excavation of the drifts and have been continued since then.

Prior to heating convergence rates average 0.25 %/a in horizontal direction and 0.3 %/a in vertical sections. The differing values in either direction are mainly a result of the local stress field.

Immediately after the start of heating the convergence rates in the heated area accelerate considerably up to twelve times the amount (Fig. 4.2-3 and 4.2-4). For a short time they are nearly constant. About three months after the beginning of heating the rates are already decreasing again due to the creep of the salt and the beginning support by the backfill. The increasing resistance of the backfill to drift closure caused by its increasing density and rigidity reduces the convergence rates more and more up to the end of 1993. As a result of the higher thermal power output in 1994 the convergence rates then remain almost constant over more than a year (Fig. 4.2-4). After the repair of the heater control system the rates are decreasing again in 1995 reaching 0.46 - 0.57 %/a in horizontal direction at the moment. The present vertical rates amount to 0.62 - 0.74 %/a. These values are still twice as much as before heating.

In the non-heated sections the convergence rates remain unchanged at first. Three months after the heaters have been switched on, the temperatures start to rise gradually in the cold sections E1 and E2 as well (Fig. 4.1-5). The closure of the drifts subsequently accelerates to double the amount (Fig. 4.2-3 and 4.2-4). Two years later in early 1993, the convergence rates decrease again. From three years after the beginning of heating up to now the rates stay almost constant. The actual rates are reaching 0.30 - 0.37 %/a in horizontal and 0.30 - 0.53 %/a in vertical direction. That is still about one and a half times of the initial closure rate and about two thirds of the rates observed in the heated area.

After the start of heating drift convergences in the southern drift are initially up to 10 % higher than in the northern drift. After two years the rates in both drifts are approximately in the same range in the heated area up to now. In the non-heated area, however, the differences between the two drifts are more significant. The convergence rates in the southern drift are still up to 20 % higher than in the northern drift.

In the sections G2 and $E1^{-1}$ the vertical convergences are not measured in the centre of the drifts but in a distance of 1 m from each wall. The recorded convergences are therefore lower than in the other sections. Generally, the vertical convergence rates on the pillar side are higher than next to the opposite wall. In the heated section G2 the difference amounts to 5 - 10 %, in the non-heated section $E1^{-1}$ even to 10 - 15 % (Fig. 4.2-5).

The comparison of measurements with calculated drift convergences /KOR 91/ reveals a good coincidence in the cold sections (Fig. 4.2-6). In the heated area, however, drift closure is considerably lower than expected. After five years of heating vertical convergences reach only two thirds of the predicted values, being already two and a half years behind the calculated course (Fig. 4.2-7). Obviously, the constitutive law applied does not fit well enough.

From the volume decrease of the drifts caused by drift closure the actual backfill porosity can be determined using the values of convergence measurements. After five years of heating the initial backfill porosity of about 35 % has been reduced to a porosity of 26.5 % to 28 % in the heated area (Fig. 4.2-8), whereas the porosity in the non-heated sections ranges between 32 % and 33.2 % (Fig. 4.2-9). In the heated area the decrease of backfill porosity is taking place much slower than predicted as a result of the lower convergence rates /KOR 91/.

The stated porosities, however, are only mean values over the respective sections. Due to the temperature gradient in the backfill from the heater casks towards the walls significant differences of the local porosity can be expected.

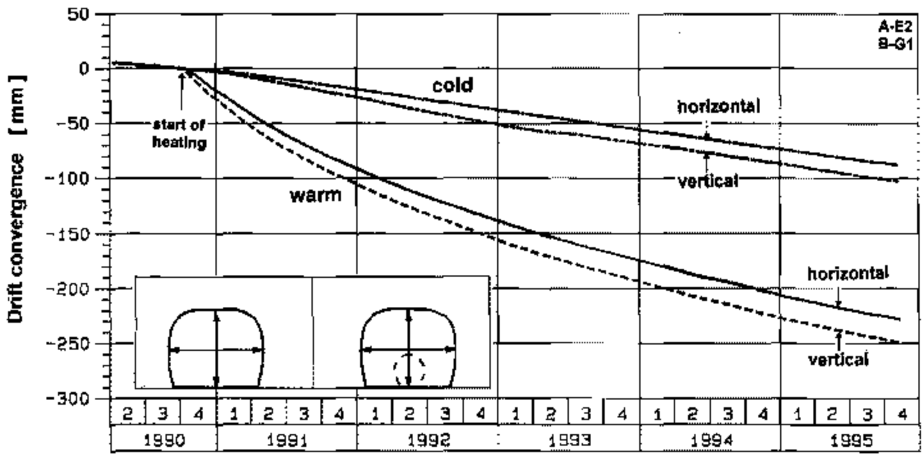

Fig. 4.2-3 Drift convergence in the heated area (section G1) compared to the non-heated area (section E2)

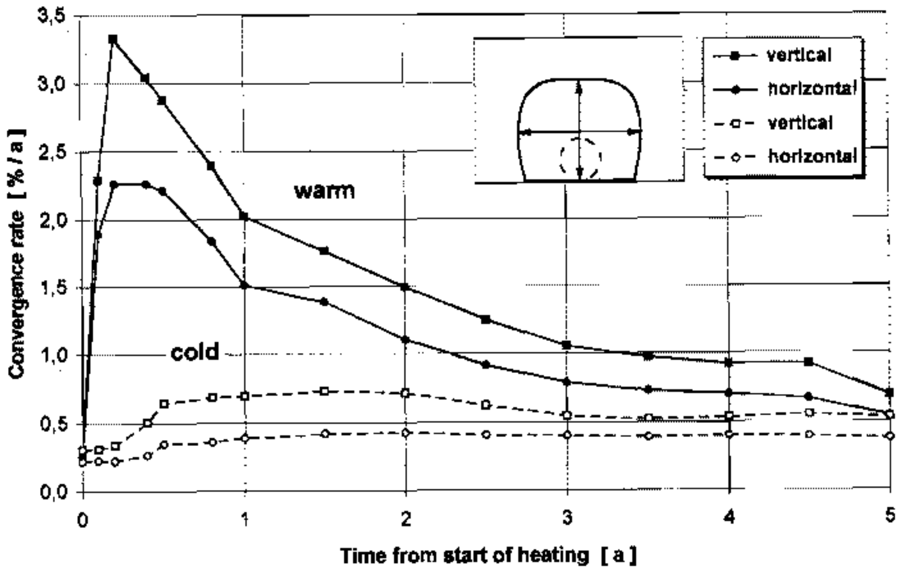

Fig. 4.2-4 Convergence rates in the heated area (section G1) compared to the non-heated area (section E2)

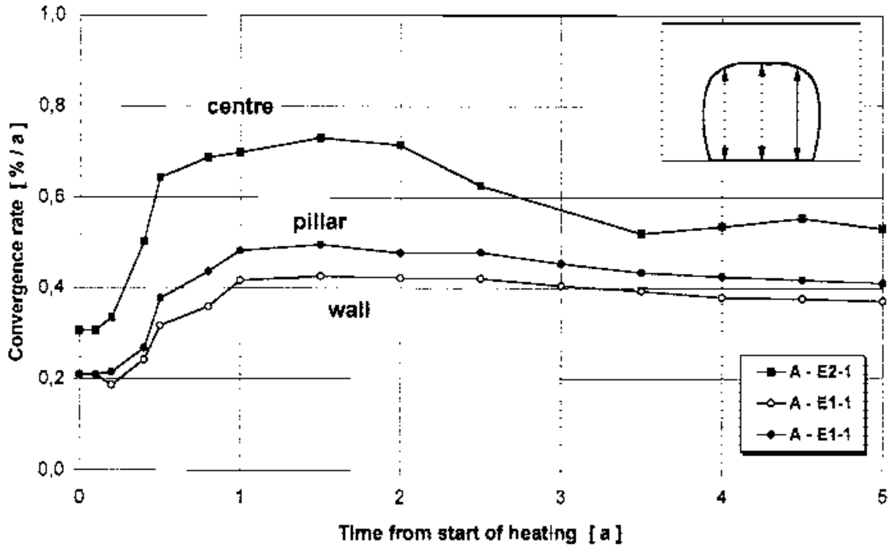

Fig. 4.2-5 Vertical convergence rates in the non-heated area (sections $E1^{-1}$ and $E2^{-1}$)

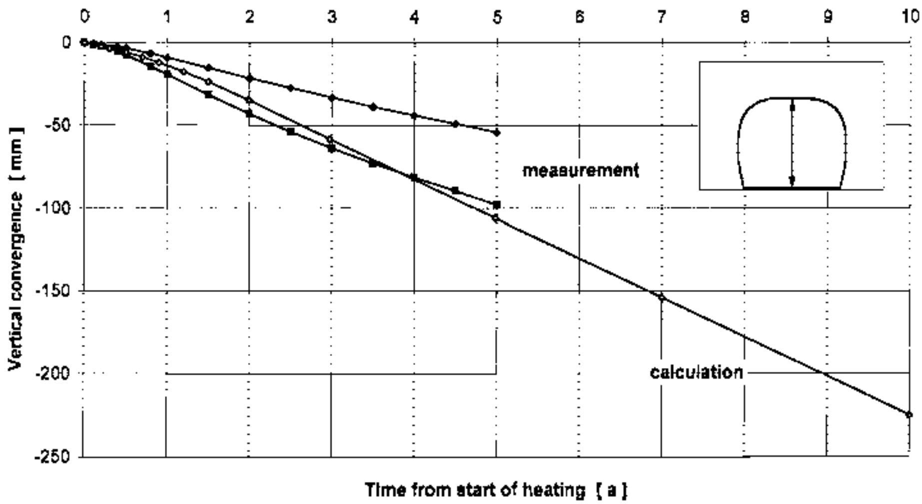

Fig. 4.2-6 Range of vertical convergences measured in the non-heated area in comparison with calculated values

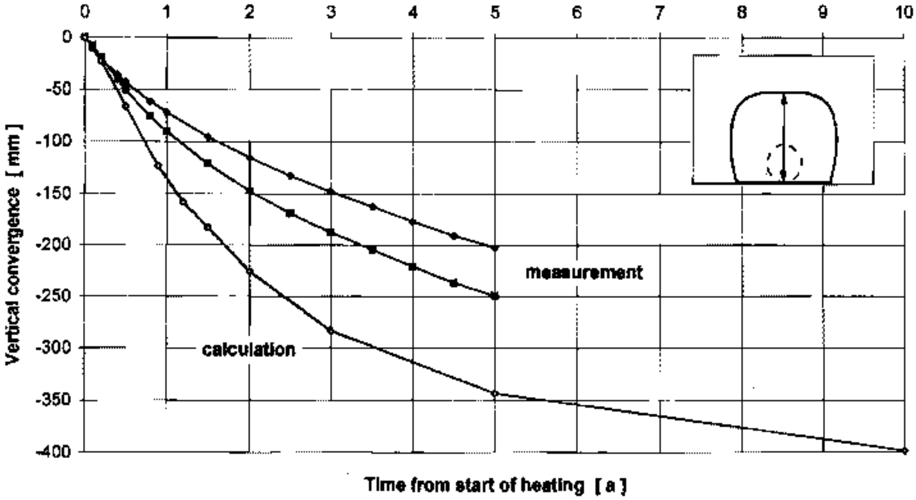

Fig. 4.2-7 Range of vertical convergences measured in the heated area in comparison with calculated values

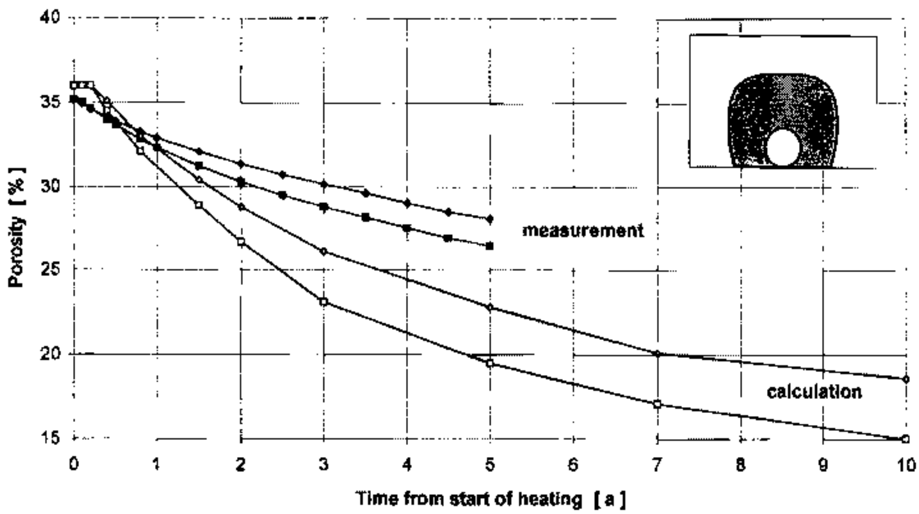

Fig. 4.2-8 Range of backfill porosity measured in the heated area in comparison with calculated values

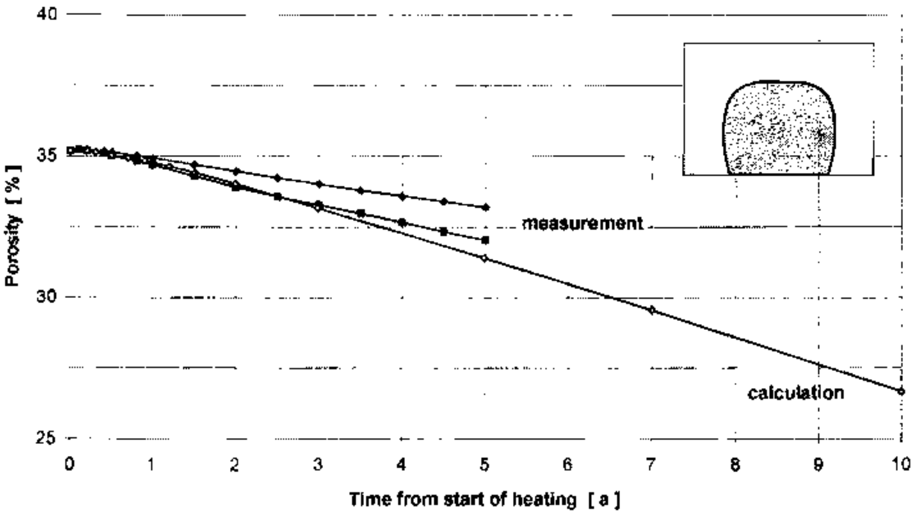

Fig. 4.2-9 Range of backfill porosity measured in the non-heated area in comparison with calculated values

4.2.2 Closing of the Roof Gap

After backfilling of a drift the settling of the backfill due to gravity leads to the opening of a gap between the roof and the top of the backfill which may be a migration path for contaminated gas or brine in a final repository.

In the test drifts the opening and closing of the gap are monitored by means of stationary measuring equipments. A whole equipment comprises three metal sheets at different levels inside the backfill to record the backfill settling. The uppermost sheet of each device is set right on the top of the backfill immediately after its emplacement. The change in distance between every sheet and the roof is monitored by electric transducers /SNE 93/.

The measuring devices are installed in the sections B^{+1}, $D1^{-1}$ and $G2^{+}$ in the heated area as well as in the non-heated sections $E1^{+1}$ and $E2^{-1}$ (Fig. 2-2).

Primary settling of the backfill induces an opening of up to 25 mm on the top of the backfill. Settling in the early backfilled sections at the far end of the test drifts has already ceased when heating starts, but still continues in sections further in front which have been backfilled just a few weeks prior to heating.

In the non-heated area the opening of the gap takes about half a year in section $E2^{-1}$ which has been backfilled at first. It lasts about four months in cross section $E1^{+1}$ right in the front of the test drifts (Fig. 4.2-10). The gap opens between 16.2 mm and 23.5 mm in the different sections depending on the local density of the backfill and the local drift convergence. If vertical drift convergence which counteracts the primary settling is taken into account, the opening of the gap in fact reaches an amount of about 22 mm to 27 mm in the non-heated zone. After maximum opening has been achieved, the size of the roof gap remains almost unchanged for a while when backfill settling and drift convergence have the same rates.

Following the gradual temperature increase in the non-heated zones in 1991, drift closure is accelerated and the gap at the roof begins to close again. Closing of the gap starts about four to ten months after the beginning of heating in cross sections $E1^{+1}$ and $E2^{-1}$ respectively (Fig. 4.2-10). About 14 months after the closing has begun, the displacements in section $E1^{+1}$ suddenly slow down considerably when the top of the backfill gets into touch with the roof. Subsequent to the closing of the gap there are still some final displacements of 1 mm to 4 mm possibly due to a compression of the disturbed zone around the drift. Unlike the backfill in the front of the test drifts the closing of the gap in cross section $E2^{-1}$ takes much longer and lasts about two years.

In the heated area most of the primary settling happens in the same way within the first month after backfilling. When heating starts about two to four months after backfilling, the opening of the roof gap reaching an amount of 5.1 mm to 11.8 mm has not come to an end yet (Fig. 4.2-11). However, settling rates are already decreasing and very low as compared with the beginning.

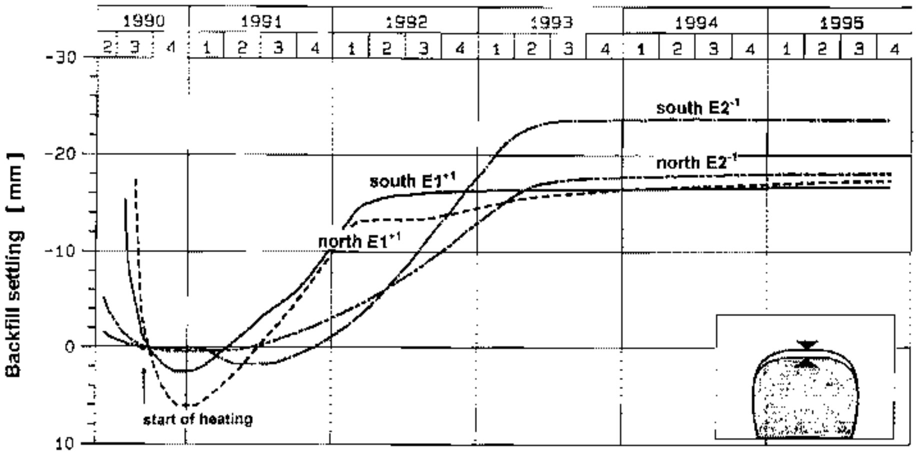

Fig. 4.2-10 Opening and closing of the roof gap in the non-heated area (sections E1^{+1} and E2^{-1})

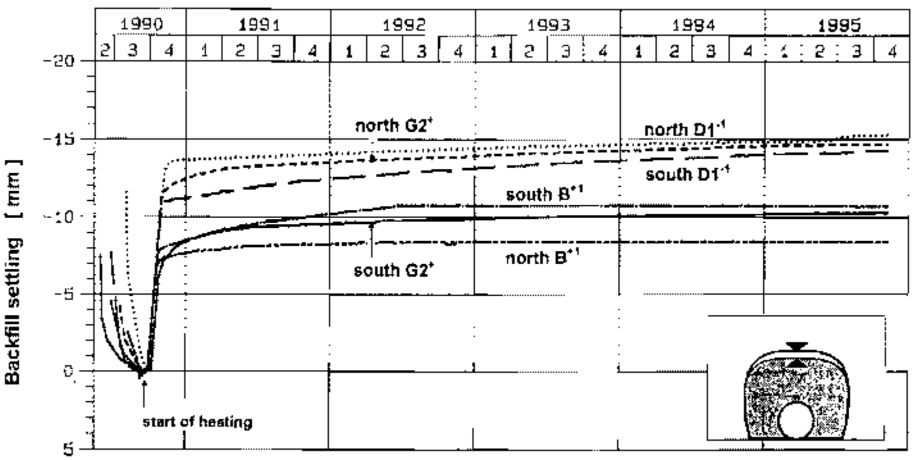

Fig. 4.2-11 Opening and closing of the roof gap in the heated area (sections G2^{+}, B^{+1} and D1^{-1})

When the heaters are switched on, the significant acceleration of drift closure almost immediately induces the closing of the roof gap. Closing starts already a few days after heating has begun. Within just about four to seven weeks the gap is closed again when the top of the backfill comes into contact with the roof, as indicated by the sudden retardation of the displacements (Fig. 4.2-11). The values recorded for the closing of the gap are up to 3 mm higher than the measured amount of opening due to the incomplete adjustment of the measuring device on the top of the backfill. Like in the non-heated area still some final displacements amounting 1 mm to 3 mm can be found after the closing of the gap when the disturbed zone around the test drifts is being compressed.

It can be assumed from the considerations above that the gaps measured in the test will not arise in a final repository. The power output of the Pollux casks will affect the surrounding rock immediately accelerating the drift closure. After backfilling the primary settling of the backfill will already be compensated by the accelerated drift convergence.

4.2.3 Backfill Settling

The settling at different levels of the backfill is recorded by the same measuring equipment used for the monitoring of the gaps /SNE 93/. The measuring devices in the sections B^{*1}, $D1^{*1}$ and $E2^{*1}$ are equipped with three gauges each, including one at the floor to measure the drift convergence, one in the middle of the drift and one on the top of the backfill to monitor the closing of the roof gap. In cross sections $G2^{*}$ and $E1^{*1}$ where separate convergence measurement devices are installed, there are two gauges in the lower and upper third of the backfill in addition to the one on the top. In this way the vertical distribution of backfill settling can be determined.

Measurements always started immediately after backfilling. Prior to heating primary settling takes place as described above.

In the non-heated area primary settling continues after the heaters have been switched on, affecting mainly the lower section of the backfill. At that time about two thirds of the compaction are taking place in the lower third of the backfill and about one third in the middle part, whereas the upper part of the backfill remains almost unchanged (Fig. 4.2-12 and 4.2-13).

As a result of the accelerated drift closure in the cold area following the gradual temperature increase in 1991, the movement in the backfill reverses about three months to ten months after the beginning of heating in the sections $E1^{+1}$ and $E2^{-1}$ respectively. While the gap at the roof is closing, the portion of backfill compaction in the central area increases. Compaction in the upper part of the backfill starts not until the gap is closed. Subsequent to the closing of the gap the settling rates at all levels in the backfill decrease with increasing percentages of backfill settling taking place in the upper part now. Since 1993, the portion of backfill compaction in the lower third is increasing again although the total compaction is still considerably lower than in the upper parts (Fig. 4.2-12 and 4.2-13).

Up to now the total compaction reaches about 23 mm in the upper third of the drifts, about 28 mm in the middle part and only around 9 mm in the lower section. The corresponding ratio of backfill settling amounts to about 40 %, 45 % and 15 % in the upper, middle and lower part respectively. Actual settling rates in the cold backfill range between 0.25 - 0.3 %/a in the upper section, 0.6 - 0.9 %/a in the middle part and 0.4 - 0.5 %/a in the lower part.

In the heated area the significant acceleration of drift closure after the start of heating almost immediately induces a reversal of the direction of displacement. Apart from primary settling, however, no compaction takes place in the beginning as the backfill which has no contact with the subsiding roof is lifted up as a whole.

Backfill compaction starts not until the gap at the roof is closed. After the closing of the gap the backfill settling takes a decreasing course running almost identical in the same cross sections of the two test drifts (Fig. 4.2-14). The deviating convergence values in the southern test drift in 1993 to 1994 shown in Fig. 4.2-14 are caused by a stick-slip effect of the gauge.

Unlike the non-heated sections about 60 % of backfill compaction is taking place in the upper half of the backfill during the first months after the closing of the gap (Fig. 4.2-15). Then increasing portions of the lower part are involved until the vertical distribution of backfill compaction is approximately balanced after two years of heating. The portion of backfill compaction in the lower half keeps slightly increasing since then, but all in all the vertical distribution is still balanced up to now.

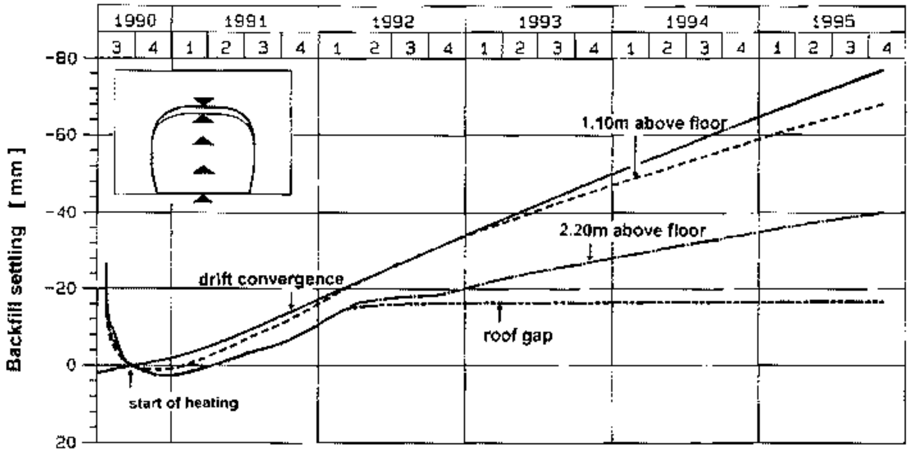

Fig. 4.2-12 Backfill settling and drift convergence at different levels in the non-heated backfill (section E1[+1])

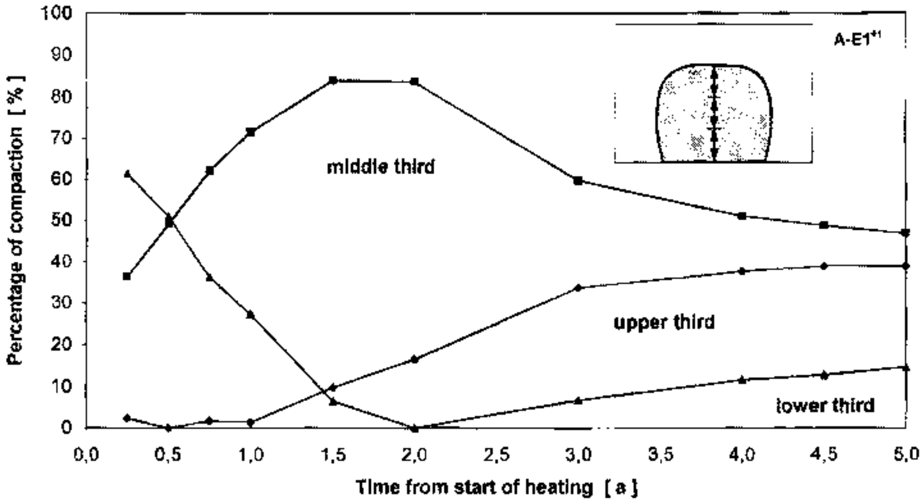

Fig. 4.2-13 Vertical distribution of backfill compaction in the non-heated backfill (section E1[+1])

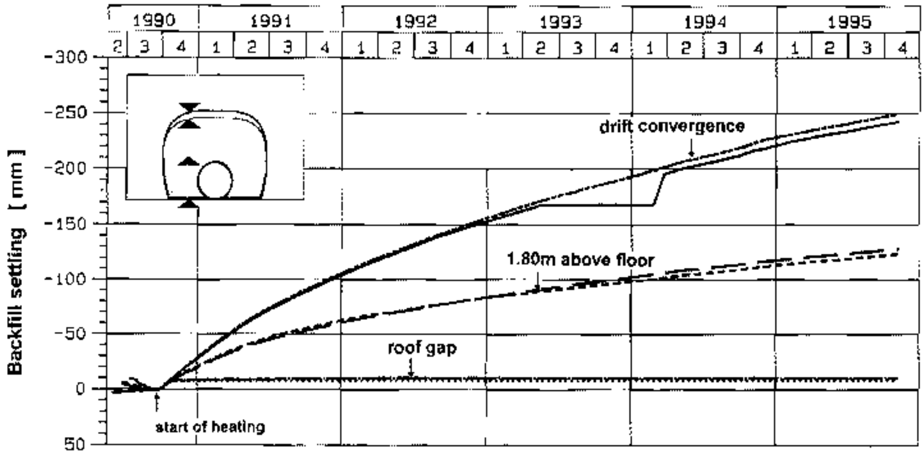

Fig. 4.2-14 Backfill settling and drift convergence at different levels in the heated backfill (section B*[1])

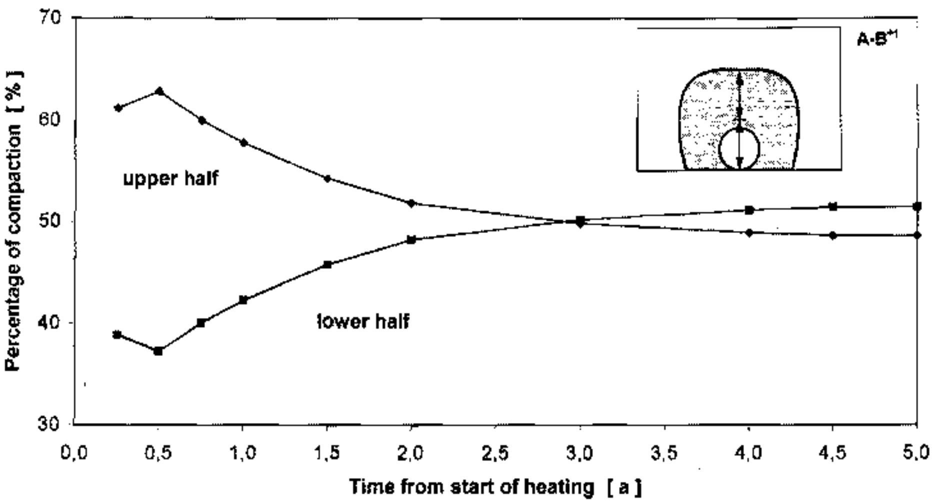

Fig. 4.2-15 Vertical distribution of backfill compaction in the heated backfill (section B*[1])

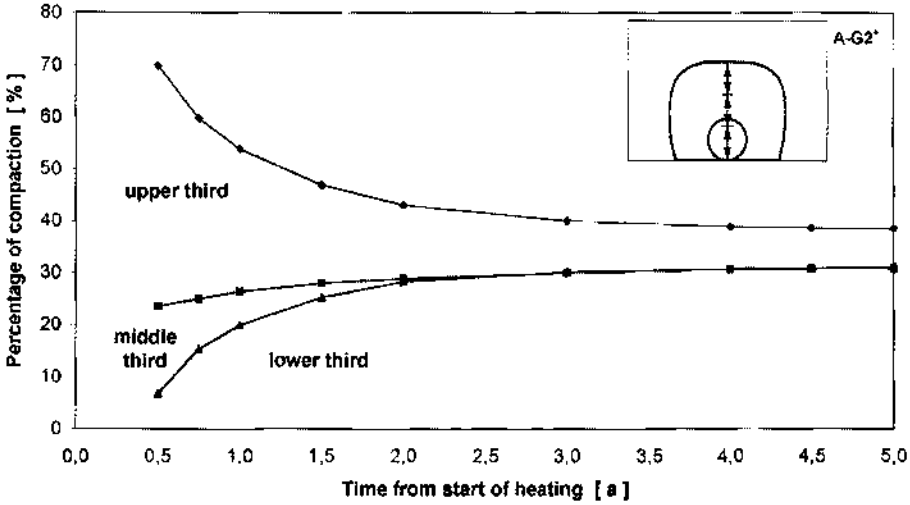

Fig. 4.2-16 Vertical distribution of backfill compaction in the heated backfill (section G2+)

A more detailed course of compaction can be obtained from section G2+ where settling gauges are installed at levels of one third and two thirds of the drifts. In the beginning about 70 % of backfill compaction is taking place in the upper third, 25 % in the central part and only 5 % in the lower section (Fig. 4.2-16). The corresponding settling rates range between about 9 %/a in the upper third to an average of approximately 5 %/a in the lower parts.

Subsequently the proportion of backfill compaction in the upper section diminishes more and more while increasing parts are taken over by the lower third of the backfill (Fig. 4.2-16). Settling in the middle part, however, increases only slightly. After two years of heating the compaction in the different parts of the backfill reaches an almost constant ratio with hardly any change up to now. The current values amount to about 40 % in the upper third and about 30 % in the middle and lower section each.

The total displacements in the heated backfill range between 57 mm to 73 mm in each of the lower thirds and 83 mm to 86 mm in the upper third at the moment. Consequently, the present compaction in the heated area reaches about three to four times the amount of the total compaction of the upper parts of the non-heated zones and even six to eight times the amount of their lower third. The current settling rates of about 0.5 %/a to 0.7 %/a, however, are in the same order as the actual rates in the cold backfill.

Actually, the highest values of backfill compaction are recorded around the central heaters in section B[*1]. Compaction decreases with increasing distance from the central heaters and is about 10 % to 25 % lower around the heaters in cross section D1[*1].

4.2.4 Axial Borehole Deformations

The axial deformations of the rock around the test drifts are monitored by multiple point glass fibre rod extensometers which are installed in boreholes in the sections A and D1 in the heated area and in the non-heated sections E1 and E2 (Fig. 2-2). In each section boreholes in the floor, in the walls, in the pillar and apart from section A in the roof as well are equipped with a set of four extensometers. In section A a set of five extensometers has been installed above each test drift from the observation drifts on the 750 m level prior to the mining of the test drifts. At the same time an additional set of eight extensometers has been installed in a vertical borehole between the test drifts in order to record the vertical displacements in the pillar between the test drifts.

Axial borehole deformations prior to heating

In the monitoring cross section A the vertical displacements above the test drifts and in the pillar are recorded on the 750 m level since April 1989.

As a result of the mining of the test drifts from the end of March until April 1989 the deformation rates right above the test drifts rise to 5 - 10 mm/a corresponding to dilatation rates of 0.25 - 0.3 %/a in the section 1.5 - 3.5 m above the drifts (Fig. 4.2-17 and 4.2-18). The movements are directed downwards towards the test drifts. Farther away in a distance of 3.5 - 31.5 m above the test drifts the deformation rates reach only 1 - 3 mm/a (Fig. 4.2-17). The dilatation rates of 0.01 %/a are very low in that area (Fig. 4.2-18). Thirteen to sixteen months after the mining of the test drifts the vertical displacements above the drifts reach steady state conditions with dilatation rates around 0 %/a. Obviously, the deformations resulting from the mining of the test drifts have already come to an end before the heating is started.

The vertical displacements in the pillar are showing the same development in the area above the level of the test drifts (Fig. 4.2-19 and 4.2-20). In the deeper part, however, a continuous uplifting is recorded until the start of heating ranging between 0.3 %/a on the level of the drifts and 0.15 %/a to 0.015 %/a below the test drifts (Fig. 4.2-20 and 4.2-22).

Axial borehole deformations during the heating

After the start of heating the deformations are accelerated four times to six times the amount with a delay of five weeks right above the test drifts to nine months 7.5 m above the drifts. In 15.5 m above the drifts the accelerated deformations start not until two years after the beginning of heating, whereas the measuring points 31.5 m away are recording the first effects of heating after four years (Fig. 4.2-17).

About one year after the start of heating the deformation rates above the test drifts are already decreasing indicating the beginning support by the backfill. The actual deformation rates 1.5 m above the drifts amount to 8.5 mm/a. They are decreasing to 3 - 5 mm/a in 7.5 m corresponding to dilatation rates of 0.1 %/a (1.5 - 3.5 m) to 0.04 - 0.07 %/a (7.5 - 15.5 m). Farther away the dilatation rates reach only 0.006 - 0.02 %/a (Fig. 4.2-18).

In the pillar the vertical displacements on the level of the test drifts are accelerated almost immediately after the start of heating to five times to ten times the amount (Fig. 4.2-19). Beneath the level of the drifts the deformations are going up twice to four times the amount with a delay of two or three months (Fig. 4.2-21). Above the drifts there is a delay of about six months (Fig. 4.2-19).

The initially upward movement on the level of the test drifts reverses about half a year after the beginning of heating (Fig. 4.2-19). The displacements are now directed downwards like the movements in the area above the test drifts. The displacements below the level of the test drifts, however, are still directed upwards (Fig. 4.2-19 and 4.2-21).

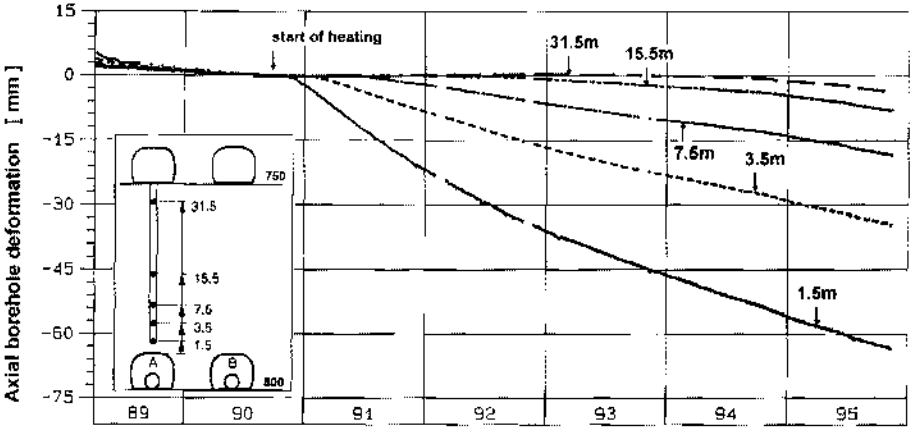

Fig. 4.2-17 Vertical deformations above the heated drifts (section A)

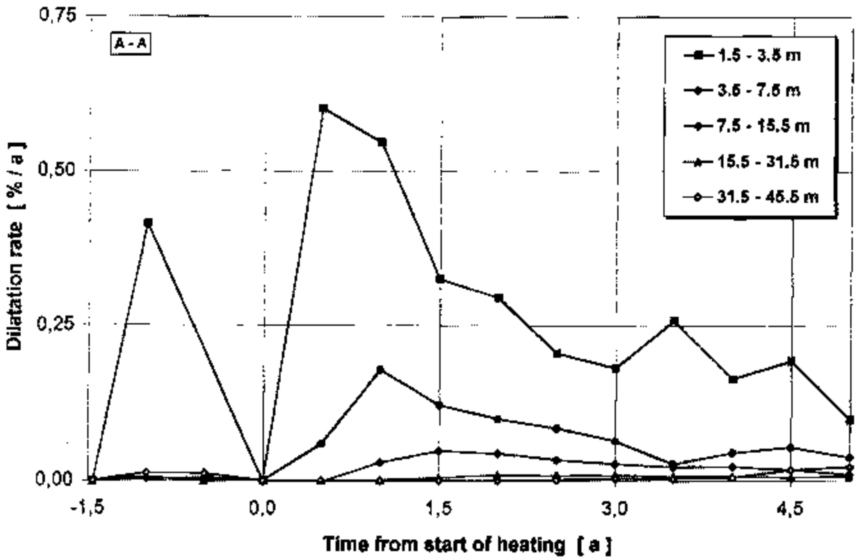

Fig. 4.2-18 Dilatation rates above the heated drifts (section A)

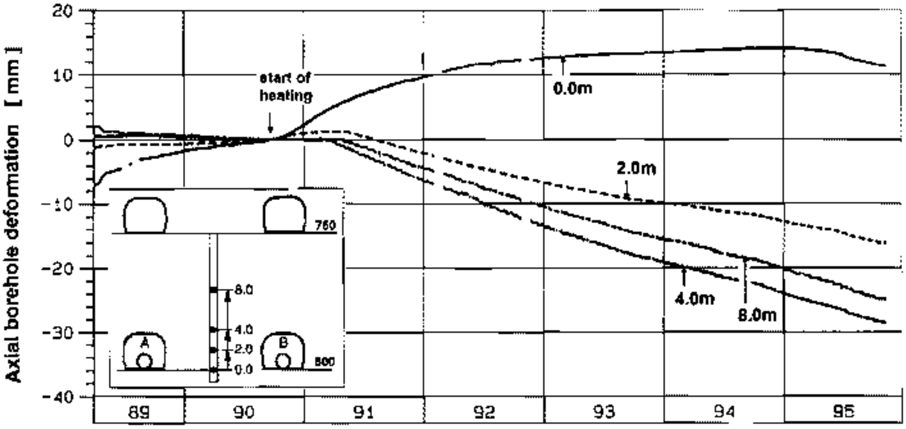

Fig. 4.2-19 Vertical deformations in the pillar above the heated drifts (section A)

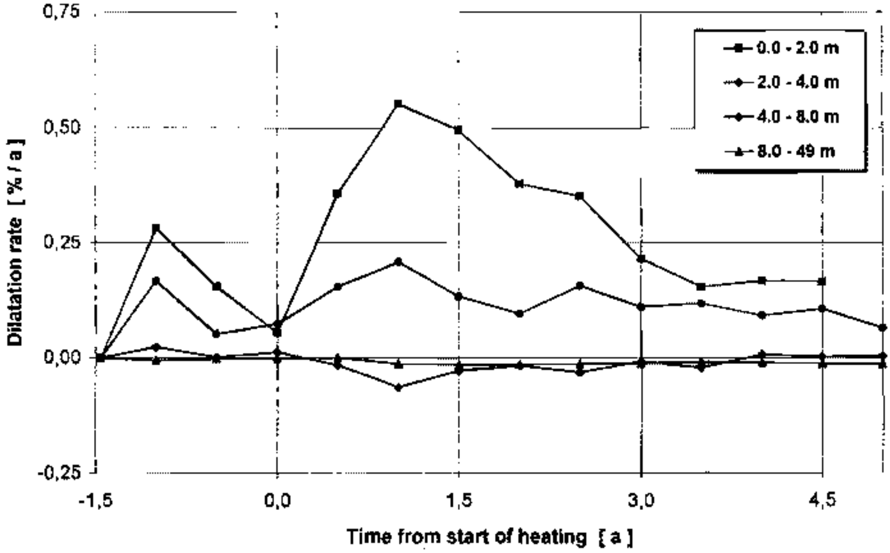

Fig. 4.2-20 Dilatation rates in the pillar above the heated drifts (section A)

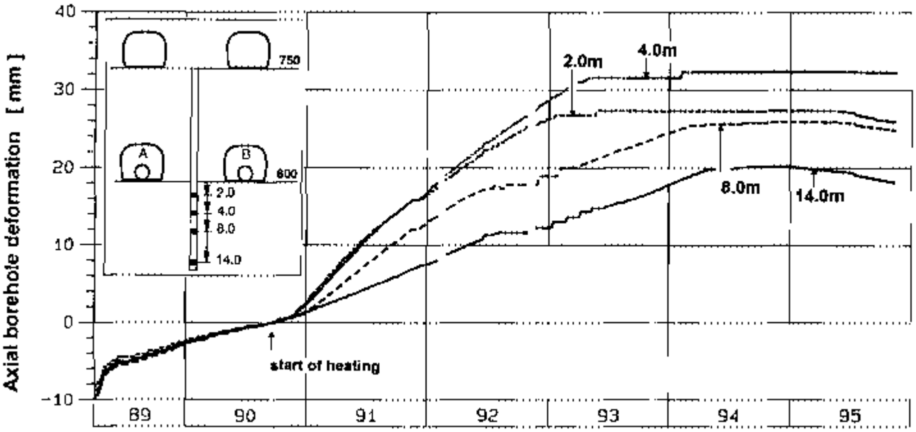

Fig. 4.2-21 Vertical deformations in the pillar below the heated drifts (section A)

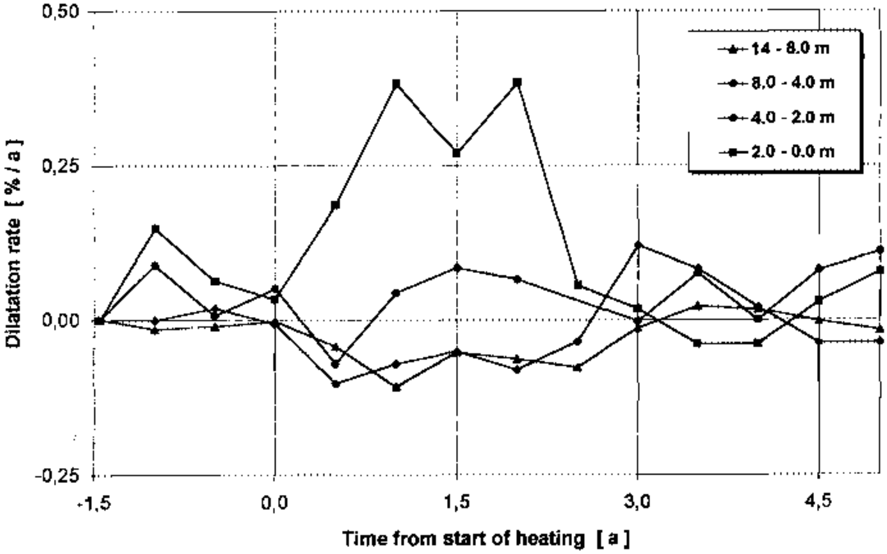

Fig. 4.2-22 Dilatation rates in the pillar below the heated drifts (section A)

About one year after the heating has been started the dilatation rates reach their maximum (Fig. 4.2-20 and 4.2-22). The highest values of up to 0.55 %/a are recorded on the level of the test drifts. After that the rates are decreasing again reaching 0.15 %/a on the level of the drifts at the moment. Right above the drifts the maximum dilatation rates in the pillar amount to 0.2 %/a decreasing to 0.1 %/a up to now. In the area more than four metres above the test drifts the dilatation rates are only very small ranging between 0.001 - 0.03 %/a.

The deeper part of the pillar, however, is affected much more by the heating. Even 14 m below the level of the drifts a doubling of the deformation rates is been observed. Since 1993 all gauges in the deeper part of the pillar do not record any further deformations. The deformations, however, have not come to an end yet. Presumably, the glass fibre rods of these extensometers got stuck due to the rock pressure leading to the failure of the gauges. In 1995, two additional boreholes in the deeper part of the pillar were equipped with a set of four extensometers each to compensate for the failures. Measurements are starting soon.

The axial deformations around the test drifts are recorded on the 800 m level since September 1990.

In the heated area the first and largest deformations are observed by the extensometers in the floor right below the heated casks. Within one week after the heaters have been switched on, the deformations are accelerated ten to twenty times the amount (Fig. 4.2-23). After initial deformation rates of up to 106 mm/a and dilatation rates of up to 4 %/a in a depth of 0 - 2.5 m, the rates are decreasing again already two months later. After three years deformation rates of 15 - 20 mm/a are registered. In the end of 1993, all of the floor extensometers in the heated area have failed, the reasons for which will be explained in chapter 4.4.1.

In 2.5 m below the heater casks the accelerated deformation starts with a delay of two to five weeks. During the next four to six months the deformation rates amount to 23 - 33 mm/a, decreasing afterwards to 14 mm/a just before the failure of the gauges in 1993.

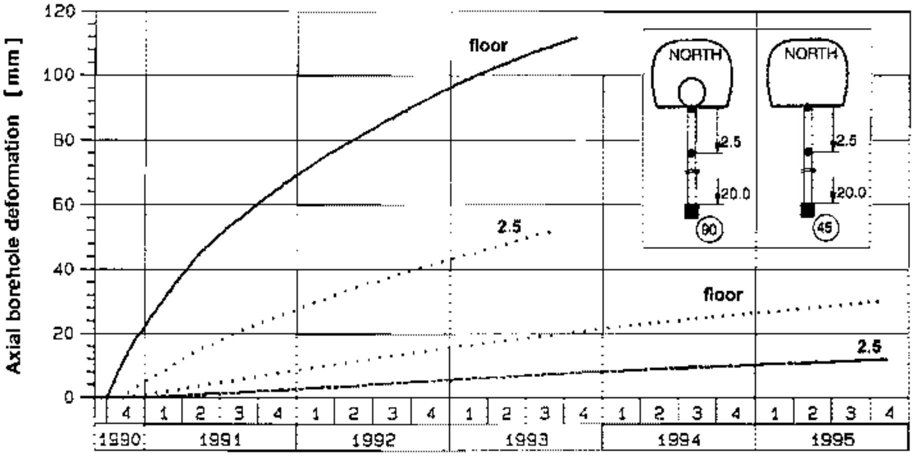

Fig. 4.2-23 Vertical deformations beneath the drifts (floor extensometers in sections A and E1)

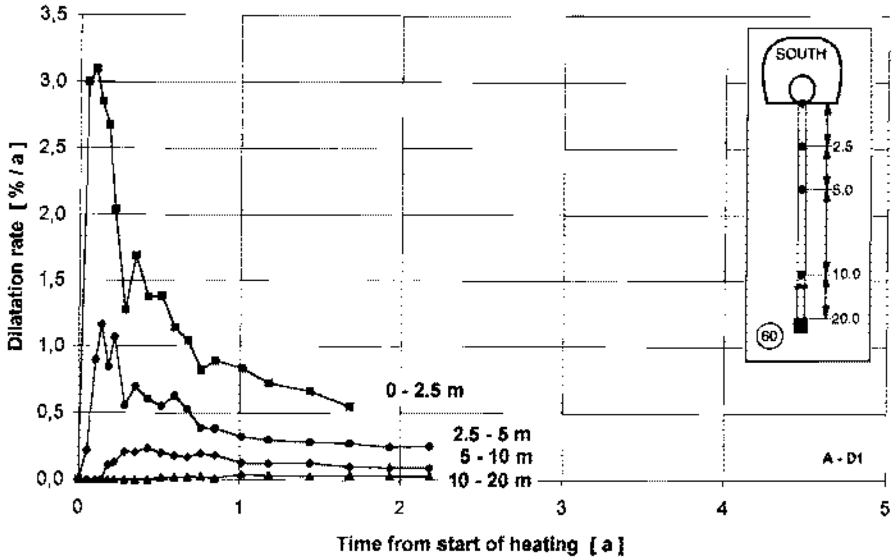

Fig. 4.2-24 Dilatation rates beneath the heated drifts (floor extensometer in section D1)

In 5 m and 10 m below the heater casks the first effects of heating are recorded after two to four months and four to ten months respectively. After an initial increase to 10 - 17 mm/a the deformation rates in 5 m depth decline to 6 - 7 mm/a in 1993. In a depth of 10 m nearly constant deformation rates of 3 - 5 mm/a are observed. The corresponding dilatation rates are shown in Fig. 4.2-24. Up to a depth of 5 - 10 m below the test drifts the uplifting of the floor reaches double the amount of the vertical displacements in the pillar on the same level. In the deeper area the deformation rates are in the same range.

The horizontal extensometers in the walls are showing a delayed reaction to the heating and in the beginning lower deformation rates than the floor extensometers (Fig. 4.2-25 and 4.2-26). At the drift wall the accelerated deformations start between one to two weeks after the heaters have been switched on with maximum deformation rates of 38 - 51 mm/a. In 2.5 m depth rates of 10 - 18 mm/a are recorded. The dilatation rates in 0 - 2.5 m reach up to 1.3 - 1.8 %/a. About two to three months later the deformation rates are already decreasing again. After nine months they are in the same range as the vertical displacements in the floor. Up to the end of 1993 the rates keep on going down. Due to the higher thermal power output in 1994 the deformation rates then remain almost constant over more than a year. After the repair of the heater control system the deformation rates are decreasing again reaching 13 - 15 mm/a at the drift wall at the moment and 7 - 9 mm/a in 2.5 m depth.

In a depth of 5 m in the walls the acceleration of the deformations starts not until three to five months after the beginning of heating. After eight to ten months maximum rates of 6 - 9 mm/a are reached going over to almost constant rates of 4 - 7 mm/a up to now. The measuring points in 10 m depth are indicating the first effects after nine to twelve months of heating. The displacements are still taking a linear course at constant deformation rates of 2 - 3 mm/a. In Fig. 4.2-26 the horizontal dilatation rates between the measuring points are shown.

The actual deformations of the horizontal extensometers in the walls are mainly measured by additional devices which have been installed in 1994 in three additional boreholes after the failure of most gauges. The boreholes have been drilled in horizontal direction in the sections A and D1 from the observation drifts on the 800 m level.

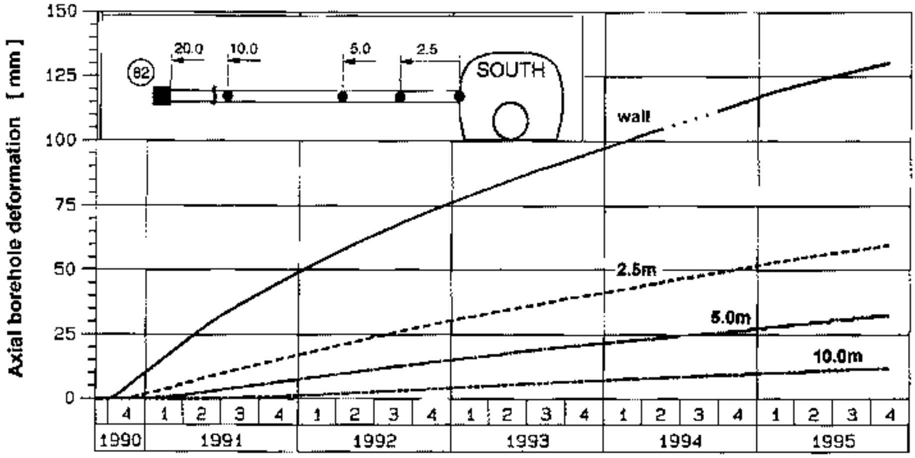

Fig. 4.2-25 Horizontal deformations beside the heated drifts (wall extensometer in section A)

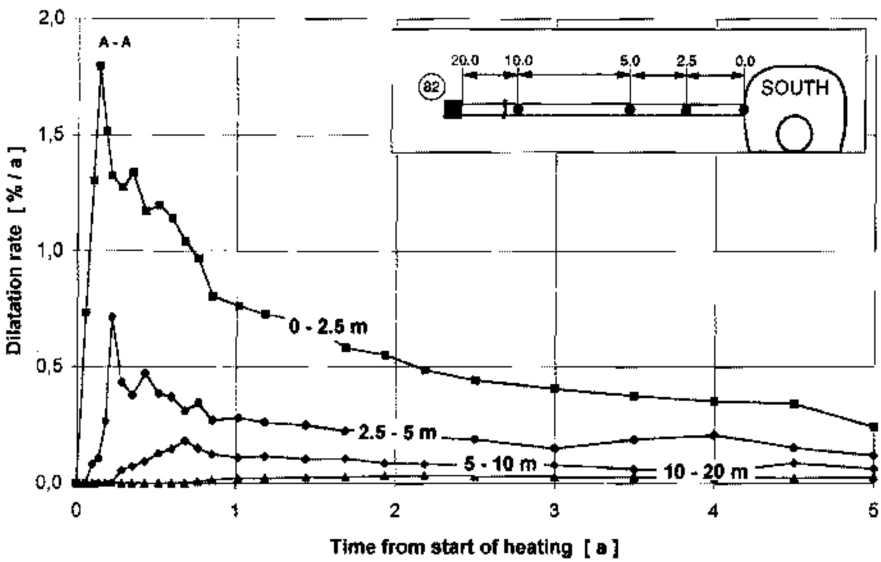

Fig. 4.2-26 Dilatation rates beside the heated drifts (wall extensometer in section A)

At the pillar wall the horizontal displacements are about 10 - 30 % higher than the deformations at the opposite side (Fig. 4.2-27). Maximum deformation rates of 48 - 64 mm/a are reached after three months. After that the rates decrease again. Four years after the beginning of heating almost all gauges in the pillar have failed with the exception of one extensometer at the drift wall recording a deformation rate of 15 mm/a at the moment (Fig. 4.2-27). A replacement of the instrumentation in the pillar is not feasible in horizontal direction.

In 2.5 m depth the horizontal deformation rates in the pillar are initially about 30 % higher than in the opposite wall. After three months the deformation rates reach their maximum as well but remain almost constant then at a level of 15 - 24 mm/a for about half a year. After that the rates are decreasing likewise. About one to two years after the beginning of heating the deformation rates in the pillar are approaching the rates of the other wall extensometers in the same depth.

While the horizontal deformation rates in the pillar and the walls are quite similar, there are differences between the dilatation rates of the measuring points. In 0 - 2.5 m depth the dilatation rates are reaching a maximum of 1.3 - 1.8 %/a in the beginning on both sides. After that, however, the rates in the pillar are decreasing more slowly than in the opposite wall (Fig. 4.2-28). In 2.5 - 5 m depth the dilatation rates in the pillar are twice as much as in the wall. In the beginning they amount up to 1 %/a. From nine months after the start of heating on they are showing the same course as the dilatation rates of the wall extensometers in a depth of 0 - 2.5 m. At the time of the failure of most pillar extensometers the horizontal dilatation rates in the inner and the outer part of the pillar are almost in the same range (Fig. 4.2-28).

The vertical deformations of the roof extensometers are lower and more delayed than the displacements of the other extensometers because of their greater distance from the heater casks. Their deformation rates are comparable to a floor extensometer which is shifted about 2.5 m (Fig. 4.2-29).

At the roof and in 2.5 m depth maximum deformation rates are reached after three to six months. They amount to 33 - 36 mm/a and 11 - 12 mm/a respectively. Afterwards the rates are decreasing again. By 1993 the roof extensometers in section D1 have all failed.

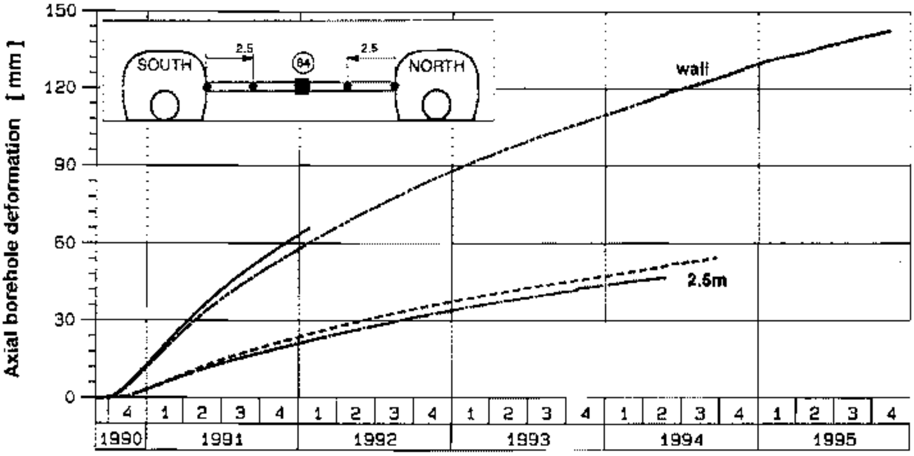

Fig. 4.2-27 Horizontal deformations between the heated drifts (pillar extensometer in section A)

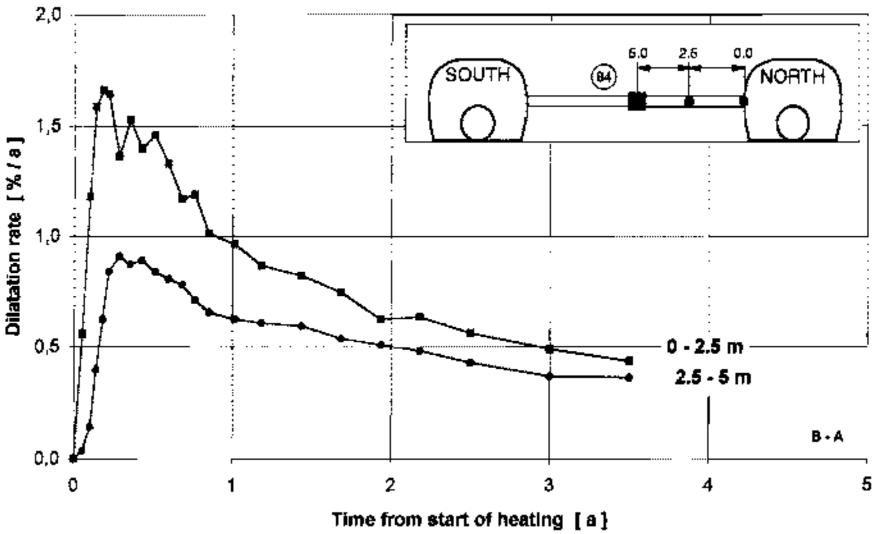

Fig. 4.2-28 Dilatation rates between the heated drifts (pillar extensometer in section A)

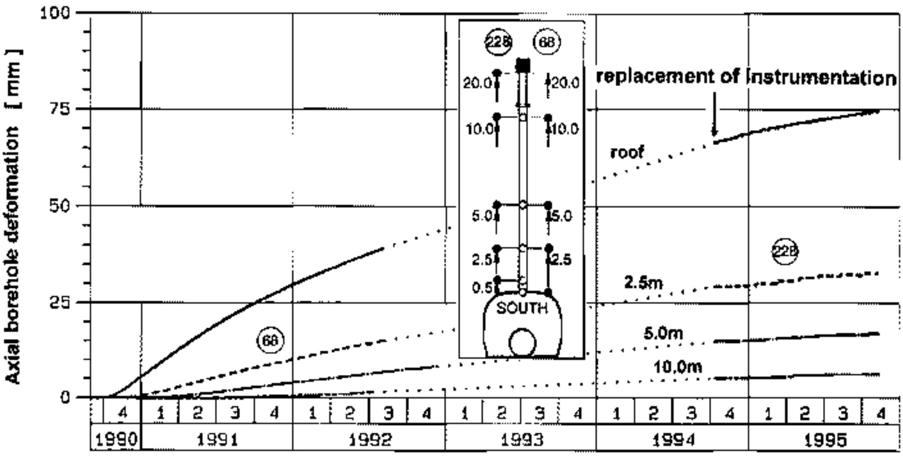

Fig. 4.2-29 Vertical deformations above the heated drifts (roof extensometer in section D1)

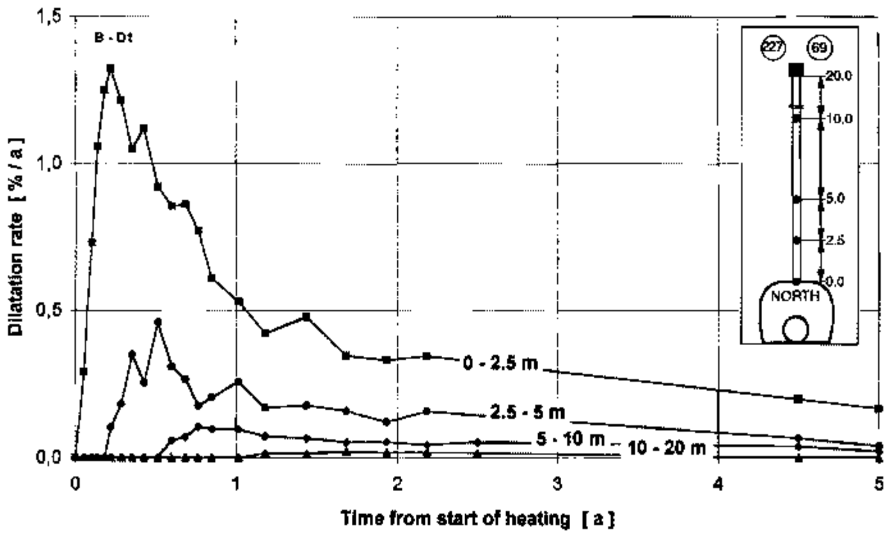

Fig. 4.2-30 Dilatation rates above the heated drifts (roof extensometer in section D1)

In 1994, two additional boreholes are drilled from the observation drifts on the 750 m level in section D1. They are equipped with five extensometers each which replace the failed gauges. The actual deformation rates measured by these extensometers amount to 6 - 7 mm/a right above the roof and to 3 - 4 mm/a in 2.5 m depth.

In 5 m depth the accelerated deformations start not until five to seven months after the beginning of heating. Reaching their maximum after nine to ten months the deformation rates are then decreasing slowly and amount to 2 - 3 mm/a at the moment. In a depth of 10 m the effects of heating are first recorded after one year. In this area the displacements take a linear course at constant deformation rates of 1 - 2 mm/a.

The dilatation rates of the roof extensometers in section D1 are shown in Fig. 4.2-30. They are in the same range as the rates of the extensometers above the test drifts in section A which have been installed from the 750 m level.

In Fig. 4.2-31 the dilatation rates next to the heated drifts in 0 - 2.5 m depth are compared for different positions. The maximum dilatation rates of up to 4 %/a in the beginning are recorded in the floor of the test drifts. The horizontal rates rise up to 1.8 %/a while the rates in the roof reach up to 1.3 %/a. About half a year after the start of heating the dilatation rates in the floor become like the rates of the other extensometers. The further decrease of the dilatation rates is in the same range in all positions with the lowest rates still occuring in the roof.

It can be concluded from Fig. 4.2-31 that the vertical convergence of the heated drifts is composed by two thirds of the uplifting of the floor and only by one third of the downward movement of the roof. The horizontal displacements, however, show not much difference. The deformations on the pillar side are contributing between 50 % and 60 % to the horizontal movements and are not distinctive higher than the deformations on the opposite side. Consequently, an approximately uniform compaction of the test drifts from both sides can be assumed.

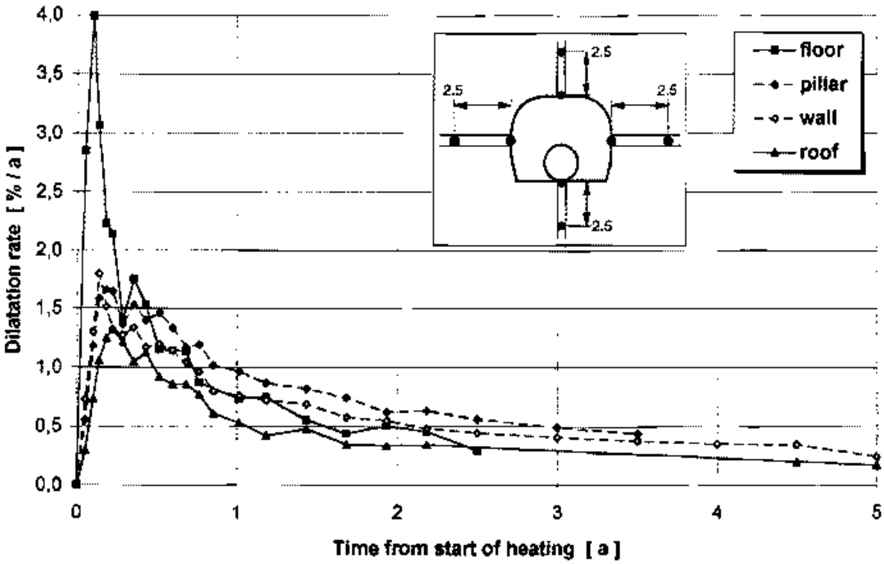

Fig. 4.2-31 Dilatation rates next to the heated drifts (0 - 2.5 m)

In the non-heated area the sections E1 and E2 have been equipped with the same extensometer instrumentation as in the heated area to enable an assessment of all the deformations. The total deformations in the non-heated area amount only to about 30 % of the displacements in the heated sections (Fig. 4.2-32 and 4.2-33). The largest deformations are recorded by the floor extensometers whereas the lowest ones are again occuring in the roof. The proportion of the uplifting of the floor, however, is much lower than in the heated area. It contributes just between 50 % to 60 % to the vertical displacements of the cold sections.

The deformations at the drift outline are similar for all measuring points in the cold sections. Due to the gradual temperature increase in the non-heated sections in 1991 the deformation rates are gradually increasing. After one to one and a half year of heating maximum rates of 10 - 12 mm/a are reached at the walls and the roof, while some higher rates of 12 - 14 mm/a are recorded at the floor. The maximum dilatation rate in 0 - 2.5 m amounts to 0.4 %/a. After that the rates are slowly decreasing again reaching 8 - 9 mm/a at the moment in horizontal direction and lower rates of 5 - 7 mm/a at the roof and the floor.

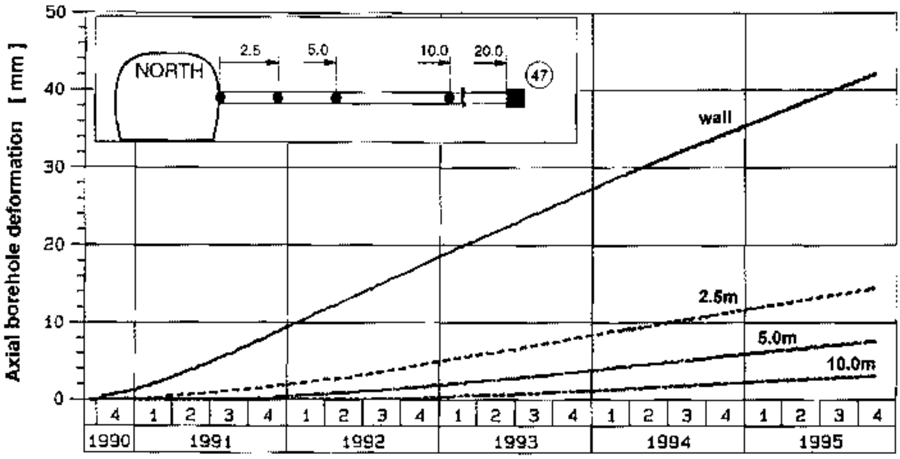

Fig. 4.2-32 Horizontal deformations beside the cold drifts (wall extensometer in section E1)

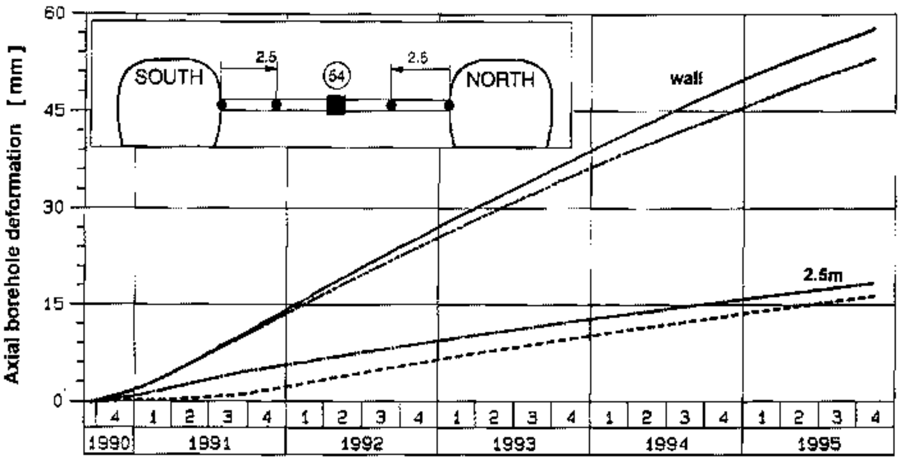

Fig. 4.2-33 Horizontal deformations between the cold drifts (pillar extensometer in section E2)

These deformation rates as well as the actual dilatation rates of 0.1 - 0.3 %/a in 0 - 2.5 m are in the same range as the present rates in the heated sections (Fig. 4.2-34 and 4.2-35).

In 2.5 m depth the deformations start with some delay but take a similar course as the displacements at the drift outline (Fig. 4.2-32). After one to one and a half year maximum deformation rates of 11 - 20 mm/a are reached in the walls and the floor and 7 - 10 mm/a in the roof. These rates keep nearly unchanged up to now. In the heated area, however, the deformation rates in 2.5 m depth are decreasing the whole time after the maximum rates have been reached. The present rates in the heated sections are in the same range as the rates in the non-heated area. The actual dilatation rates of 0.03 - 0.07 %/a in 2.5 - 5 m depth in the cold area are likewise comparable with the heated sections (Fig. 4.2-34).

A differing behaviour, however, is observed in the pillar. In 2.5 - 5 m depth the dilatations reach maximum rates of 0.2 %/a after one year. After five years the rates in the pillar amount to 0.11 - 0.13 %/a and are still twice to three times as much as the dilatation rates in the opposite walls (Fig. 4.2-35). In the heated area the horizontal dilatation rates in the inner and the outer part of the pillar are in the same range after two years (Fig. 4.2-28). In the non-heated pillar, however, the dilatation rates in 0 - 2.5 m depth are still double the amount of the rates in the inner part of the pillar (Fig. 4.2-35).

In depths of 5 m and 10 m the deformations in the non-heated area are only very small. In 5 m the deformations are rising about half a year to one year after the beginning of heating (Fig. 4.2-32). The deformation rates are almost constant at 2 - 3 mm/a in the walls and in the floor. The roof extensometers are recording rates of 0.4 - 0.9 mm/a. In 10 m the deformations start after one to two years. The rates amount to 0.9 - 1.5 mm/a in the walls, to 0.6 - 0.9 mm/a in the floor and to 0.2 - 0.4 mm/a in the roof. The dilatation rates reach 0.01 - 0.04 %/a in 5 - 10 m depth and 0.002 - 0.01 %/a in 10 - 20 m depth (Fig. 4.2-34).

Actually, in areas further away from the test drifts the horizontal deformation rates in the heated walls are still twice as much as in the non-heated area. In the heated roof and floor the present vertical deformation rates are even three to five times the amount of the cold sections. Unlike the area next to the drifts the deformation rates of the heated and the cold sections are still not approaching up to now.

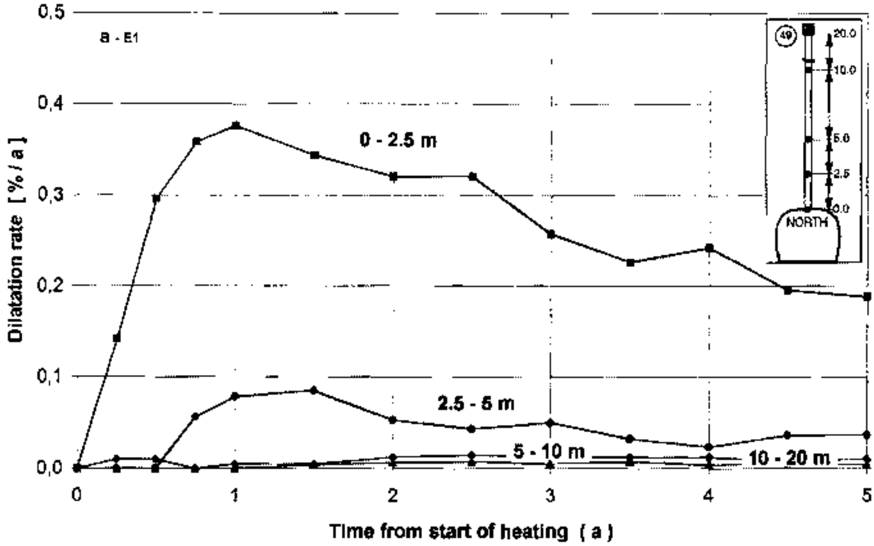

Fig 4.2-34 Dilatation rates above the cold drifts (roof extensometer in section E1)

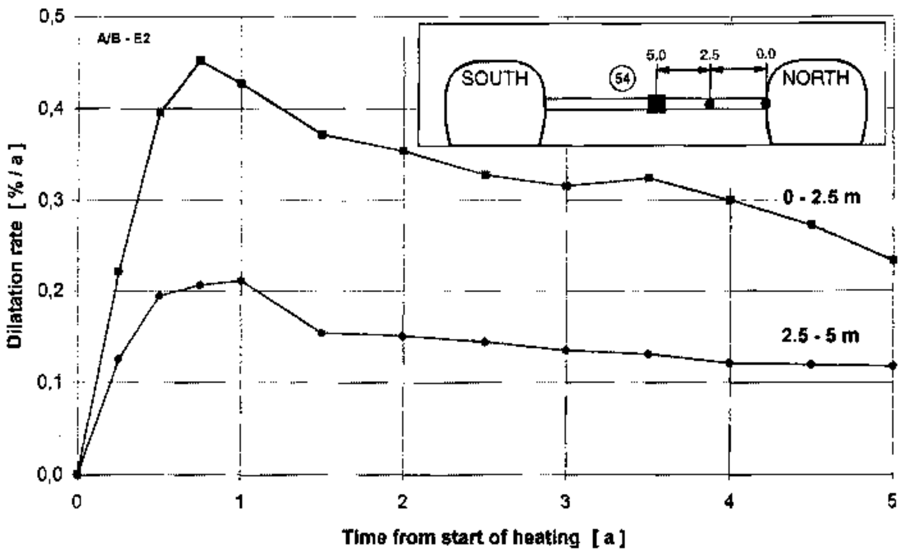

Fig. 4.2-35 Dilatation rates between the cold drifts (pillar extensometer in section E2)

The development of the deformation rates in the heated and the non-heated area after two and five years of heating is shown in Fig. 4.2-36 to 4.2-39 for increasing depths. The deformation rates of the extensometers in different depths are set in relation to the rates at the drift outline.

In the heated area the proportions of the deformation rates of all extensometers apart from the pillar are quite similar after two years of heating. In 2.5 m depth about 50 % of the rates at the drift outline are reached (Fig. 4.2-36). Up to a depth of 10 m the values decrease to approximately 5 %. After five years of heating the proportion of the rates in 2.5 m depth decreases to 30 % at the roof extensometers (Fig. 4.2-37). At the horizontal extensometers the proportion of the area next to the drifts up to 5 m increases slightly. In the area further away from the drifts, however, the proportion of the rates increases more significantly to about 10 % in 10 m depth. The extensometers in the floor have all failed at that time.

In the non-heated area the proportions of the deformation rates in 2.5 m depth are reaching between 25 % of the rates at the drift outline at the roof extensometers to 35 % at the floor extensometers after two years of heating (Fig. 4.2-38). In the pillar even 55 % are recorded. Up to a depth of 10 m the values are decreasing to 3 - 5 %. Five years after the beginning of heating the proportions of the rates have hardly changed in the non-heated area (Fig. 4.2-39). The horizontal extensometers in the walls are the only ones with a noticeable increase of the values in the area further away from the drifts.

In Fig. 4.2-40 the start of the accelerated deformations in the heated area is summarized for the different extensometers in relation to the distance of the measuring points from the heated drifts. From that diagram the activating time of the accelerated deformations for distant areas can be estimated.

The comparison of the extensometer measurements with calculated rock deformations reveals significant differences in the heated area. Like the drift convergences the horizontal deformations in the walls and the pillar reach only two thirds of the predicted values (Fig. 4.2-41). The vertical deformations in the floor are even much lower than expected. At the time of the failure of the extensometers they have reached just about the half of the calculated amount.

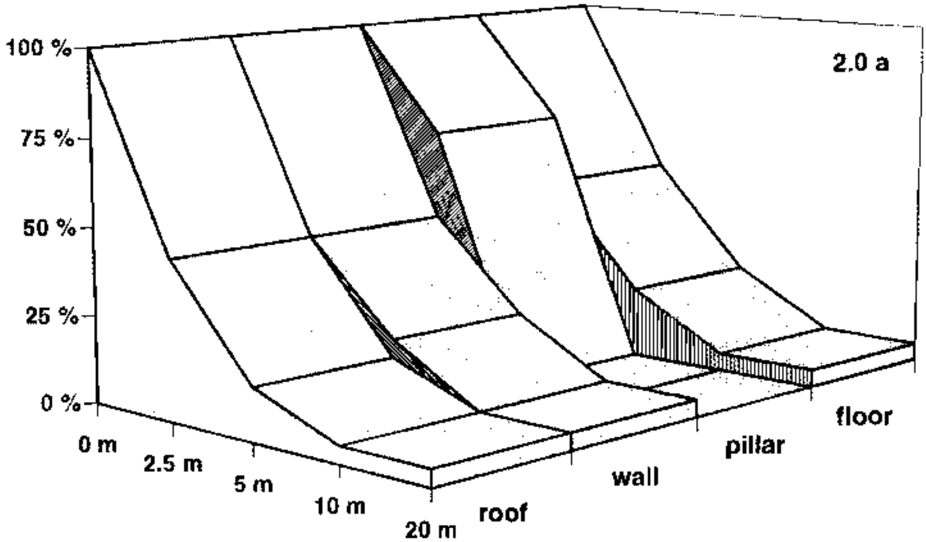

Fig. 4.2-36 Decrease of deformation rates with increasing depth in the heated area after two years of heating (drift outline = 100%)

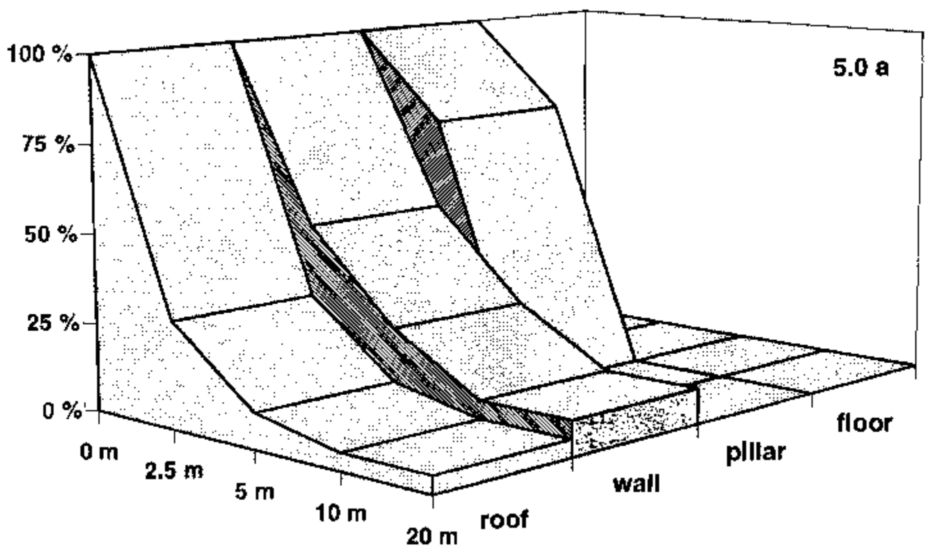

Fig. 4.2-37 Decrease of deformation rates with increasing depth in the heated area after five years of heating (drift outline = 100%)

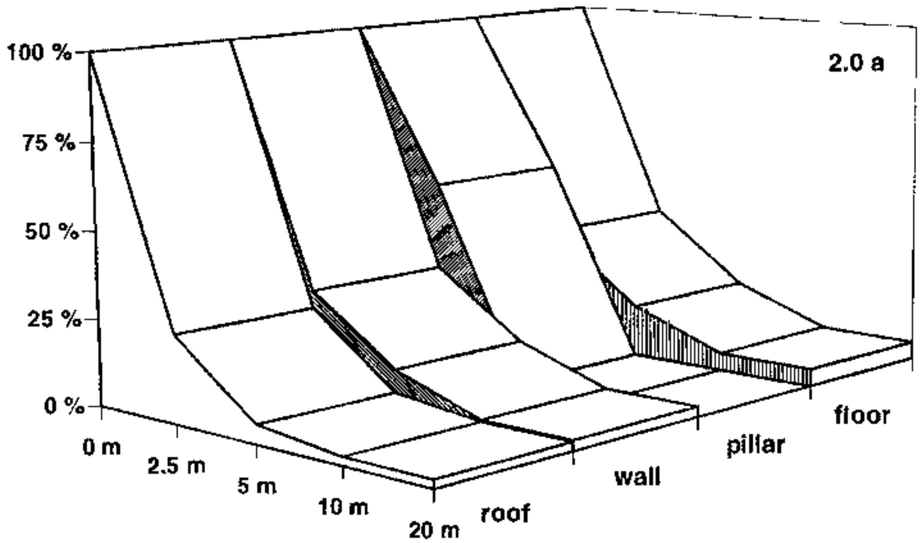

Fig. 4.2-38 Decrease of deformation rates with increasing depth in the cold area after two years of heating (drift outline = 100%)

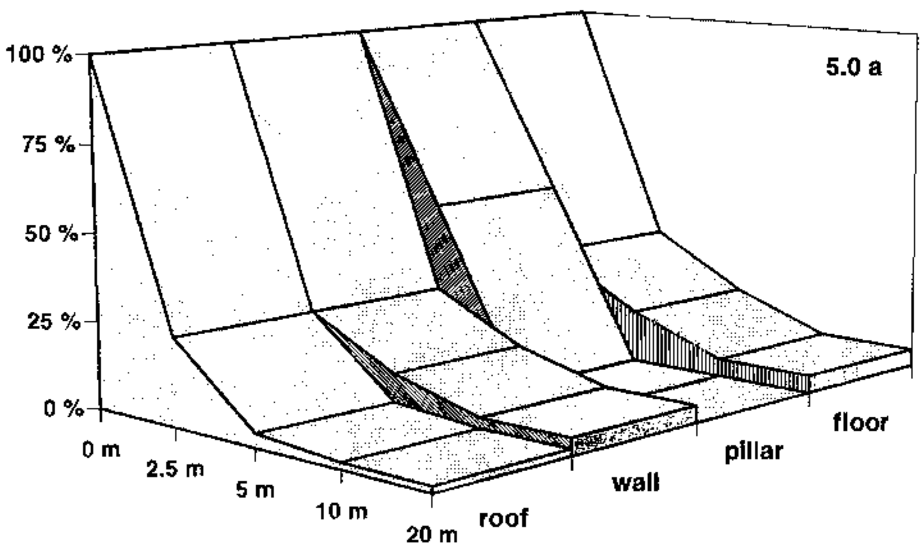

Fig. 4.2-39 Decrease of deformation rates with increasing depth in the cold area after five years of heating (drift outline = 100%)

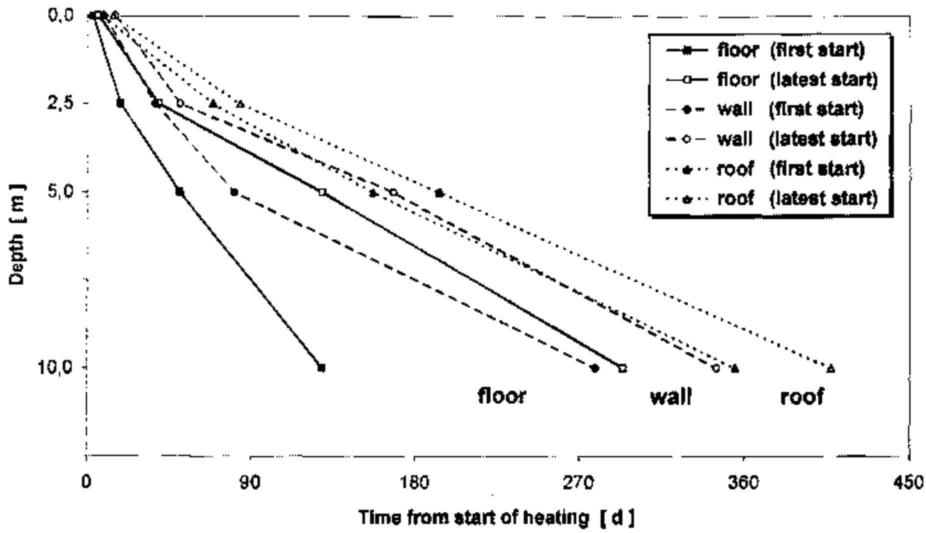

Fig. 4.2-40 Start of the accelerated deformation in the heated area

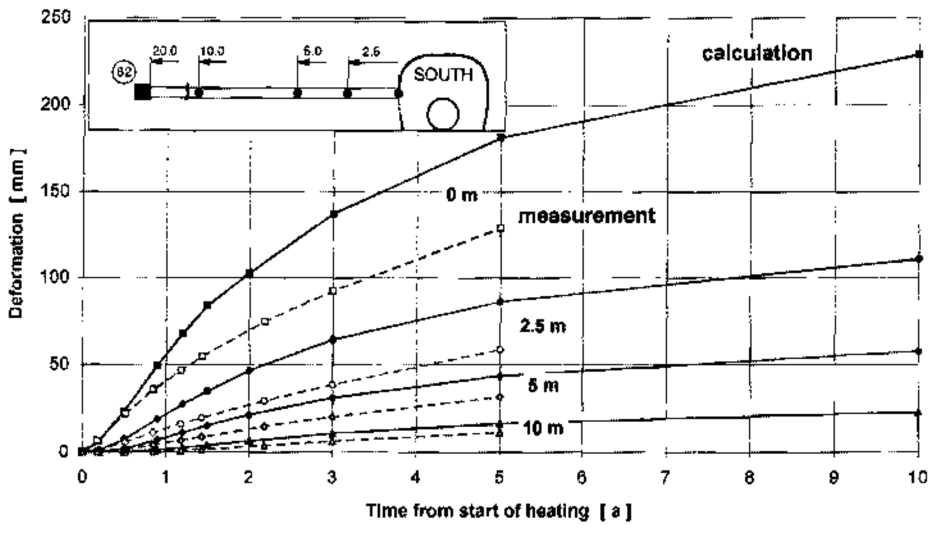

Fig. 4.2-41 Comparison of calculated and measured deformations beside the heated drifts (wall extensometer in section A)

In summary the heating causes a significant acceleration of the rock deformations around the heated area towards the test drifts. The closer the measuring points are located to the heater casks the earlier the deformation starts and the higher are the deformation rates.

Next to the heated drifts the deformation rates are decreasing again after two to three months indicating the beginning support by the backfill. Since that time the rates are continuously decreasing approaching the steady state creep. However, the time when that steady state will be reached cannot be estimated up to now.

Unlike the deformations next to the heated drifts the rates of the distant extensometers as well as the rates in the non-heated sections are still constant. An assessment of the future development of the deformations in these areas away from the heated drifts is not possible at the moment.

4.3 Pressure

4.3.1 Backfill Pressure

The increasing compaction of the backfill due to drift closure is creating a rising pressure between backfill and surrounding rock which improves the stability of the repository. The connection between backfill pressure and drift convergence is indispensable to the validation of numerical models. In the test drifts the backfill pressure is recorded by Glötzl type hydraulic pressure cells which are installed at the floor, at the roof and at the walls of the drifts. Measurements are carried out in the heated sections B, D1, D2 and G1 as well as in the non-heated section E1.

The pressure in the cold backfill is not affected by heating at first. The gauges in cross section E1 measure only a minor decrease in pressure of about 0.025 MPa. Approximately one year after the start of heating the pressure begins to rise slowly due to the gradual temperature increase in the non-heated sections in 1991. From 1992 onwards, the pressure development takes a seasonal course with a stagnating pressure in summer time. Since the end of 1994, the pressure in the northern drift rises faster than in the southern drift. Current values range between 0.10 - 0.16 MPa in the southern drift and between 0.13 - 0.17 MPa in the northern drift (Fig. 4.3-1).

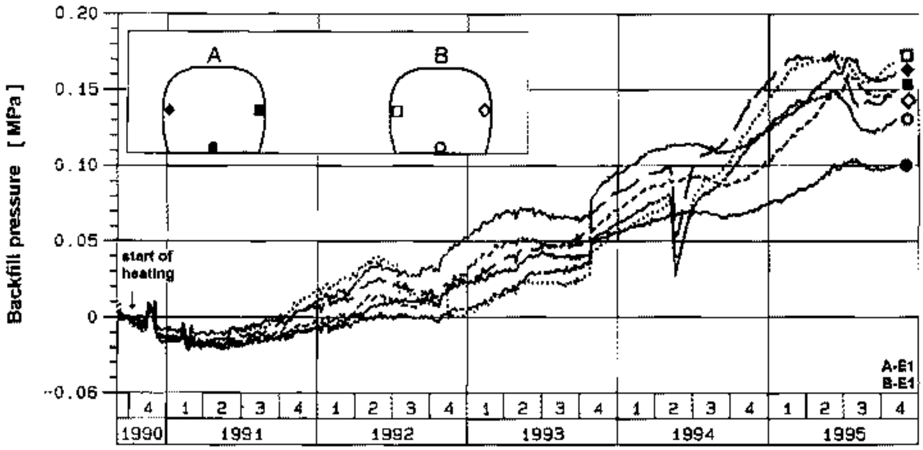

Fig. 4.3-1 Backfill pressure in the cold area (section E1)

In the northern drift the cold backfill has already obtained a higher rigidity. This is indicated by a slightly higher pressure increase up to now as well as by a distinct drop in pressure of 0.04 - 0.05 MPa in May 1994 after a 75 hour heater breakdown (Fig. 4.3-1). The short drop in heater temperature caused by the breakdown does not affect the temperatures in section E1. The short pressure decrease in the northern drift has to be attributed to the relaxation of the more rigid backfill due to thermal contraction. Another heater breakdown of 15 hours in June 1995 once again leads to an immediate drop in pressure of 0.02 - 0.03 MPa in the northern drift. This time the backfill in the southern drift reacts as well but with a delay of about six weeks and a lower pressure decrease of just about 0.01 MPa.

In the heated area the pressure cells at the walls measure an immediate increase in pressure after the beginning of heating. Pressure increase at the roof, however, starts not until three months after the heaters have been switched on. Since that time all the gauges at the walls and at the roof record a pronounced rise in pressure indicating the support by the backfill (Fig. 4.3-2). This observation is corresponding to the data of convergence measurements where the drift closure rate decreases about three months after the start of heating as mentioned above.

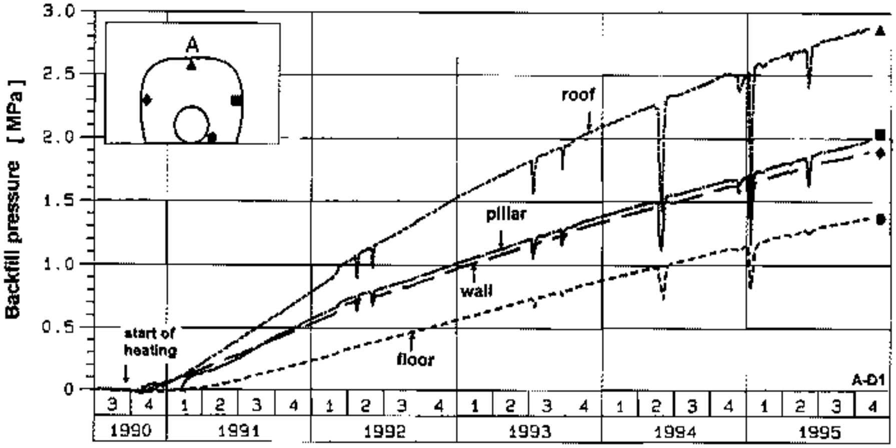

Fig. 4.3-2 Backfill pressure in the heated area (section D1)

Unlike the other gauges the pressure cells at the floor first register a minor decrease in pressure of about 0.025 MPa after the heaters have been switched on. Pressure increase at the floor starts not until six months after the heating has begun.

Since the beginning of 1991 most pressure gauges record a linear rise in pressure. Some short drops are due to short heater breakdowns resulting in a thermal induced relaxation of stress (Fig. 4.3-2). The response of the gauges to the interruption of the power output proves their correct function. While the breakdowns in June 1991 and August 1991 can hardly be recognized at a few measuring points at the roof and the walls, the failures in April 1992 and June 1992 cause significant stress changes at most gauges except for the pressure cells at the floor. The breakdowns in July 1993 and September 1993 are the first to be recorded by the gauges at the floor as well.

In May 1994, January 1995 and June 1995 further failures cause distinct drops in pressure at all pressure cells. The increasing sensitivity of the backfill to power failures in the course of time implies a rising rigidity of the backfill starting from its upper part.

About two years after the start of heating the rates of pressure increase are mostly decreasing. They will change to constant or increasing rates again as soon as drift convergence creates a significant increase in the rigidity of the backfill.

In the sections B, G1 and D1 a sudden pressure increase in March 1992 is caused by an overcoring of boreholes required for geophysical measurements in cross section G1. In the end of 1994 the previously steady pressure development is disturbed by the change of thermal power output due to the already mentioned problems at the heater control system.

Generally, the highest values of backfill pressure are observed at the roof, currently ranging between 2.5 MPa to 2.9 MPa in the southern drift and 2.2 MPa to 2.25 MPa in the northern drift (Fig. 4.3-3). In each cross section the pressure at the walls reaches about 50 % to 80 % of the pressure at the roof. Pressures at the walls amount to about 1.5 MPa to 2.9 MPa in the southern drift and 1.15 MPa to 1.8 MPa in the northern drift (Fig. 4.3-4 and 4.3-5). The values are always a bit higher at the pillar side. The pressures at the floor are ranging between 1.0 MPa to 1.85 MPa in the southern drift and 1.1 MPa to 1.45 MPa in the northern drift, corresponding to about 50 % to 65 % of the pressure at the roof (Fig. 4.3-6).

A few pressure cells record lower stress values either caused by an insufficient bond with the surrounding rock or a damage at the hydraulic pressure lines or due to local inhomogeneities in the backfill.

Usually, backfill pressures in the northern drift are reaching only about 70 % of the stresses in the southern drift. In cross section D2, however, the pressures in the northern drift are about 10 % to 50 % higher than in the southern drift. As described in the previous chapters, there are only little differences in the backfill compaction and convergence of the two drifts. Obviously, the differing stress values are a result of the varying local rigidity of the backfill.

The difference between the pressure at the bottom and the top of the backfill is caused by the heater casks which are working as hard inclusions in the less rigid backfill. The forces are concentrated at the casks what is leading to decreasing pressures in the backfill towards the drift floor.

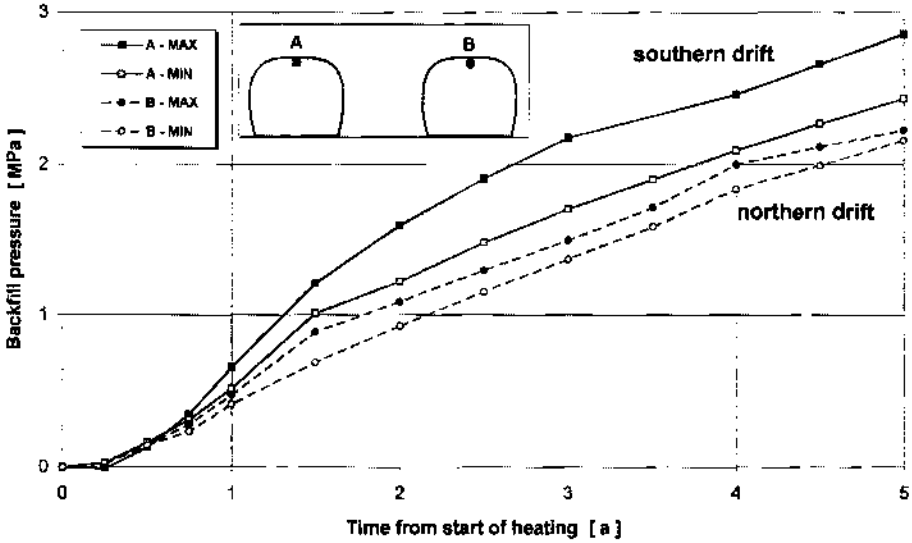

Fig. 4.3-3 Range of backfill pressure at the roof in the heated area

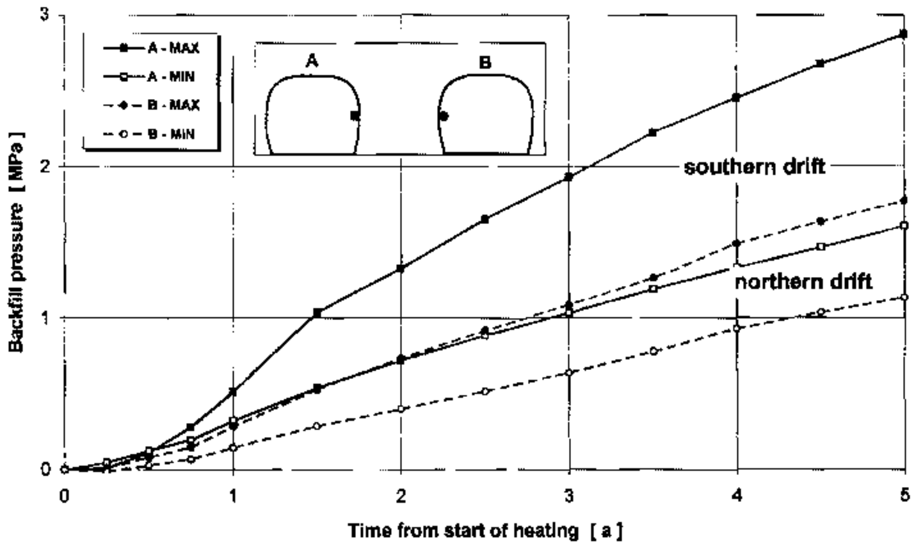

Fig. 4.3-4 Range of backfill pressure at the pillar in the heated area

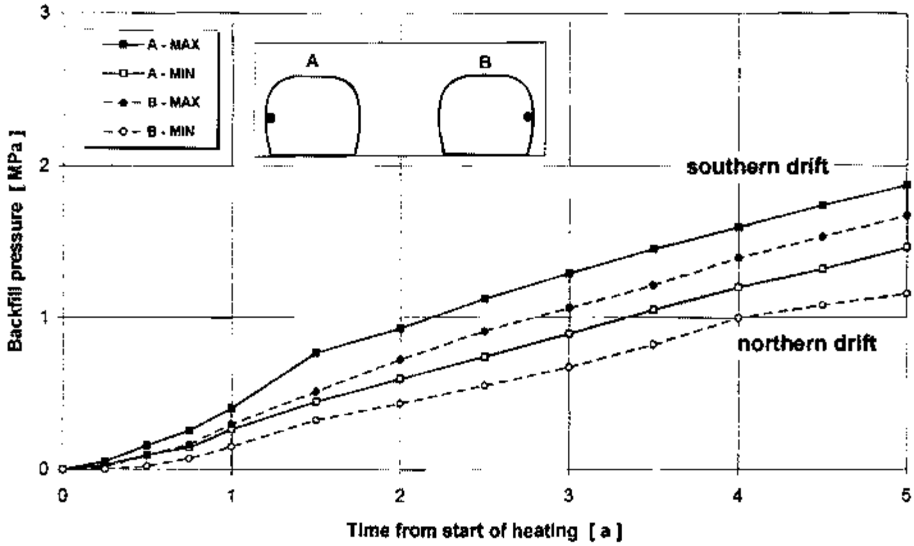

Fig. 4.3-5 Range of backfill pressure at the wall in the heated area

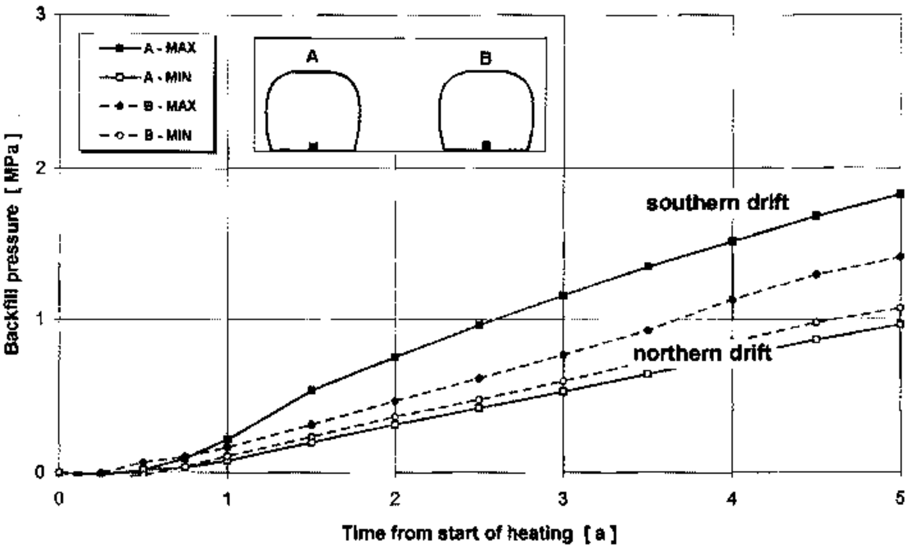

Fig. 4.3-6 Range of backfill pressure at the floor in the heated area

The comparison of measured and calculated backfill pressures is shown in Fig. 4.3-7 for section 1 around the central heaters and in Fig. 4.3-8 for section 3 around the heaters on the exterior /KOR 91/. As the pressure increase at the walls and at the roof starts earlier than expected, the measured values at these positions are higher in the beginning. The gauges at the floor, however, record almost the same pressure increase at first as calculated. Starting about one and a half year after the beginning of heating, the calculated rates of pressure increase exceed the measured rates considerably. After five years of heating the average backfill pressure is significantly lower than predicted. The difference is a result both of the differing drift convergence and the backfill description in model calculations as a compressible liquid with a homogeneous isotropic behaviour /KOR 91/.

Actually, after five years of heating the average backfill pressure at the roof of about 2.4 MPa has reached 20 % of the initial vertical stress, which has been estimated at about 12 MPa in the test field /SNE 94/.

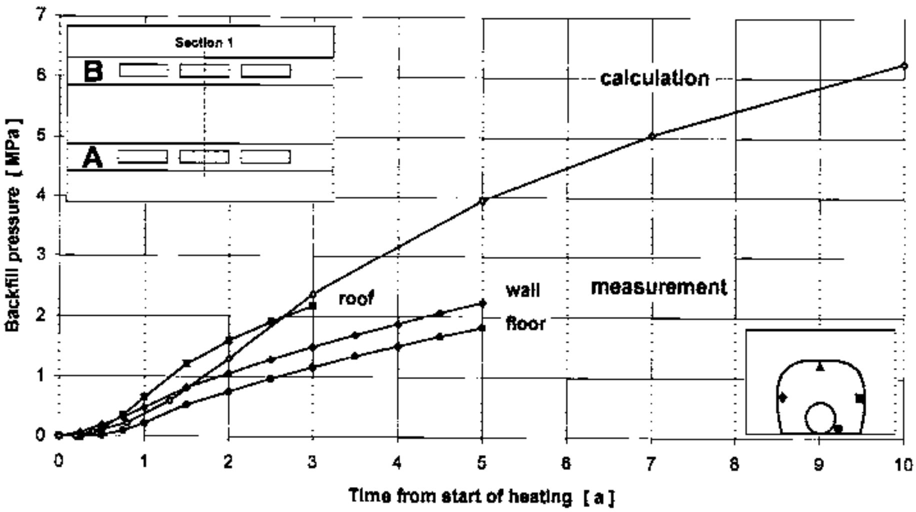

Fig. 4.3-7 Comparison of calculated and measured backfill pressure in the heated area (section 1 compared with section B)

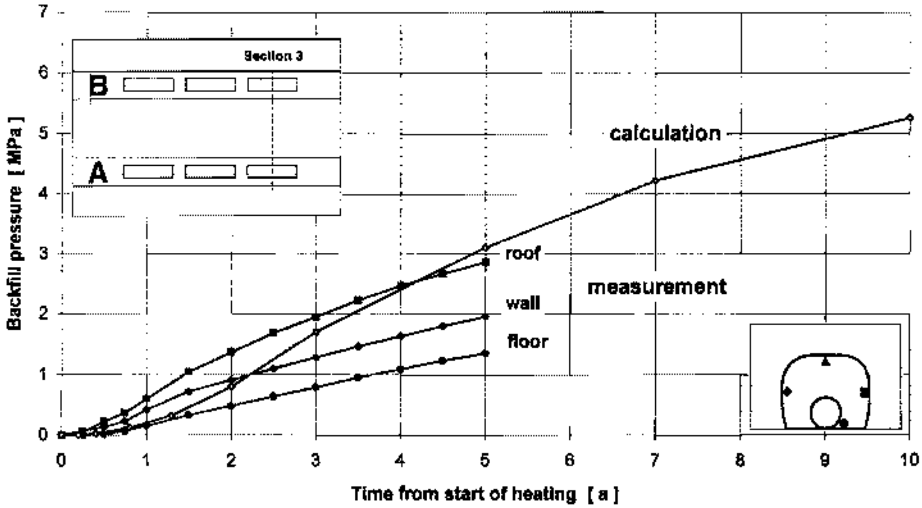

Fig. 4.3-8 Comparison of calculated and measured backfill pressure in the heated area (section 3 compared with section D1)

4.3.2 Rock Pressure

The initial state of stress in the test field has been determined by means of the overcoring method and by the measurement of stress release in slot cutting tests carried out by the BGR /SNE 94/. From these measurements an initial vertical stress of approximately 12 MPa is estimated /SNE 94/. Accordingly, the vertical stress in the test field is considerably lower than the expected rock pressure of about 18 MPa due to the overburden. The difference is caused by the mining activities in the salt mine above the test field.

For a determination of thermally induced stress changes due to heating seven stress monitoring units have been installed in vertical boreholes in cross section B. Five boreholes have been drilled from the observation drifts on the 750 m level. Two of them are located above the test drifts with a length of 45 m each. The other ones are extending 50 m into the pillar between the test drifts. With the gauges in these boreholes the effects of the excavation of the test drifts on the 800 m level are already recorded. Two additional boreholes with a length of 4 m each have been drilled below each test drift to measure the stress changes beneath the heated drifts.

The stress monitoring units are installed at a distance of 1.8 m to 3 m above the roof of each test drift and 0.8 m to 2 m above the level of the drift floor in the pillar. The devices below the test drifts are located in 2.2 m to 3.4 m beneath the drift floor.

Each stress monitoring unit is consisting of seven hydraulic pressure cells which are of the same Glötzl type used for the determination of the backfill pressure /SNE 93/. The gauges are installed with a varying orientation to record stress changes in all directions. Measurements are taken vertically, horizontally parallel, normal and at an angle of 45° to the drift axis as well as subhorizontally (45° inclined) parallel and normal to the drift axis /SNE 93/.

After the installation of the stress monitoring units the boreholes have been refilled by special concretes with a similar behaviour as the surrounding rock salt. Two of the monitoring units are embedded in Halliburton expanding cement, the other ones in saltcrete /SNE 93/.

The inclusion of the stress monitoring units in the host rock is improved by a subsequent injection of epoxy resin around the pressure cells via injection lines. The injection in February 1989 leads to a prestressing of the gauges in the saltcrete due to an injection pressure of 13 MPa to 17 MPa (Fig. 4.3-9 to 4.3-12). After the injection the pressure decreases again as the resin shrinks during its hardening. In the Halliburton expanding cement, however, prestressing has not been successful probably due to plugged outlets of the injection lines.

Rock pressure prior to heating

In March to April 1989 the excavation of the test drifts on the 800 m level causes significant stress changes which are recorded by the measuring devices installed from the observation drifts on the 750 m level. The vertical pressure above the excavated drifts is completely relieved dropping almost to null as the vertical loads are transmitted to the sides by arch action (Fig. 4.3-9). In the pillar between the test drifts, however, the vertical stress increases considerably (Fig. 4.3-11).

The stress changes in horizontal direction depend on the measuring direction of the gauges. Above the excavated drifts the horizontal pressure normal to the drift axis rises rapidly up to a magnitude of 11 MPa, whereas the horizontal stress parallel to the drift axis decreases distinctively (Fig. 4.3-9). An opposite behaviour is observed in the pillar, where the horizontal stress normal to the drift axis is reduced considerably due to the free expansion of the rock. Parallel to the drift axis, however, the pressure in the pillar increases after the excavation of the test drifts (Fig. 4.3-11).

The measurements in subhorizontal direction reveal similar stress changes as the vertical stress. Above the excavated drifts the pressure parallel to the drift axis is dropping almost to null. The subhorizontal pressure normal to the drift axis decreases distinctively as well (Fig. 4.3-10). In the pillar, however, the subhorizontal stress in both directions increases considerably (Fig. 4.3-12).

After the redistribution of the stress field due to the excavation activities the stresses change only slightly until the start of heating. The backfilling of the test drifts in the area around cross section B causes a small increase in rock pressure since June 1990.

The corresponding stress magnitudes can be taken from Fig. 4.3-9 to 4.3-12. Steady state conditions are still not reached when the heating starts in September 1990.

Rock pressure during the heating

Immediately after the start of heating most gauges record a significant rise in rock pressure of 1 MPa up to 5 MPa although the temperatures in the surrounding rock are still low. Generally, the elastic stress changes depend upon the respective measuring position.

In the pillar the thermally induced stress changes reach their maximum after two months (Fig. 4.3-11 and 4.3-12). The highest pressure of 13.5 MPa is registered in horizontal direction parallel to the drift axis. The subhorizontal stress changes are in the same order of magnitude. The lowest pressure increase is registered horizontally normal to the drift axis.

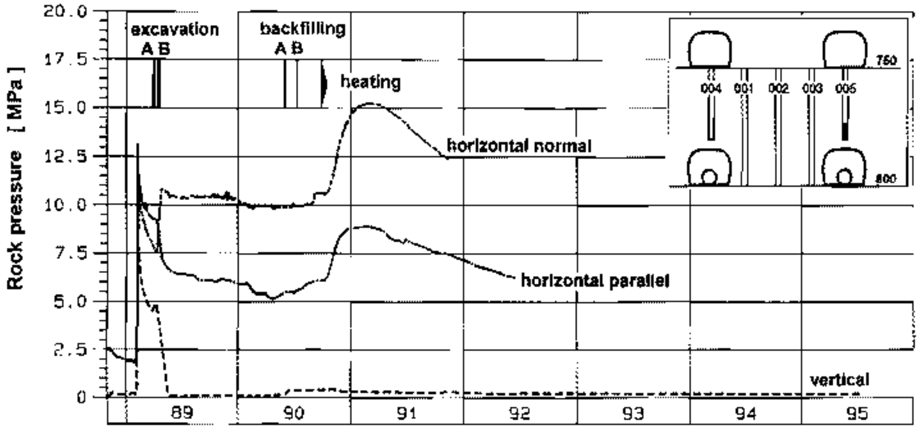

Fig. 4.3-9 Rock pressure above the heated drifts (section B)

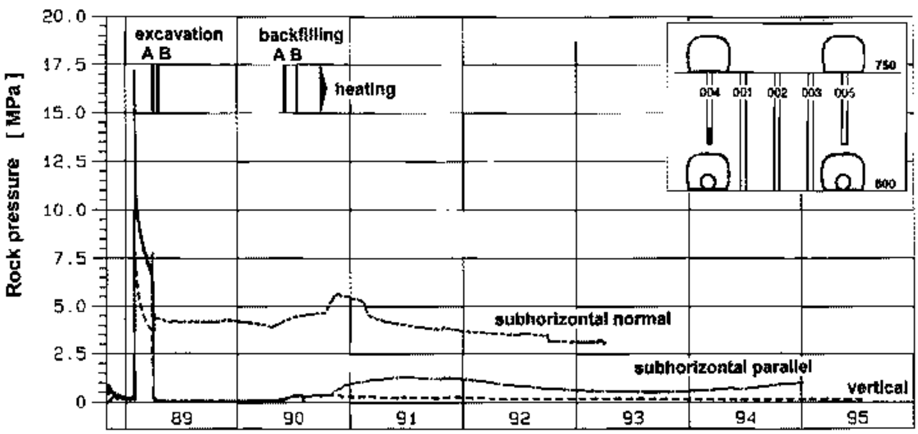

Fig. 4.3-10 Rock pressure above the heated drifts (section B)

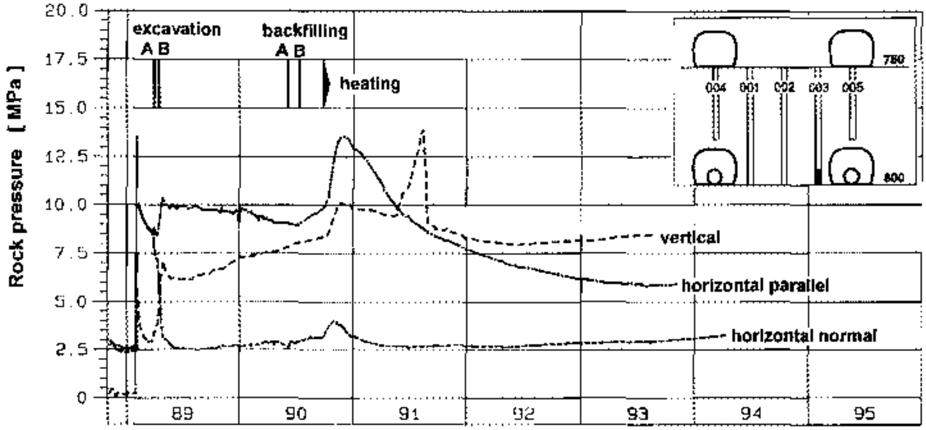

Fig. 4.3-11 Rock pressure between the heated drifts (section B)

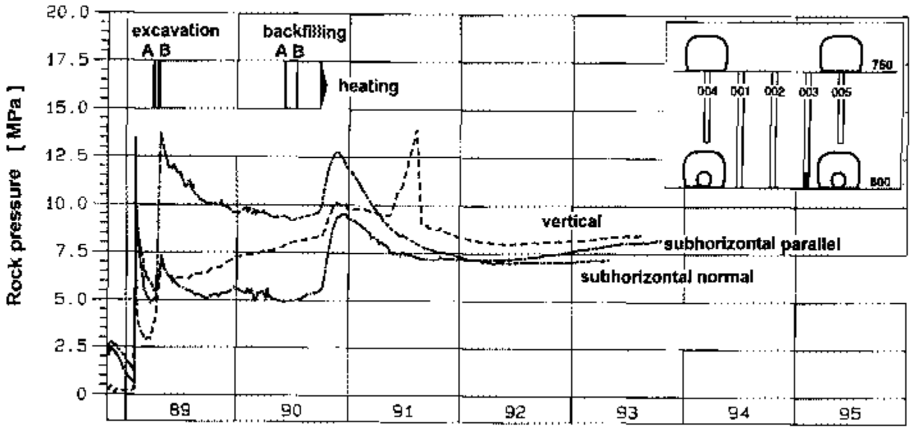

Fig. 4.3-12 Rock pressure between the heated drifts (section B)

Above the test drifts, however, the stress maximum is recorded three to five months after the heaters have been switched on with a maximum value of 15 MPa in horizontal direction normal to the drift axis (Fig. 4.3-9). The subhorizontal stress changes are much lower. The pressure rises slowly after the beginning of heating without a pronounced maximum (Fig. 4.3-10). The vertical stress above the test drifts is hardly affected by the heating. Only a minor pressure decrease of approximately 0.1 MPa is registered by the gauges.

The stress monitoring units in the floor beneath the test drifts are operating since July 1990. The stress changes show a similar behaviour as above the heated drifts. However, the elastic pressure increase in horizontal direction is more pronounced reaching up to 7 MPa (Fig. 4.3-13). About two to three months after the start of heating the maximum stress is attained. Due to the missing overburden the vertical stress below the drift floor approaches almost null. Like above the drifts the vertical stress decreases slightly after the beginning of heating by approximately 0.1 MPa.

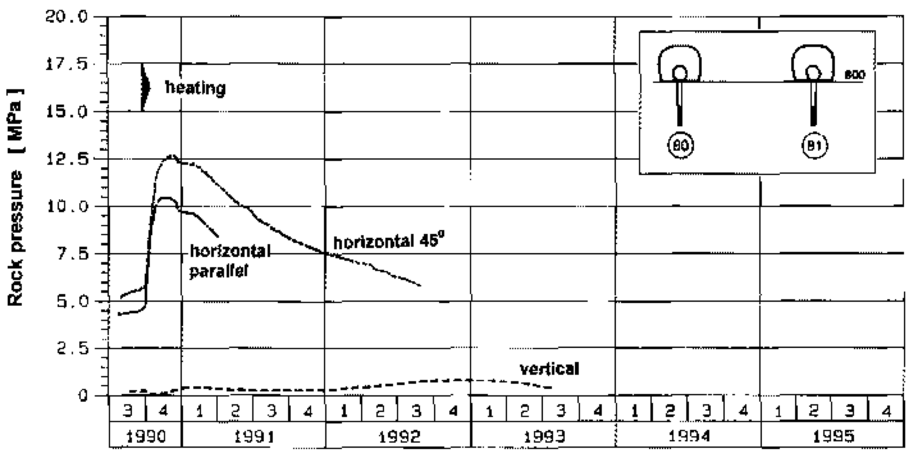

Fig. 4.3-13 Rock pressure beneath the heated drifts (section B)

Actually, the magnitude of thermally induced stress sometimes even exceeds the initial state of stress in the test field. The pressure peaks, however, are only a short-term effect. Subsequently, the rock pressure decreases again due to relaxation of the induced stress by creeping of the rock salt. The original state of stress prior to heating is approached again within two years. In the pillar the original stress values are already reached about half a year to one year after the beginning of heating. Afterwards some gauges even record pressure decreases below the original values. Occasionally, the pressure increases once again during the relaxation phase (Fig. 4.3-11). These pressure peaks, however, are only temporary phenomena as they are reduced again within a short time.

In the pillar the vertical and subhorizontal stress as well as the horizontal stress normal to the drift axis rise again since June 1992 (Fig. 4.3-11 and 4.3-12). At the same time the vertical stress beneath the drift floor increases a little (Fig. 4.3-13). The reason for this is the support by the backfill in the heated drifts which takes up an increasing part of the rock pressure.

The accelerated deformations around the heated drifts cause an increasing failure of the pressure gauges what will be dealt with in chapter 4.4.1. Especially the stress monitoring units beneath the heated drifts which are located right below the heater casks are involved at first. By 1995, almost all monitoring units have failed.

In July 1995, five additional boreholes which have been drilled from the observation drifts on the 750 m level in section B" are equipped with stress monitoring units of the same type. The additional gauges are replacing the failed devices in the pillar and above the heated drifts in cross section B. The monitoring units are embedded in special K-UTEC saltcrete. Up to now the gauges record a pressure increase up to 1.5 MPa which is still much lower than the prevailing stress. A subsequent injection of epoxy resin will be carried out soon to improve the inclusion of the stress monitoring units in the host rock.

The results of model calculations by Korthaus (1992) are summarized in Fig. 4.3-14 and 4.3-15. The development of rock pressure since the excavation of the test drifts is shown disregarding the small pressure increase due to the backfilling of the drifts.

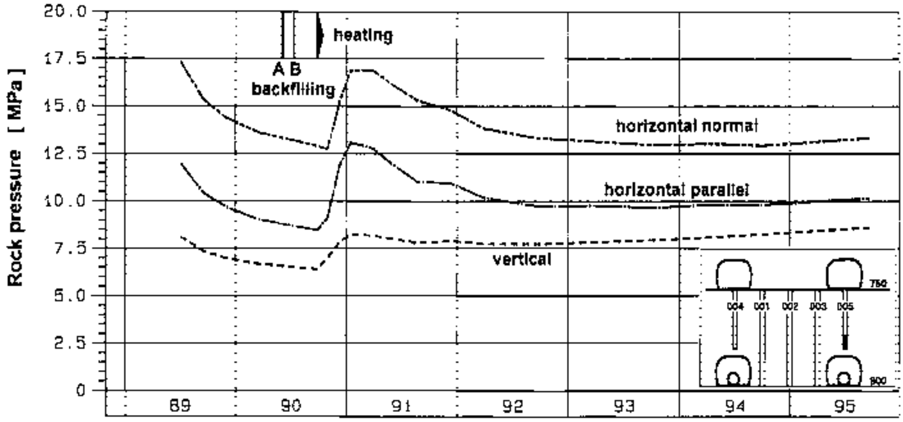

Fig. 4.3-14 Calculated rock pressure above the heated drifts (section B)

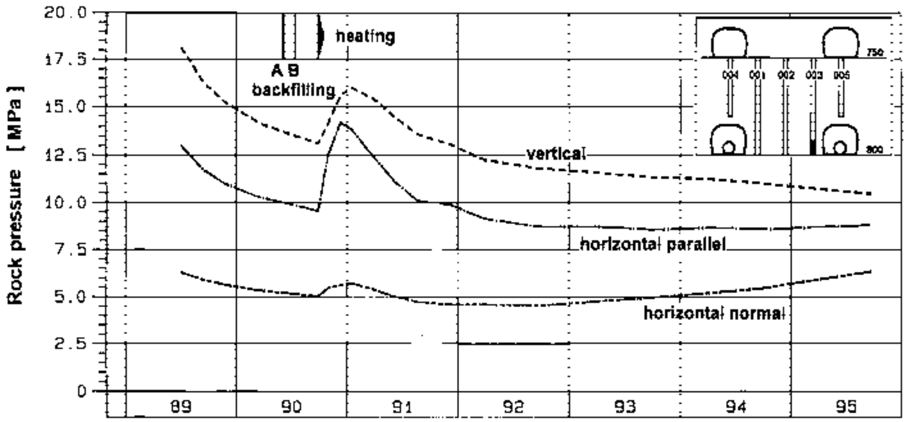

Fig. 4.3-15 Calculated rock pressure between the heated drifts (section B)

Above the test drifts the development of the horizontal stress corresponds quite well with the measurements even though the magnitudes of stress are different (Fig. 4.3-14 and 4.3-9). The horizontal stress normal to the drift axis differs by about 1 MPa from the recorded values, the rock pressure parallel to the drift axis by approximately 2 MPa. The vertical stress, however, is much lower than the calculated pressure of approximately 7.5 MPa. Unlike the calculations, no pressure increase is registered in vertical direction after the beginning of heating.

In the pillar the horizontal stress changes reveal an adequate coincidence as well (Fig. 4.3-15 and 4.3-11). The magnitude of stress normal to the drift axis is about 2 MPa lower than calculated. The horizontal stress parallel to the drift axis reaches almost the predicted values at first. Only in the phase of relaxation the difference increases. Again the vertical pressure is much lower than expected. When the heating starts the pressure still increases considerably as the vertical stress has not reached its final state yet (Fig. 4.3-11). The thermally induced pressure peak is not as pronounced as calculated for the vertical stress. After a relaxation phase of one and a half year the vertical stress increases again approaching the calculated values more and more.

Generally, the model calculations correspond quite well with the stress measurements with regard to the development of the stress changes. The differences in the magnitudes of stress are mainly a result of the constitutive law of rock salt which does not fit well enough.

In summary the heating causes a significant rise in rock pressure. The thermally induced elastic stress changes, however, are only a short-term effect. Subsequently, the rock pressure decreases again to the original state of stress prior to heating due to relaxation of the induced stress by creeping of the rock salt.

4.4 Reliability of the Measuring Systems

In the TSS test the measuring systems are operating under standard repository conditions. By that the reliability of the installed measuring equipment for the safety monitoring of a salt repository can be determined.

4.4.1 Failure of Gauges

The measuring equipment in the test field is exposed to extraordinary conditions. Both the accelerated deformations around the test drifts as well as the high temperatures put a lot of strain and stress on the gauges and the measuring lines. Consequently, an increasing number of measuring points fails since the beginning of heating as the measuring equipment is damaged. In the following the failures are dealt with for the different types of gauges.

Failure of temperature gauges

The temperatures in the test field are recorded by a number of about 750 resistance thermometers. When heating starts in September 1990, about 2 % of the gauges have already failed due to damages during the installation or in the preliminary phase.

About one year after the beginning of heating the failure quota of the temperature gauges starts to rise gradually up to 6.5 % in the end of 1995 (Fig. 4.4-1). Considering the large number of thermometers, this quantity is negligible and the measuring programme can be carried on without any problems.

The losses are occurring mainly in the heated sections where 82 % of the failures are observed. In the cold sections only 18 % of the defects are noticed. Closer examinations reveal that the troubles in the cold sections are all caused by damages at the measuring cables, whereas about 20 % of the failures in the heated area arise from defects at the gauges. The damaged thermometers are all installed next to the heated drifts up to a distance of 2.5 m from the drifts where the prevailing high temperatures cause the failure of the thermometers. About 80 % of the failures in the heated sections, however, are due to damages at the measuring lines which are squeezed together leading either to short-circuited or broken cables.

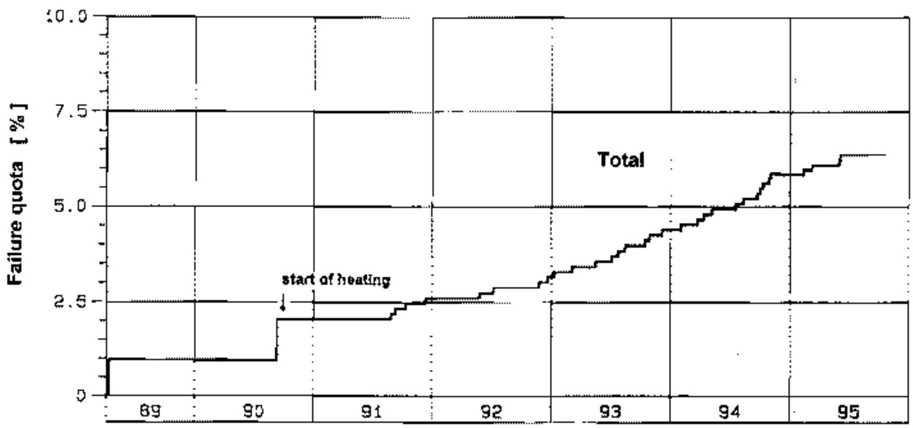

Fig. 4.4-1 Failure of temperature gauges

Failure of deformation gauges

The deformations in the test field are determined by specially designed measuring equipments which are assembled durably to be resistant both against the strain during backfilling and heating. The design proves to be successful as up to now no damages at the gauges are detected. The measuring lines, however, are the weak points of the measuring systems. Especially the multicore cables are affected by the accelerated deformations around the test drifts leading to an increasing number of failures.

After the start of heating the failure quota is quite low at first (Fig. 4.4-2). Since 1992, however, the quota increases considerably up to 34 % in 1994. A subdivision into the different types of gauges reveals only moderate percentages of failures for the drift convergence gauges and the extensometers in the cold sections (Fig. 4.4-3). The equipments measuring the backfill settling are still operating completely. The major part of losses is recorded for the extensometers in the heated area with a failure quota up to 75 % in 1994.

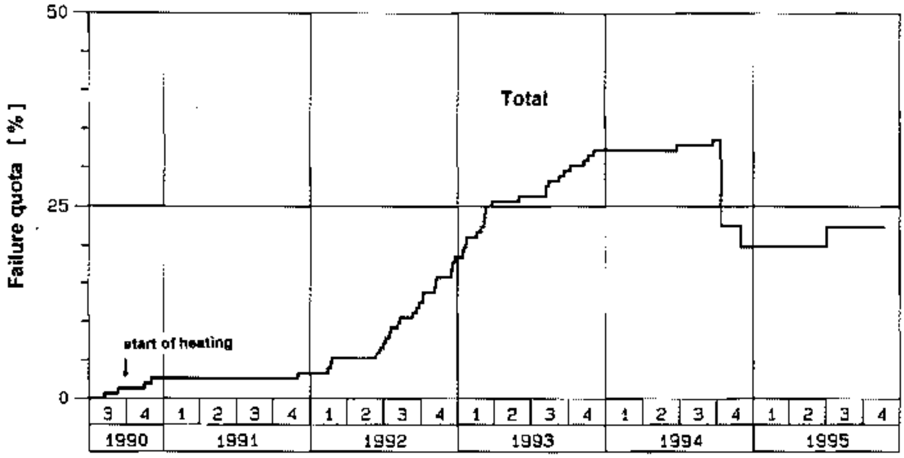

Fig. 4.4-2 Failure of deformation gauges

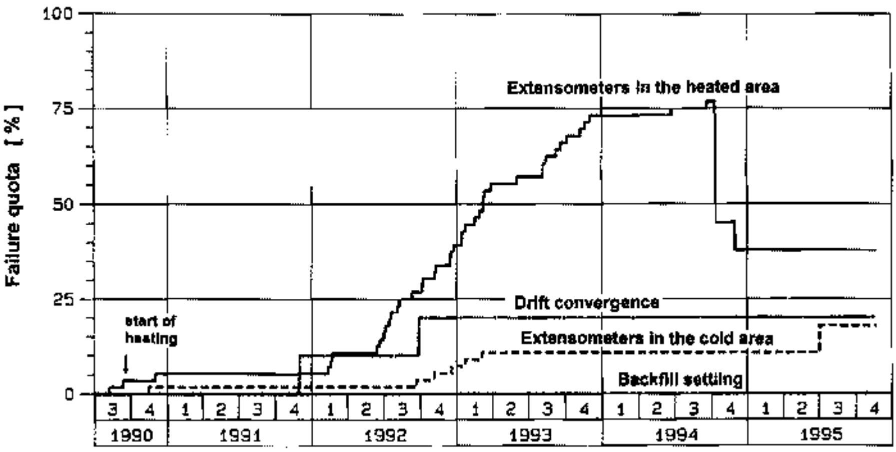

Fig. 4.4-3 Failure of different types of deformation gauges

An investigation of the defects carried out by the manufacturer turns out that almost all damages are affecting the measuring cables. About 30 % of the failures are caused by electrolytes inside the measuring lines. By this all gauges which are connected to the same multicore cable are set out of order one after the other. The majority of about 70 % of the failures, however, has to be ascribed to the squeezing of the cables which leads gradually to short-circuited or broken cores of the multicore cables.

A determination of the fault positions is feasible by means of a reflex analyzer device which operates by the impulse reflection method. Although the length of the measuring lines has not been determined precisely after their installation and the temperature increase after the beginning of heating causes deviations in the impulse reflections, an adequate assessment of the respective fault position is possible.

The examinations prove that 55 % of the failures are located in the cable ducts of both test drifts. Both cable ducts are arranged close to the roof of the drifts leading from cross section E2 to the exit of each drift. The damages are restricted to a certain area extending from cross section D1 up to a distance of 10 m to the east (Fig. 2-2). About 28 % of the faults can be assigned to positions inside the boreholes and 17 % to places in the cable slots in which the cables are laid between each borehole and the cable duct.

Obviously, the design of the multicore cables with diameters up to 16.6 mm is not suited for the heated area since they are protected unsufficiently against damages. The thin cables of the temperature gauges with a diameter of 4.4 mm, however, are less sensitive as they are presumably able to get out of the way of most of the deformations.

The large failure quota of extensometers in the heated area up to 1994 impedes the deformation assessment around the heated drifts considerably. Therefore, a replacement of the instrumentation in the heated area is carried out in 1994 by which the failure quota of extensometers is reduced to 38 % in the warm sections (Fig. 4.4-3). The total quota of failed deformation gauges decreases to 20 % (Fig. 4.4-2). The stated values are referred to the total number of gauges respectively which has of course increased after the installation of the additional instrumentation. By these measures the extensometer array in the test field is completed again as far as a further continuation of the deformation measuring programme is guaranteed.

The replacement extensometers are of the same type as the failed devices. As already described in chapter 4.2.4 the gauges are installed in additional boreholes which have been drilled both in horizontal direction from the observation drifts on the 800 m level and in vertical direction from the 750 m level. They are replacing the failed extensometers in the walls and the roof. A substitution both of the gauges in the drift floor and the horizontal instrumentation in the pillar is not feasible as these sites are not accessible any more.

Although the deformation measurements have been interrupted sometimes for a longer time, the results of the failed gauges are resumed immediately by the respective replacement extensometers proving their correct function (Fig. 4.4-4).

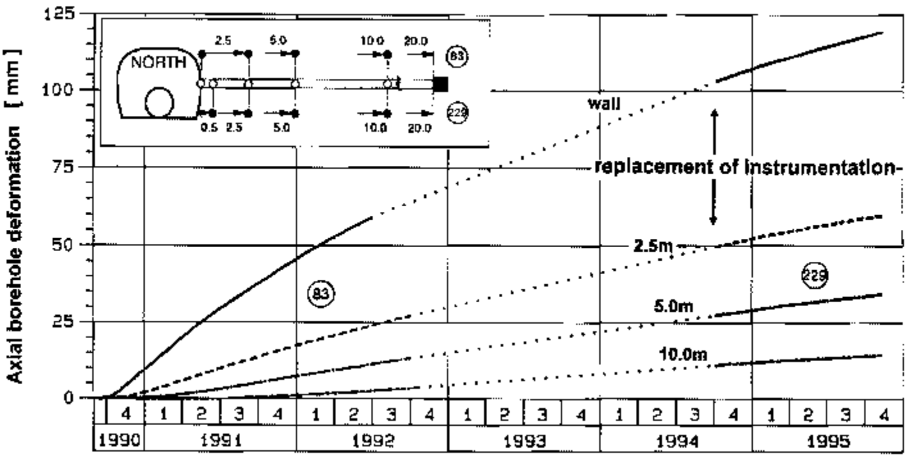

Fig. 4.4-4 Resumption of deformation measurements after the replacement of failed extensometer gauges

Failure of pressure gauges

The Glötzl type hydraulic pressure cells used for the measurements of backfill and rock pressure are proved to be reliable under severe conditions. Since the beginning of heating the durability of the hydraulic system under extraordinary temperature conditions is examined in the test field.

The first pressure cells are operating since 1988. They have been installed as stress monitoring units from the 750 m level as described in chapter 4.3.2. In 1989, about 14 % of these gauges have already failed (Fig. 4.4-5). After the instrumentation of the measuring equipment on the 800 m level in 1990, the total failure quota of all pressure gauges decreases temporarily to 9 %.

After the start of heating the failure quota increases gradually up to 56 % in 1995 (Fig. 4.4-5). The losses, however, are distributed unequally. While most of the pressure cells in the stress monitoring units have failed at that time, the failure quota of the gauges recording the backfill pressure reaches only 16 % (Fig. 4.4-6).

An investigation of the defects carried out by the manufacturer reveals that most of the stress monitoring units fail due to damages at the pressure cells. Only about 20 % of the failures are caused by defects at the hydraulic measuring lines. A certain classification of the faults, however, is not possible in any case as the common use of the return lines by all gauges of a unit excludes an examination of the pressure cells via the return lines.

Obviously, the pressure pads in the boreholes are affected considerably both by the temperature increase and the accelerated deformations after the beginning of heating. The monitoring units beneath the heated drifts which are located right below the heater casks are the most involved.

As already described in chapter 4.3.2 a replacement of the borehole instrumentation is carried out in 1995 from the observation drifts on the 750 m level. By this the respective failure quota is reduced to 43 % referring to the increased number of gauges (Fig. 4.4-6). The total quota of failed pressure gauges decreases to 39 % (Fig. 4.4-5). With the additional instrumentation the stress monitoring programme is almost complete again allowing the further observation of stress changes in the rock around the heated drifts.

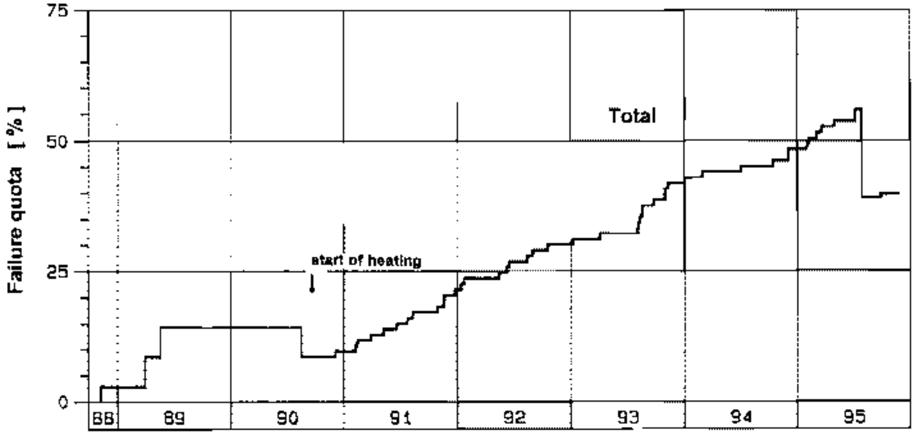

Fig. 4.4-5 Failure of pressure gauges

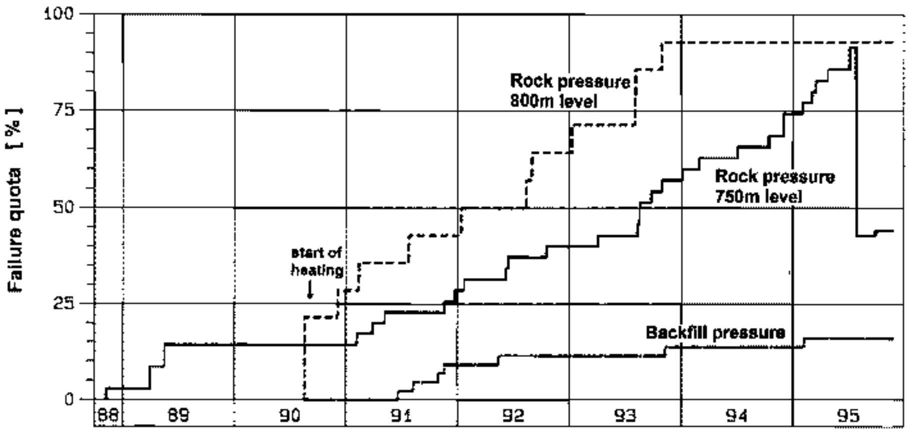

Fig. 4.4-6 Failure of different types of pressure gauges

Unlike the devices in the boreholes most of the gauges recording the backfill pressure are still operating. The continuation of the measurements is not affected by the few failures. The losses are all limited to the heated area. Closer examinations reveal that in contrast to the stress monitoring units almost all gauges in the backfill fail due to damages at the hydraulic measuring lines. Just in one case the failure is caused by a defective pressure cell. Obviously, the position in which the backfill pressure gauges are installed around the drifts is less exposed to deformations.

Actually, the failed pressure gauges are all concentrated on a few sites implying that the damages at the measuring lines are restricted to certain places. The distribution of the failures suggests the damages to occur in the cable slots in which the lines are laid between the measuring gauges and the cable ducts. The affected areas are located in cross section B in the northern and the southern part of the cable slots in the northern and the southern drift respectively. Another point is situated in the northern part of the cable slot in cross section D1 in the northern drift (Fig. 2-2).

Unlike the stress monitoring devices a fault classification of the backfill pressure cells is definitely possible as each gauge is equipped with a separate return line allowing an examination of the defect both via the pressure and the return lines. Furthermore, the separate return line enables a continuation of the measurements of gauges with damaged pressure lines. These gauges are operated manually using the return line as a pressure line. The damaged pressure line, however, is not able to take over the function of the return line as it releases the hydraulic medium. Though the hydraulic system is not closed any more, measurements can still be carried out.

4.4.2 Testing of Measuring Techniques

An important objective of the TSS test is to prove both the correct function of the measuring equipment and the long-term stability of the measurements under standard repository conditions. The testing of the measuring techniques is carried out by the subcontractor Deutsche Gesellschaft zum Bau und Betrieb von Endlagern für Abfallstoffe (DBE).

In each test drift both the cross sections G2 in the heated zone and $E1^{-1}$ in the non-heated area are equipped with test devices (Fig. 2-2). The examinations are carried out by means of three stationary convergence measuring equipments and six temperature gauges in each section which are of the same type as the other gauges of the geotechnical investigation programme /SNE 93/.

The results of these additional temperature and convergence measurements correspond to the respective measurements of GRS and are already included in chapter 4.1.1 and 4.2.1. They are described by DBE in detailed annual reports upon which this chapter is based.

The results of the temperature measurements by DBE are summarized in Fig. 4.4-7 revealing the average rates of temperature changes in the heated section G2 and the non-heated section $E1^{-1}$. In the heated area the rates decrease more and more after the rapid temperature rise in the beginning of heating. In 1993, the changes are almost null as the temperatures approach steady state conditions. The troubles at the heater control system in 1994 cause distinct temperature changes until steady state conditions are reached again in 1995. In the cold section $E1^{-1}$ the temperatures are still increasing even though the rates decrease more and more. The temperature peak before the start of heating in 1990 is caused by a rearrangement of the data acquisition (Fig. 4.4-7).

The accuracy of the temperature gauges is given by a maximum deviation of ± 0.24 °C to ± 0.36 °C regarding the absolute temperatures resulting in deviations of ± 0.33 °C to ± 0.52 °C for the stated temperature changes. Taking these values into account, almost the same temperature development is observed in both test drifts.

The convergence measurements carried out by DBE are summarized in Fig. 4.4-8. The average convergence rates are calculated from the data of each cross section. The rates are reflecting the temperature development including the deviant behaviour in the heated area in 1994 due to the faulty heater control system. The results have already been discussed in chapter 4.2.1 especially with regard to the differences between the two test drifts and the higher vertical convergence rates on the pillar side.

The accuracy of the convergence measurements amounts to ± 3.1 mm in the heated area and to ± 1.1 mm in the cold sections implying a maximum deviation of ± 1.9 % and ± 2.5 % respectively.

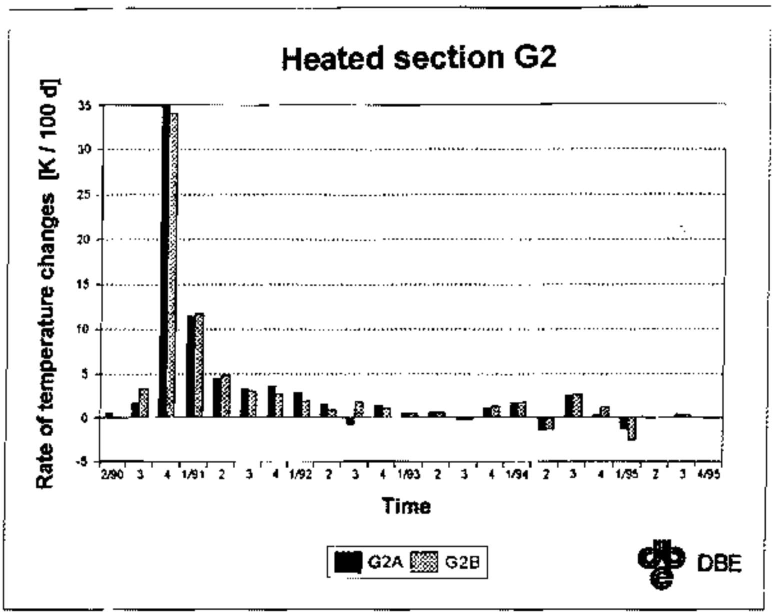

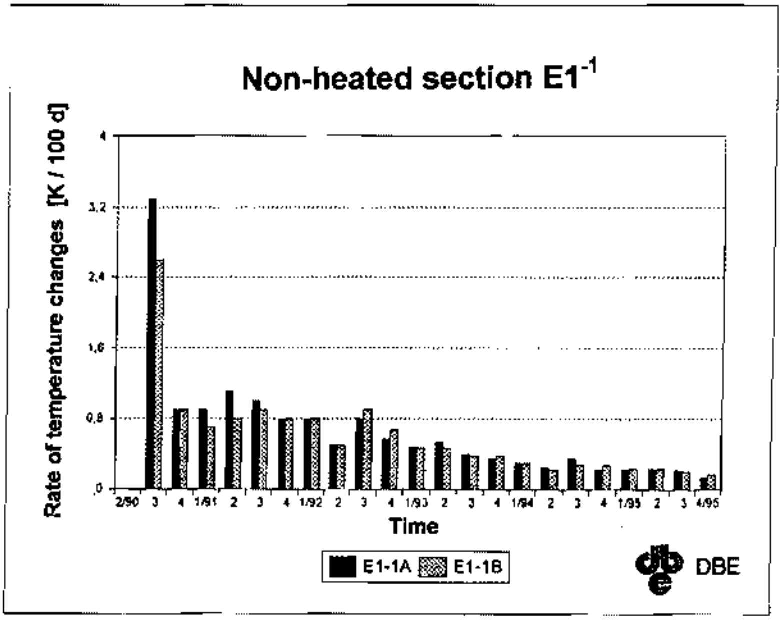

Fig. 4.4-7 Average rates of temperature changes in the heated area (section G2) and the non-heated area (section E1^{-1})

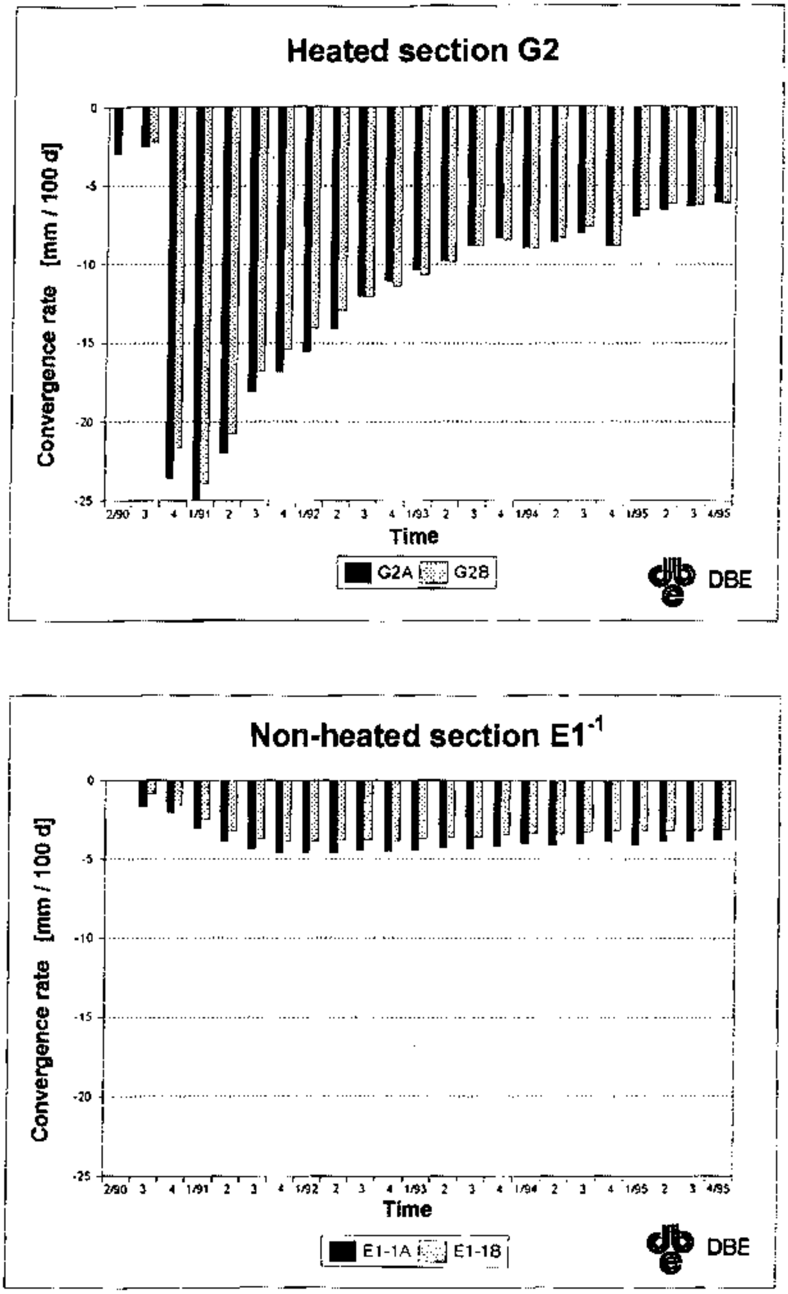

Fig. 4.4-8 Average convergence rates in the heated area (section G2) and the non-heated area (section E1^{-1})

After five years of heating most of the 24 temperature gauges of DBE are still operating without any problems. Two of the gauges have failed due to damages at the measuring cables. The cable of another gauge has been damaged but could be repaired successfully. The 12 convergence measuring equipments of DBE have been affected by only one failure up to now. This defect is caused by a damaged measuring cable as well what has already been discussed in chapter 4.4.1.

The heating of the measuring equipments in the test drifts up to a maximum temperature of 106 °C neither has an impact on their correct function nor on the long-term stability of the measuring data up to now. The data acquisition system fits the requirements as well. With the exception of the measuring cables which ought to have been protected better against damages, the designed measuring equipment proves to be successful.

5 In-situ Determination of the Backfill Compaction

To determine the compaction of the backfill material it is necessary to measure its density and porosity and their change in time. The aim is to estimate the time when the backfill is in a mechanical state comparable to the host rock.

5.1 Gravimetry

Usually, porosity is determined indirectly by measuring the backfill density of samples. All these methods depend on boreholes and samples. Their advantage is their accuracy and promptness but their results are strictly valid only for a small area. Moreover, sampling without disturbing is very difficult. Because of these disadvantages a method is required which allows an estimation of these parameters without disturbing the system. One non-destructive method for this purpose is gravimetry. This method allows an estimation of the mean bulk density of the rock from the knowledge of the disturbing body's geometry and its effect on gravity.

Estimations of the expected effect have shown that a normal field gravimeter does not have the required accuracy. Devices with a higher accuracy are used stationary in observations of the earth tides. Superconducting gravimeters have an extraordinary low drift compared to other gravimeters. In the last stage of the project it was shown that it is not possible to get results with the required accuracy from a mobile gravimeter. For this reason it was tried to measure and quantify the backfill compaction by measuring its effect on gravity from a fixed station.

A special advantage of the superconducting gravimeter is its compensation system which has no mass. A magnetic field is used to hold the sensor in a fixed position. This magnetic field is very constant over long times because the whole system is superconducting and the electric losses are extremely low. This leads to an extremely low drift and to a high accuracy compared to other gravimeters. Liquid helium is used for the necessary cooling.

The well known dip dependence of all gravimeters is compensated by two dip control devices.

After it was shown that the superconducting gravimeter can not be used for mobile measurements it was used as a stationary observatory in this stage of the project. It was tried to prove the compaction of the backfill and the rise of the salt dome. For this the drift of the gravimeter has to be known very well and a correction has to be carried out. Because these effects are very small the correction is very demanding and takes a lot of time. These investigations were done by the Institute for Geophysics of the TU Clausthal.

The long and aperiodic drift is of extraordinary importance because it possibly contains not only instrumental effects but also small changes in gravity according to changes in the rock density. To determine the drift the different physical signals have to be analyzed or computed. These are especially:

- the earth tide signal
- the air pressure correction
- the polar motion.

As one result of this work a correction for the air pressure effect could be estimated. An exact correction of its impact on the gravity recordings is not possible at this time. Several groups are working on this problem worldwide.

The determined drift (Fig. 5-1) shows an exponential decay at the beginning of the recordings which is typical for most gravimeters of this type. This is due to the gravimeters construction and negligible for later times. The longperiodic drift is approximately 13μGal/a which is very small. For a determination of the salt dome rising the gravity gradient at the observation location is required in addition.

For the determination of the gravity gradient at the observation location measurements with two gravimeters were taken by the Institute for Geophysics of the TU Clausthal. At four different points around the superconducting gravimeter the changes in gravity between two different levels were measured. The determined gradient is 210.94 μGal/m. With this gradient the recordings of the superconducting gravimeter can be related to changes in height and compared with a geodetic survey nearby.

Fig. 5-1 shows the separated long term variation of the gravimeter and the nearby measured vertical motion of the saltdome. From this diagram it is clear that the real long term drift of the gravimeter is 48 μGal in three years. Because this drift is higher at the beginning of the recordings than at the end this superconducting gravimeter is clearly superior to other gravimeters. On the other hand even this small drift is not sufficient to monitor changes in the backfill density. Therefore the superconducting gravimeter is not suitable for this purpose.

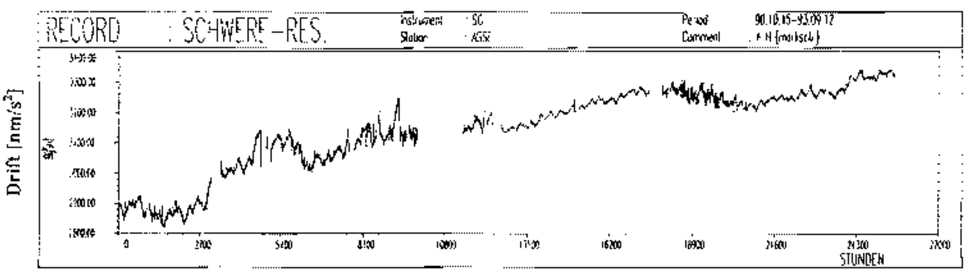

Fig. 5-1 Long-term drift of the superconducting gravimeter

5.2 Radiometry

The density determination with radiometric γ-γ-borehole devices is successfully applied in worldwide measurements. It works by placing a source of γ-radiation in the borehole and counting the scattered radiation at different distances from the source. The counted rate of γ-impulses depends on the density of the electrons in the surrounding material which for natural rocks is approximately proportional to the bulk density. As the rate of γ-impulses is counted at different distances from the source the bulk density at different distances from the borehole can be estimated.

For the observation and monitoring of backfill compaction the knowledge of the absolute density is important. The required calibration of the density probes is a problem which is solved only in approximation by measurements in calibration areas where the density is well known and in the same order as in the backfill material.

For the in-situ measurements of the backfill density with a γ-γ-borehole probe the same boreholes as in the former stage of the project were used /SNE 93/. The boreholes are extending from the 750 m level into the test drifts on the 800 m level. They are 52 m long and 56 mm in diameter. Because of the failure of the casing in the heated area in late 1991 the original plastic casing had to be replaced by a new steel casing.

In total six boreholes ($\gamma\gamma$18 - $\gamma\gamma$23) were drilled. The boreholes $\gamma\gamma$18 and $\gamma\gamma$19 are passing through the northern test drift in the non-heated sections E1 and E2 respectively. The boreholes $\gamma\gamma$21 and $\gamma\gamma$22 are passing through the heated section G1 in the southern and northern drift respectively. The boreholes $\gamma\gamma$20 and $\gamma\gamma$23 serve for an additional check of the surrounding rock salt. Because of logistic problems the borehole $\gamma\gamma$20 was not part of the measuring program in the last years.

In the sections passing through the test drifts the boreholes in the non-heated area ($\gamma\gamma$18 and $\gamma\gamma$19) are cased with a carbon enhanced plastic casing. Since these casings could not stand the pressure of the rock in the heated area of the boreholes $\gamma\gamma$21 and $\gamma\gamma$22, they were replaced by steel casings over the whole length of the boreholes in March 1992.

Because of the required high accuracy of the absolute density values the calibration of the γ-γ-probes is a problem. By means of calibration bodies with a bulk density comparable to the expected densities in the backfill it was tried to determine the impact of the different casings on the counted rate. According to informations of the contractor BPB Instruments Ltd. & Co. GmbH, in spite of all efforts the accuracy of the absolute values is much less than one of the relative values.

The measurements were carried out by BPB Instruments Ltd. & Co. GmbH. The scattered γ-radiation was measured at different distances from the source ("short" and "long" spacing) with a non-directed (DD2) and a directed (DD3) borehole device. The directed measurements allow to estimate the impact of the casings roughness on the counted rate. In this case, however, the required corrections could be neglected.

The values were digitally recorded on disks in the international LAS-format. This allows an online check and an easy application of PC-based programs for the further presentation and interpretation. The spacing between two records is 0.01 m. The resolution of the density values is 1 kg/m^3.

During this stage of the project (1993 - 1995) six measurements in approximately half year intervals were carried out.

Non-heated area

The measurements in the non-heated area are carried out in the boreholes $\gamma\gamma$18 and $\gamma\gamma$19. As an example the recorded density values (short and long spacing) and the calibre logs are shown in Fig. 5-2. The values for borehole $\gamma\gamma$19 are similar. The intact rock salt above the test drifts shows a density of approximately 2000 kg/m^3 which is slightly lower than the real density of 2200 kg/m^3. This deviation is caused by the calibration procedure. Because the probes are calibrated in boreholes with casings the measurements in the uncased part of the borehole $\gamma\gamma$18 give results which are too low. In the small area above and below the test drift where the casing reaches into the intact rock the probes show the correct density value of 2200 kg/m^3.

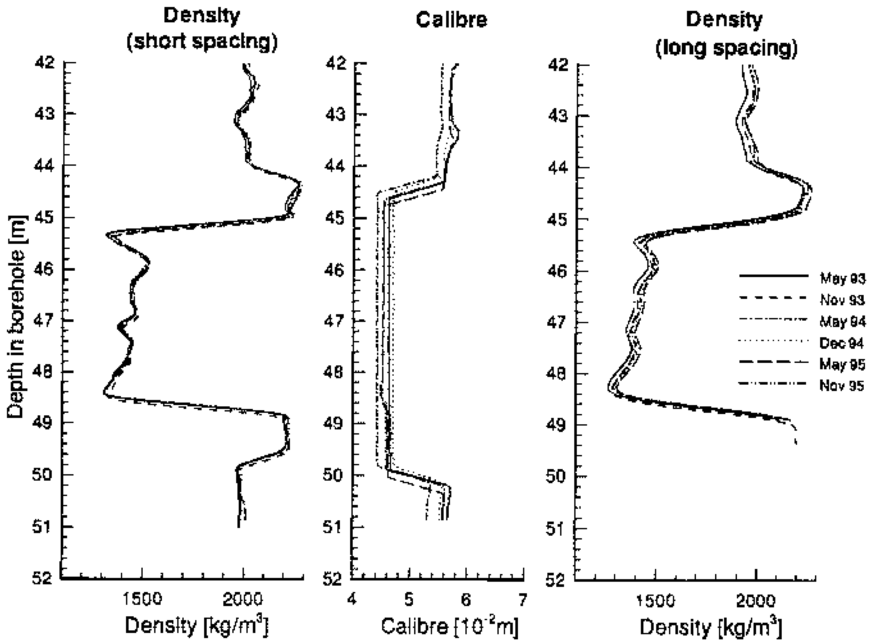

Fig. 5-2 Density variation in the non-heated area (section E1)

At the top of the test drift the density drops to 1200 kg/m³. This very low density could be caused by a loosened zone around the casing. Then the density increases sharply to over 1500 kg/m³. Towards the bottom the density decreases again to values between 1200 kg/m³ and 1300 kg/m³. This general trend of an increasing density towards the roof is caused by the slinger technique which was used for the backfilling of the test drifts. Because the coarser grain fraction was falling faster than the fine grains the grade of sorting is high on the bottom of the drifts and decreases towards the top. The porosity and therefore the density depend on the grade of sorting. A high grade of sorting implies a high porosity and a low density. Therefore the increasing density values towards the top are caused by the decreasing grade of sorting.

Over the years the curves do not change very much but all values increase slightly in time due to the compaction of the backfill. With the density of rock salt (ρ_{salt} = 2160 kg/m³) it is possible to estimate the related porosity $\Phi = 1 - \rho_m / \rho_{salt}$ where Φ is the porosity of the backfill, ρ_m the measured density and ρ_{salt} the density of rock salt.

In Fig. 5-4 the measured compaction and the related porosity in the backfill are shown for the non-heated and the heated area. Compared with the results of the geotechnical estimations of porosity these values are lower. This could be due to the already mentioned difficult calibration procedure of the γ-γ-probes. Another reason is that the geotechnical estimations compute a total porosity over the whole drift. The density values from the γ-γ-measurements, however, are only representative for a small area around the casing (about 1 - 2 dm) and this area could be disturbed e.g. by the drilling process.

Heated area

The measurements in the heated area are carried out in the boreholes $\gamma\gamma$21 and $\gamma\gamma$22. In Fig. 5-3 the results of the short spacing density logs are shown for the different measurements. As the original plastic casings were replaced by continuous steel casings in March 1992 the calibration steps at the top and bottom of the drifts are missing. In spite of the same casing the curves from the boreholes show a very different character. The overall characteristics of the curves do not change very much in time but are shifted towards higher densities due to the compaction of the backfill.

The logs of borehole $\gamma\gamma$21 do not show the low density at the top of the drift which is characteristic for a loosened area. This favours the assumption that the gap at the roof is been closed soon after the start of heating. But similar to the boreholes in the cold area the density decreases towards the bottom of the drift which is again explained by the separation of the backfill during its emplacement in the test drifts.

Compared to the boreholes in the cold area the increase of the density in time is much faster (Fig. 5-4). The average density increases from approximately 1400 kg/m^3 in May 1993 to approximately 1520 kg/m^3 in December 1994. The rate of this increase is nearly constant and at the moment there is no hint of an asymptotic approaching of the final density.

In contrast to borehole $\gamma\gamma$21 the logs of borehole $\gamma\gamma$22 in the heated area show a completely different characteristic (Fig. 5-3). The curves show an increasing density towards the bottom of the drift. This trend, however, is caused by numerous local extreme values. Before the replacement of the plastic casing the logs of this borehole were the same as in borehole $\gamma\gamma$21. During the replacement of the casings the pressurized air which was used as a flushing agent had a large impact on the surrounding area.

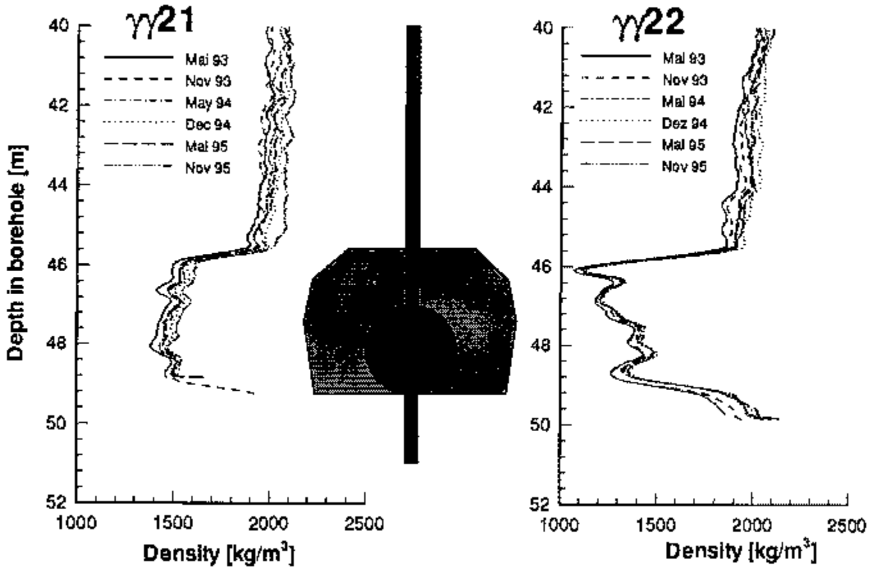

Fig. 5-3 Density variation in the heated area (section G1)

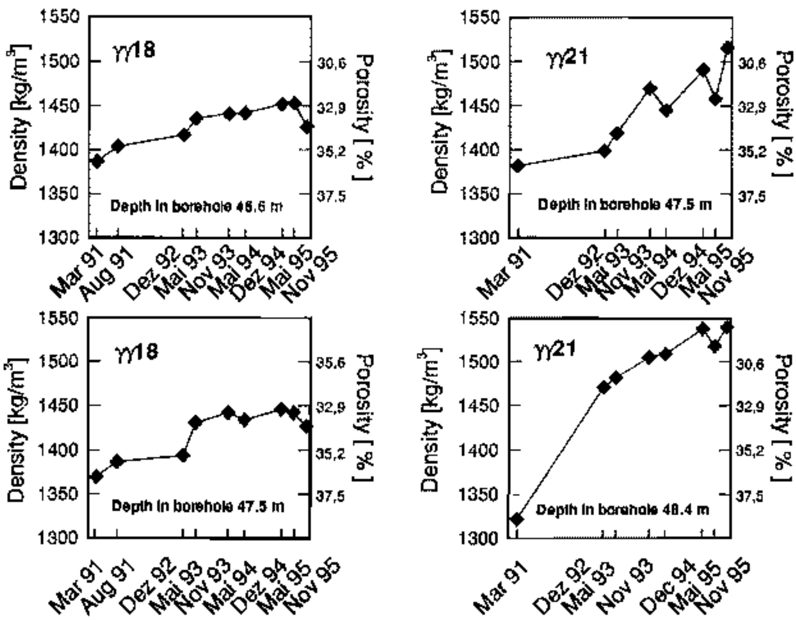

Fig. 5-4 Compaction of the backfill in the non-heated area (γγ18 in section E1) and the heated area (γγ21 in section G1)

The trend to higher densities with time is the same as in borehole $\gamma\gamma$21 and much more pronounced than in the boreholes in the cold area.

The γ-γ-method was successfully applied for the density determination in the backfill material. The required calibration of the probes for the determination of absolute density values and the quantification of the influence of the casing is a problem which is only partly solved by calibration bodies.

The results show clearly that with the slinger technique used for the backfilling of the test drifts the aimed high density is not achieved. This technique produces a separation of the different grain fractions which implies a heterogeneous spatial density distribution being conserved during compaction.

The rate of compaction in all areas is lower than expected. A steady state with densities comparable to the intact rock is not predictable even after five years of heating.

5.3 Sonic Measurements

An important parameter for the petrophysical characterization of the backfill is the porosity. This parameter can only be determined by measurements of the grain and bulk density. A parameter which is sensitive for changes in density is the acoustic velocity. This effect is used in standard to estimate porosity with borehole probes. A pilot test on crushed salt under pressure confirmed the relation between density / porosity and acoustic velocity and showed that small changes in density could be observed /SNE 93/. After the successful completion of these pilot tests the achieved experiences were used to design an in-situ experiment for recording the spreading of the acoustic wave field in the backfill and for relating the different results to the change in density. Because of the low temperature resistance of the equipment the experiment was only feasible in the cold area. As it is seen from the γ-γ-measurements in this area the compaction rate and therefore the change in density is very low. Moreover only compressional waves could be recorded because a suitable source of shear waves was not available.

According to the high grade of loosening of the backfill the attenuation of seismic waves above 10 kHz is very high. Since signals with high frequency are necessary for the exact determination of small time intervals this attenuation limits the expressiveness of the results.

For the determination of the velocity of compressional waves five experiment sites were designed. Each site consists of a piezoelectric source which radiates a short acoustic impulse and a piezoelectric receiver which converts the impinging waves to electric signals which are amplified and digitally recorded. The distance between source and receiver is 200 mm. Both components are mounted on a metal frame. For the acoustic isolation of the piezos a layer of plastic is placed between the piezos and the frame. The required cables for the source and the receiver are placed in pipes running through the backfill and are connected with the source generator and the transient recorder for each measurement.

The acoustic source is a piezoelectric crystal which is excited with its resonance frequency. This frequency is about 33 kHz. The excitation with the resonance frequency is advantageous because of the higher release of acoustic energy. The attenuation of the vibration is achieved by sending an adjustable double impulse. The signal generator is self designed and is specially adjusted to the used piezoelectric crystal.

For the receivers commercial accelerometers of Piezotronics (PCB) (type: 308B02) are used. Their resonance frequency is between 29 kHz and 31 kHz. They are equipped with an internal amplifier. Up to approximately 10 kHz the output voltage is proportional to the acceleration. Above 10 kHz up to the resonance frequency the sensitivity increases more than proportional with frequency. For protection against the rising backfill pressure the receivers are coated by steel. The electrical output is amplified again externally and stored with the input signal on a digital transient recorder.

The used recorder is a signal-memory-recorder with four channels. This device stores the signals digitally in CPM-format on disks. The maximum sampling frequency is 454 kHz which means a maximum accuracy in time of $2.2 \cdot 10^{-6}$ s. The travel time can be determined directly on the screen.

Each of the experiment sites consists of the metal frame on which the source and receiver are mounted. Overall five sites in different levels in the backfill were constructed. The first location is 0.35 m above the drift floor. The four other sites follow in 0.70 m distance in height each.

In the actual stage of the project six measurements were conducted. Because of the loose backfill and the implied high attenuation of the compressional waves most of the energy travelled along the metal frame in spite of several protective measures as plastic isolation of source and receiver from the frame. For this reason no measurement of the travel time with the required accuracy could be obtained. However, the change in the properties of the backfill material could at least be monitored according to the change of the received signal in the frequency domain. With progress in time the received amplitudes increased and the frequency characteristic was shifted towards lower values. This demonstrates the compaction of the backfill. It was also tried to quantify these results by defining a relative quality factor but it failed because of the poor quality of the signals.

The dependence of the transfer function of acoustic waves on the rock porosity is well known and was successfully demonstrated for the backfill material in a pilot test. But the high porosity of the backfill material even after five years of compaction causes many experimental problems. This leads to the conclusion that with the current configuration of the experiment only qualitative statements concerning the state of the backfill compaction can be made.

6 Gas Release in the Backfill

6.1 Concentration of the Gas Components

The Staßfurt Halite of the Zechstein Series is mainly composed of halite. Additionally, it contains minor and trace minerals, such as polyhalite, anhydrite, kieserite, clay, carbonates and bitumen. Geochemical analysis of rock salt samples taken from the backfill of the test field indicate that the major components are halite (92.7 to 96.3 wt%) and anhydrite (4.0 to 7.0 wt%). Gases and brines are trapped in inclusions so called "negative crystal" cavities within the crystal or adsorbed to the crystal boundaries.

As a result of the drift mining or the borehole drilling as well as by elevated temperatures or gamma radiation due to the disposed radioactive waste, the equilibrium in the salt dome is disturbed leading to the release of volatile components and the decomposition of thermally or radiolytically unstable minerals.

One of the principal purposes of the demonstration test is the determination of gas generation and release from the backfill as a result of thermal desorption, thermal decomposition and corrosion of the casks. For that purpose 24 glass filters are attached to the surface of the casks and to the roof of the drifts covering areas with different temperatures. In the northern drift four additional glass filters are installed at the floor next to the central cask. The gas samples are taken from measuring points in the sections A, B and C of the test drifts (Fig. 2.2). From each glass filter a teflon tube is leading to a valve at the entrance of the drifts.

Gas sampling started already on September 4^{th}, 1990. Sampling from the pore volume of the backfill is done by a membrane pump which is connected to the corresponding valve of the teflon tube at the entrance of the drifts. About 400 ml of gas are collected into a special gas bag.

The geochemical analysis is performed in an underground laboratory using gas chromatography with specific columns and detectors like flame ionization detector, thermal conductivity detector and flame photometric detector, respectively. In the gas chromatograph the concentration of the components hydrocarbons C_1 to C_4, CO_2, CO, H_2S, SO_2, HCl and H_2 is determined.

Within the first nine months gases were sampled each week. Subsequently the intervals were prolonged to one and to three months. Parallel to gas sampling, the water content in the pore volume is determined by connecting a moisture analyzer to the valves of the teflon tubes and by pumping ten liters of gas through the apparatus within a period of ten minutes. Additionally to the gas from the pore volume of the backfill, the mine air at the entrance of the test drifts has been analyzed. Its composition is:

• CO_2	between	300	and	800	vpm
• CH_4	between	0	and	5	vpm
• other hydrocarbons	less than			5	vpm
• CO	less than			5	vpm
• H_2S	less than detection limit of			0.1	vpm
• SO_2	less than detection limit of			0.1	vpm
• HCl	less than detection limit of			1	vpm
• H_2	less than detection limit of			1	vpm

The great variation of the concentration in CO_2 and CH_4 is caused by the mine ventilation, the traffic and the mining activities.

The Fig. 6-1 to 6-28 show the values of H_2, CH_4 and CO_2 versus time at the bottom (1), midplane (2) and the top (3) of the central cask as well as at the roof of the drift (4) in the sections A, B and C of the southern and northern drift, respectively.

The nomenclature for the gas measuring points in the corresponding position is (Fig. 6-1 to 6-28):

- Position (x / yz) with
  - x representing the drift A or B
  - y indicating the section A, B, C (Fig. 2-2)
  - z giving the position of the measuring point in the cross section at the bottom (1), midplane (2) and the top (3) of the cask and at the roof of the drift (4).

The remaining measuring points (B / I1 to B / I4) are located at the drift floor right in front of the outer cask in section I1 of the northern drift.

Prior to heating the concentration of the major gas components in the pore volume at the measuring points B / B1 to B / B4 is:

- H_2 in the range of 28 to 44 vpm
- CH_4 in the range of ≤ 4 vpm
- CO_2 in the range of 35 to 75 vpm

Assuming that the pore volume of the backfill was initially filled with mine air these results indicate that H_2 is already generated at the ambient temperature of approximately 36 °C by corrosion or chemical interaction. The concentration of CO_2 in the gas phase is considerably lower than in the mine air. The reason for that is the capability of the crushed salt to adsorb CO_2 at its surface.

After starting heating on September 25, 1990 the backfill temperature gradually rises to 200 °C within about three months. The concentration of the sampled gases increases subsequently during the next three to six months:

- H_2 up to 550 vpm
- CH_4 up to 40 vpm
- CO_2 up to 3000 vpm

These results indicate that corrosion is accelerated by the rising temperatures leading to an enhanced hydrogen concentration. The carbon dioxide originally adsorbed at ambient temperatures is desorbed at elevated temperatures. More carbon dioxide is generated by the oxidation of hydrocarbons or the release from the crystal lattice. Methane is desorbed from the surface of the backfill and from the crystal lattice as well as it is generated by the thermal decomposition of higher hydrocarbons.

The results of Fig. 6-1 to 6-28 show a varying concentration of the components in the range of 20 % within a comparatively short time. This fluctuation correlates directly with the air pressure changes at the entrance of the backfilled drifts which varies in the range of 50 mbar caused by changes in the mine ventilation several times a day and by the variation of the atmospheric pressure.

Due to the high porosity and permeability of the backfill, the concentration of the generated and released gases is constantly diluted.

After about one year of heating, the concentration of hydrogen, methane and carbon dioxide in the pore volume of the backfill decreases indicating that the gas production is lower than the escaping amount of gases.

In March 1992 the pore volume of the backfill in drift A and B is flushed with mine air due to an overcoring of boreholes required for geophysical measurements in cross section G1 (Fig. 2-2). Subsequently the concentration of all components decreases. The measuring points at the roof are the first which record increasing concentrations again.

Some of the measuring points in drift A fail prematurely probably due to recrystallizations at the surface of the glass filters resulting in an obstruction of the sampling point.

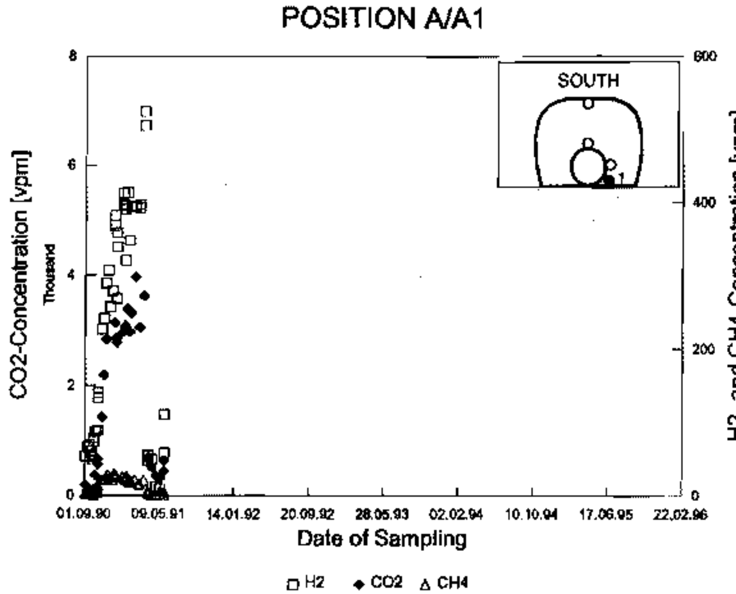

Fig. 6-1 Content of carbon dioxide, hydrogen and methane versus time at measuring point A / A1

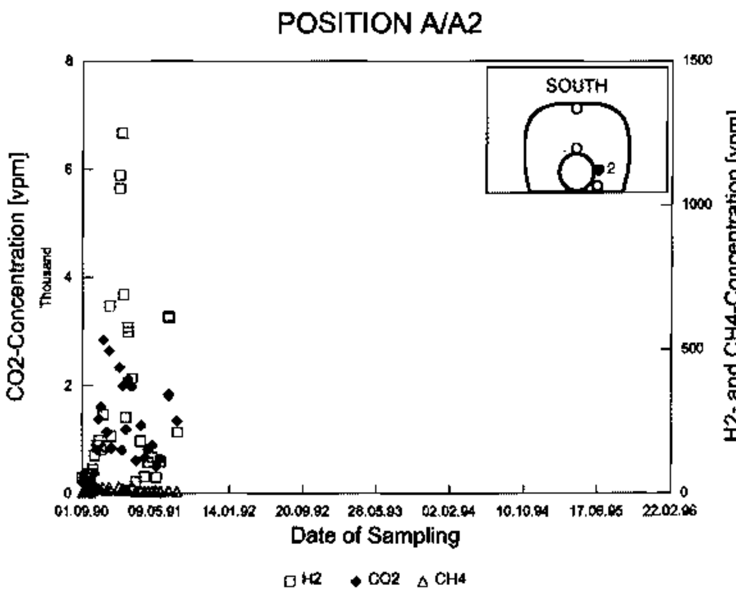

Fig. 6-2 Content of carbon dioxide, hydrogen and methane versus time at measuring point A / A2

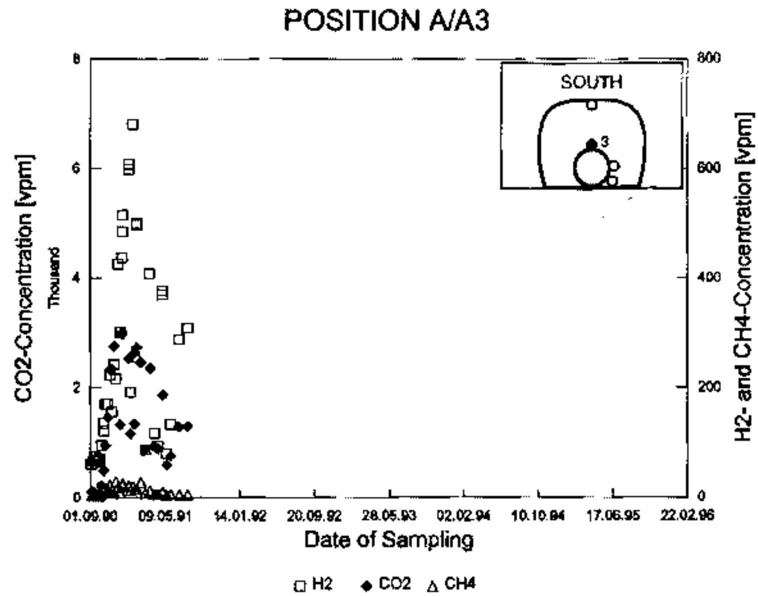

Fig. 6-3 Content of carbon dioxide, hydrogen and methane versus time at measuring point A / A3

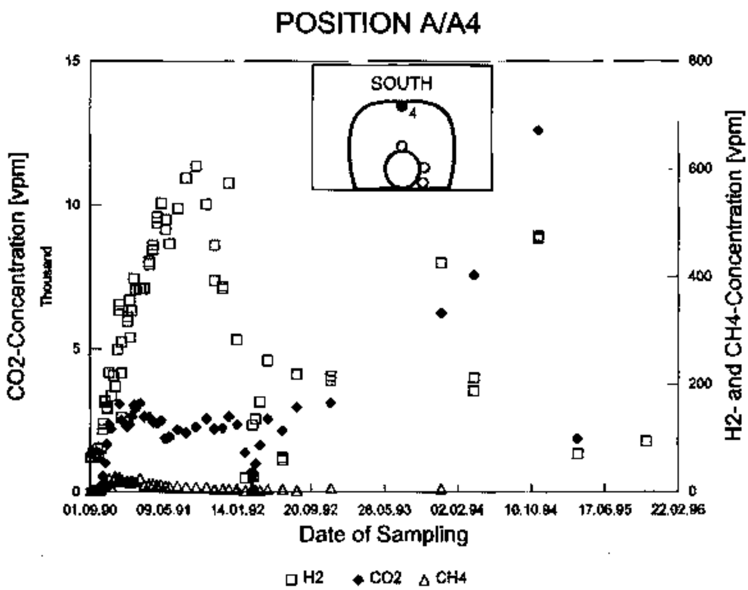

Fig. 6-4 Content of carbon dioxide, hydrogen and methane versus time at measuring point A / A4

POSITION A/B1

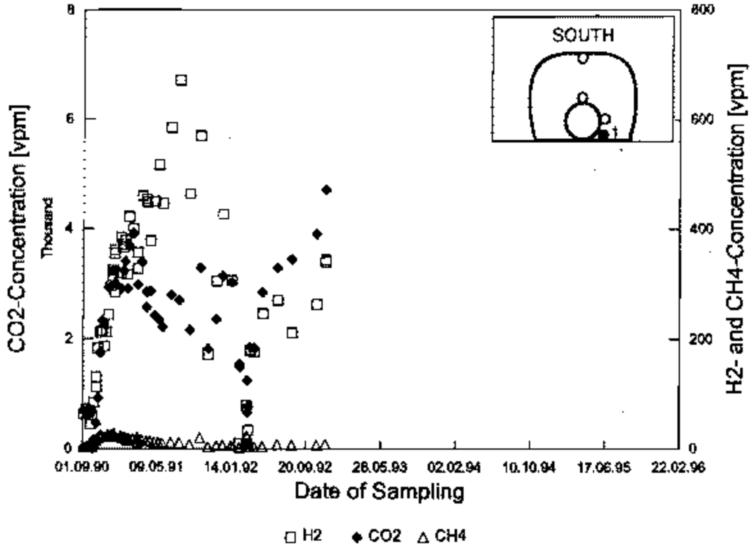

Fig. 6-5 Content of carbon dioxide, hydrogen and methane versus time at measuring point A / B1

POSITION A/B2

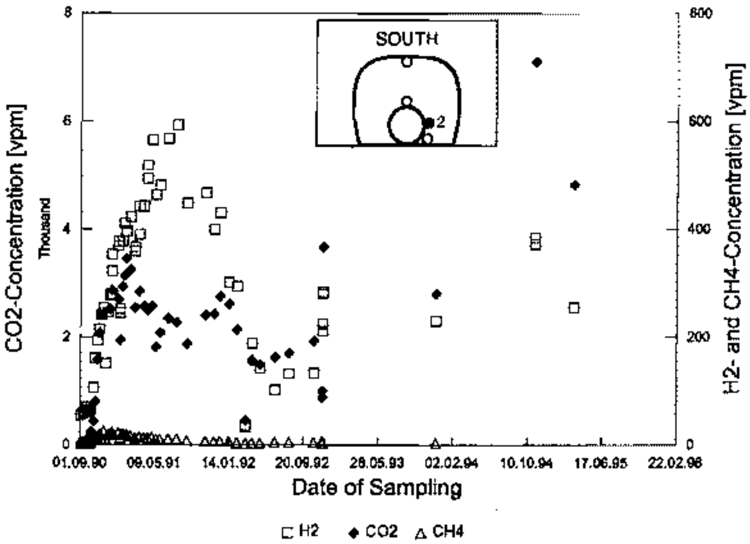

Fig. 6-6 Content of carbon dioxide, hydrogen and methane versus time at measuring point A / B2

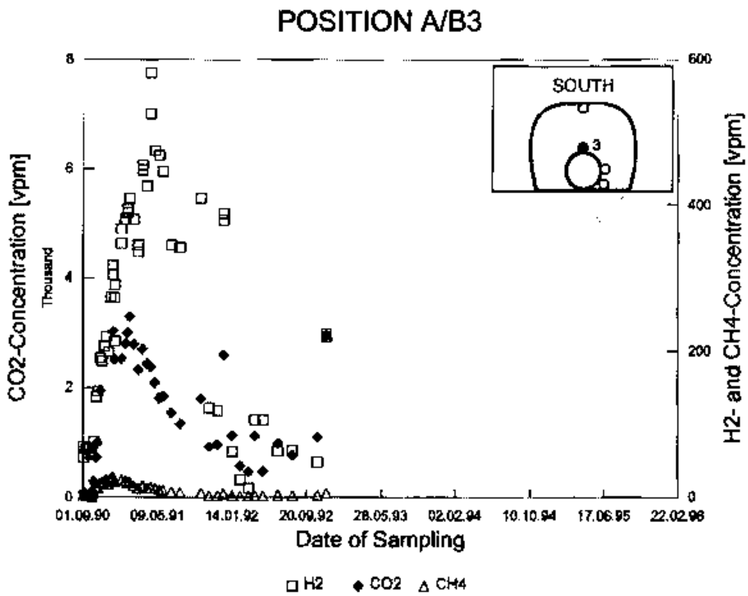

Fig. 6-7 Content of carbon dioxide, hydrogen and methane versus time at measuring point A / B3

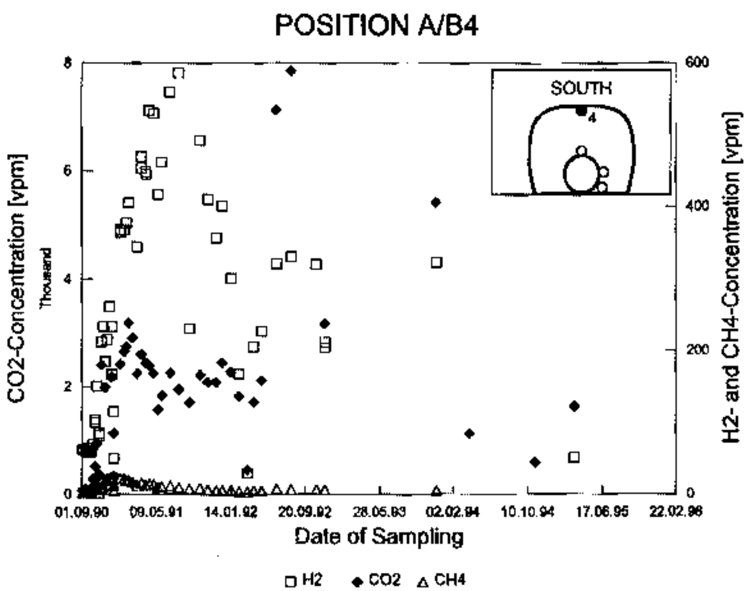

Fig. 6-8 Content of carbon dioxide, hydrogen and methane versus time at measuring point A / B4

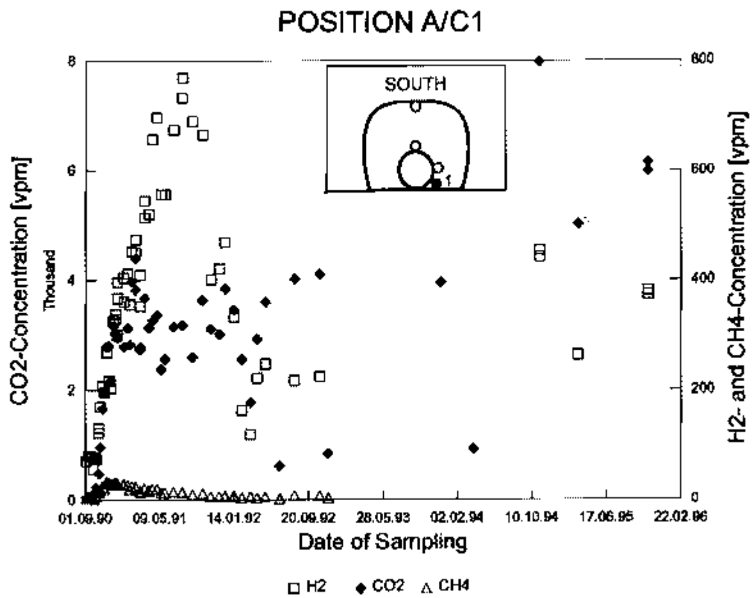

Fig. 6-9 Content of carbon dioxide, hydrogen and methane versus time at measuring point A / C1

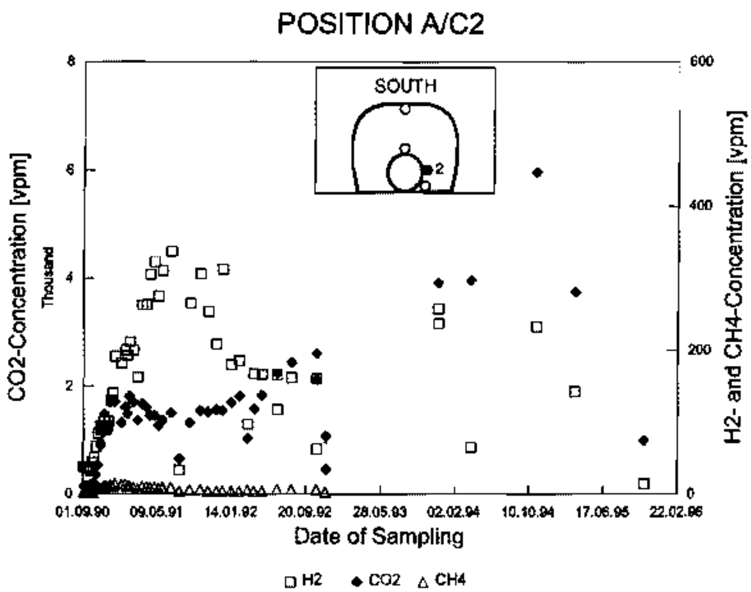

Fig. 6-10 Content of carbon dioxide, hydrogen and methane versus time at measuring point A / C2

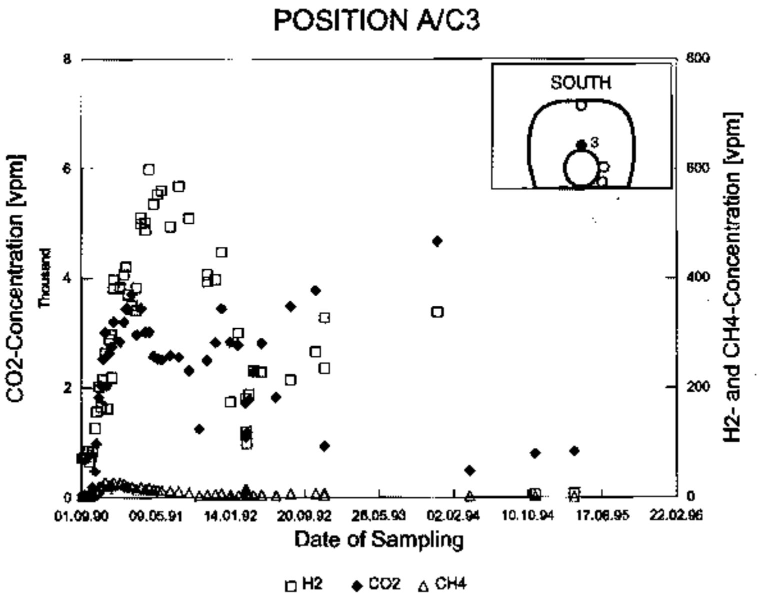

Fig. 6-11 Content of carbon dioxide, hydrogen and methane versus time at measuring point A / C3

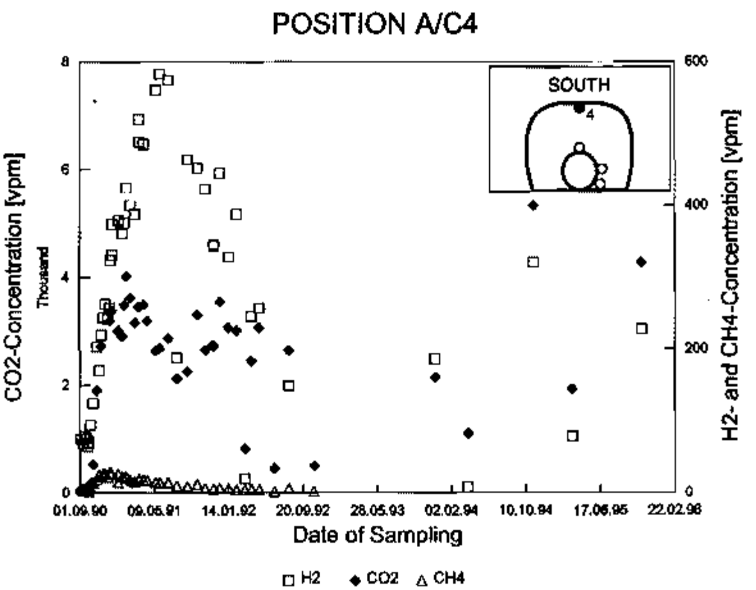

Fig. 6-12 Content of carbon dioxide, hydrogen and methane versus time at measuring point A / C4

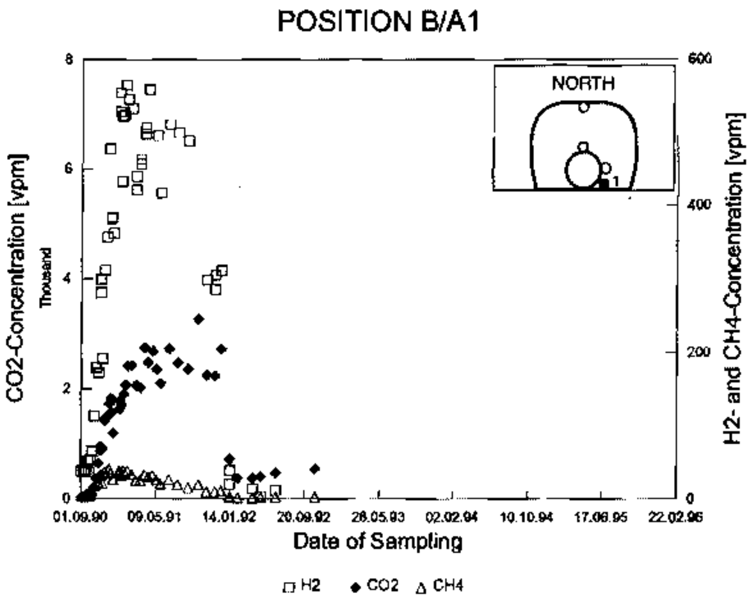

Fig. 6-13 Content of carbon dioxide, hydrogen and methane versus time at measuring point B / A1

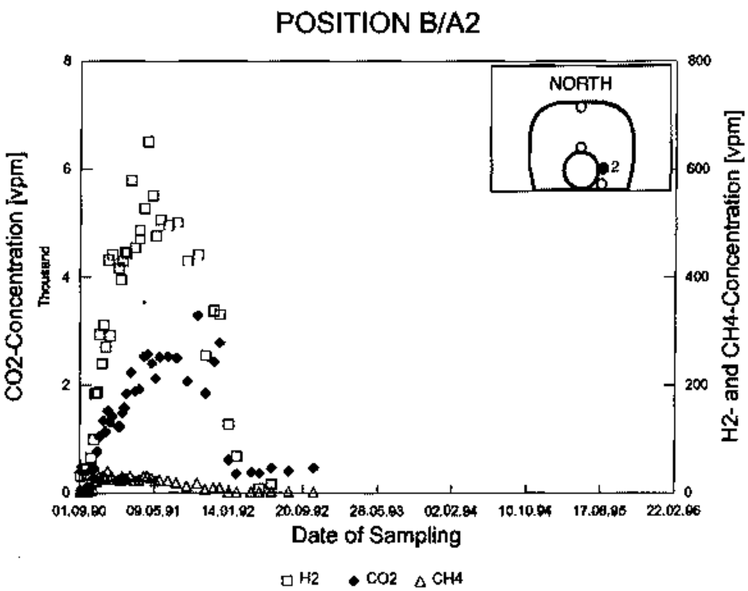

Fig. 6-14 Content of carbon dioxide, hydrogen and methane versus time at measuring point B / A2

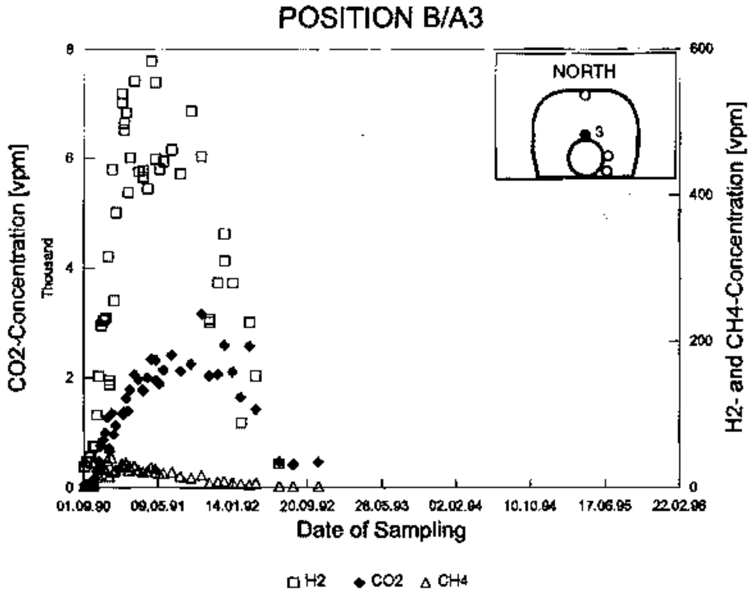

Fig. 6-15 Content of carbon dioxide, hydrogen and methane versus time at measuring point B / A3

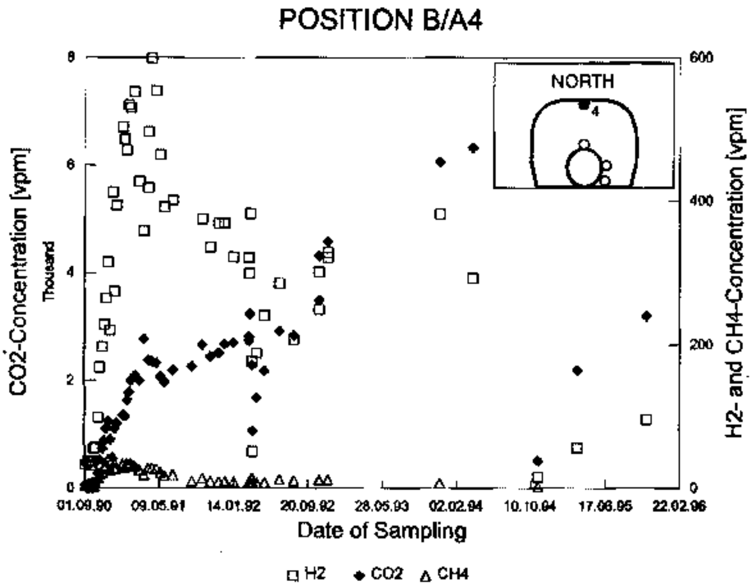

Fig. 6-16 Content of carbon dioxide, hydrogen and methane versus time at measuring point B / A4

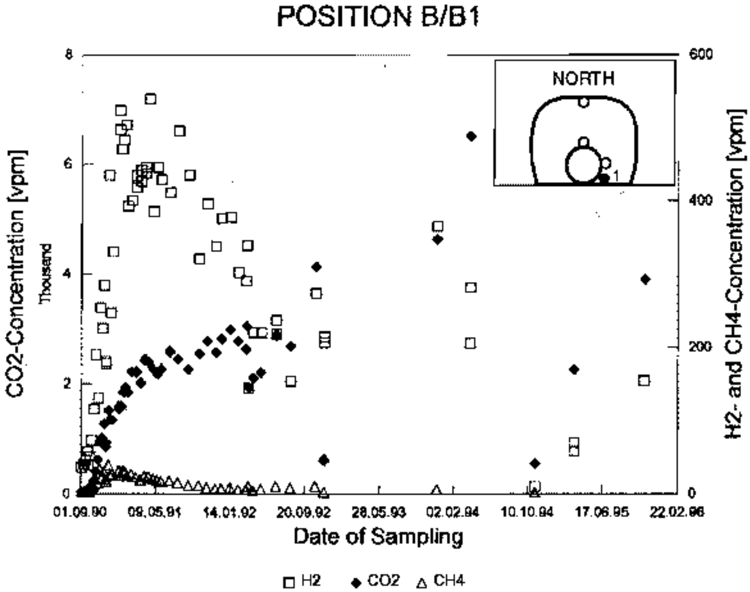

Fig. 6-17 Content of carbon dioxide, hydrogen and methane versus time at measuring point B / B1

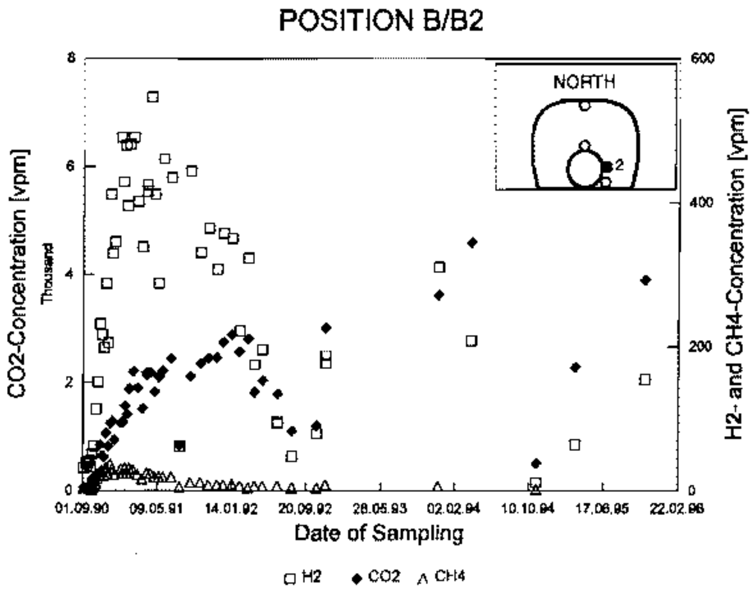

Fig. 6-18 Content of carbon dioxide, hydrogen and methane versus time at measuring point B / B2

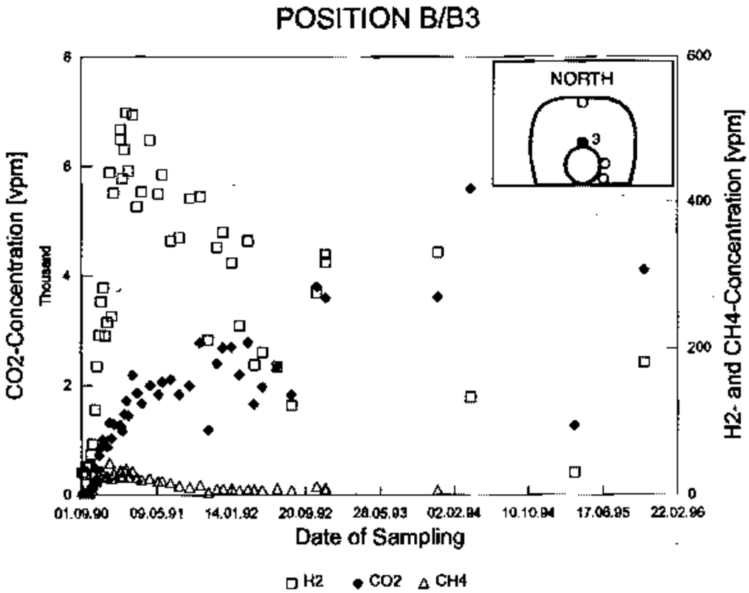

Fig. 6-19 Content of carbon dioxide, hydrogen and methane versus time at measuring point B / B3

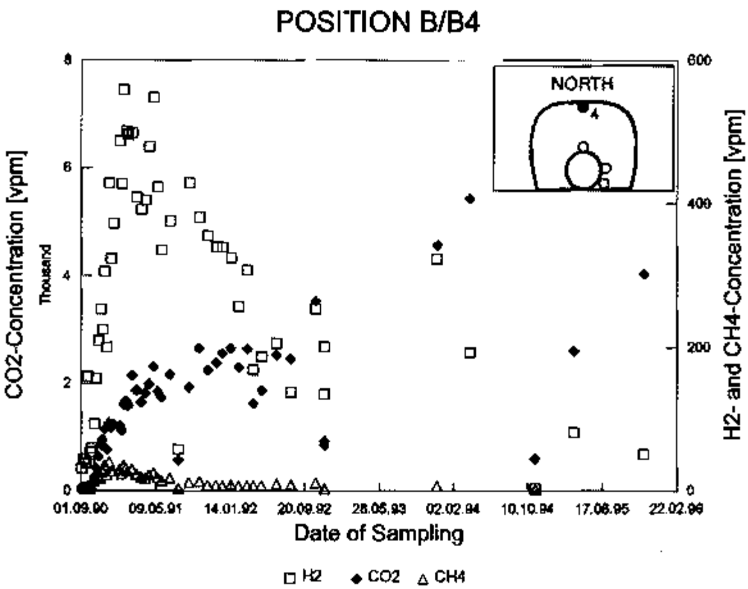

Fig. 6-20 Content of carbon dioxide, hydrogen and methane versus time at measuring point B / B4

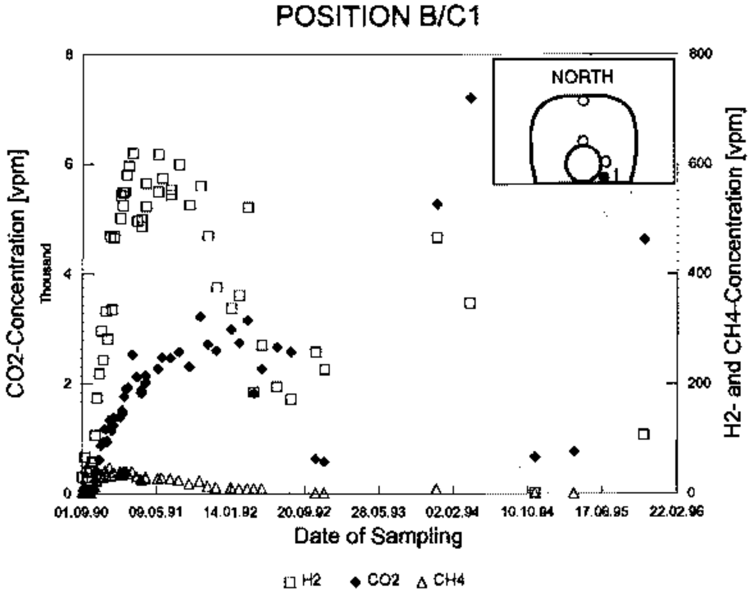

Fig. 6-21 Content of carbon dioxide, hydrogen and methane versus time at measuring point B / C1

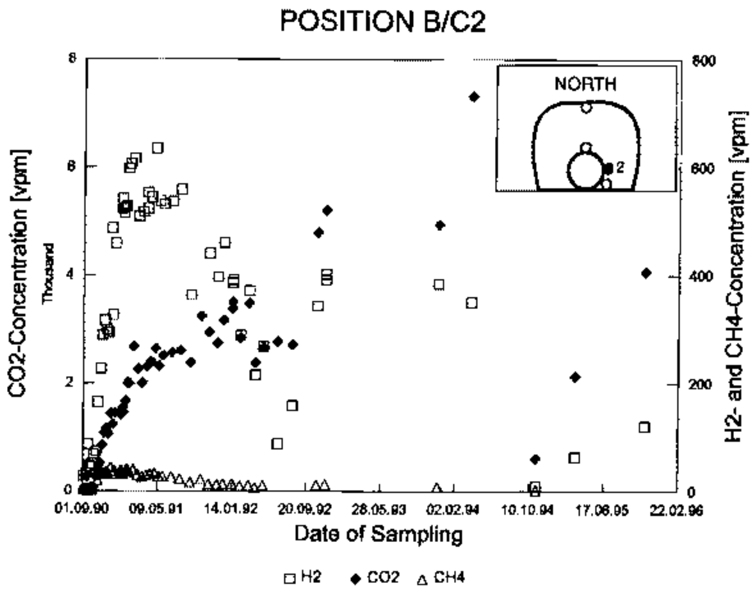

Fig. 6-22 Content of carbon dioxide, hydrogen and methane versus time at measuring point B / C2

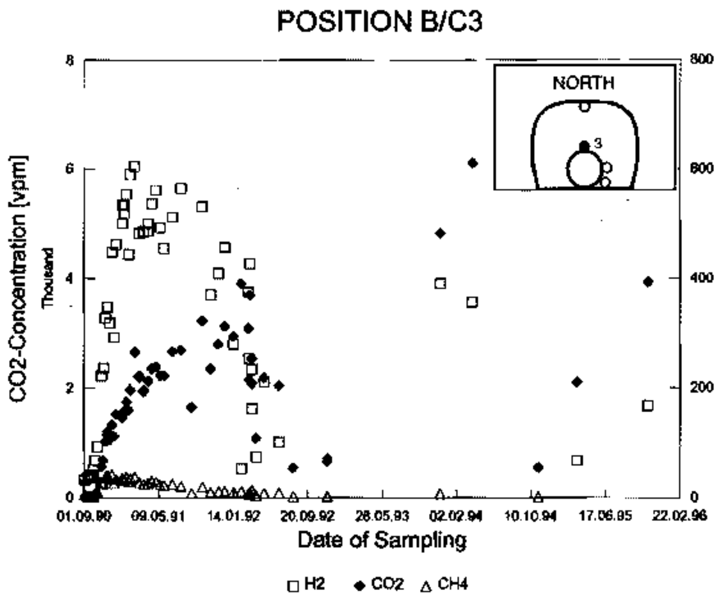

Fig. 6-23 Content of carbon dioxide, hydrogen and methane versus time at measuring point B / C3

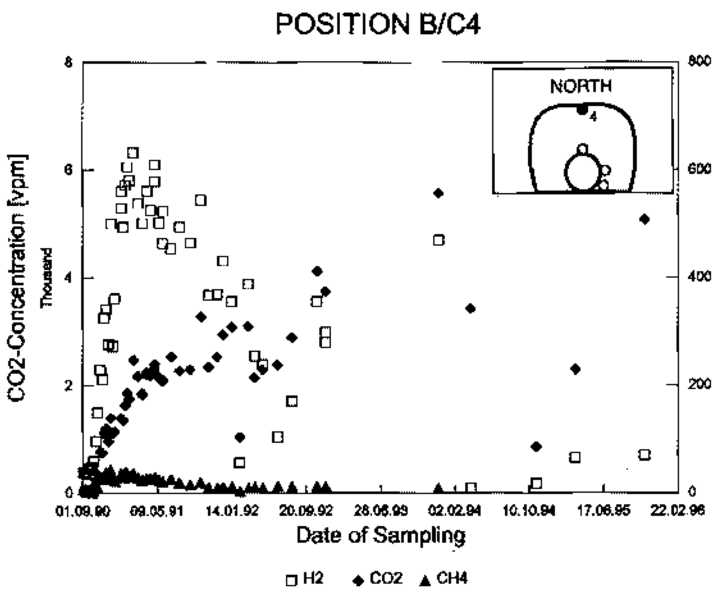

Fig. 6-24 Content of carbon dioxide, hydrogen and methane versus time at measuring point B / C4

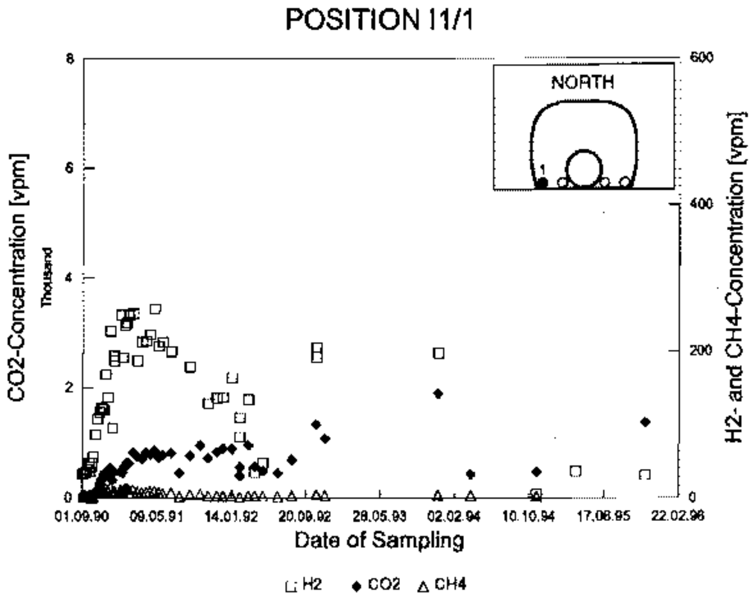

Fig. 6-25 Content of carbon dioxide, hydrogen and methane versus time at measuring point B / I1

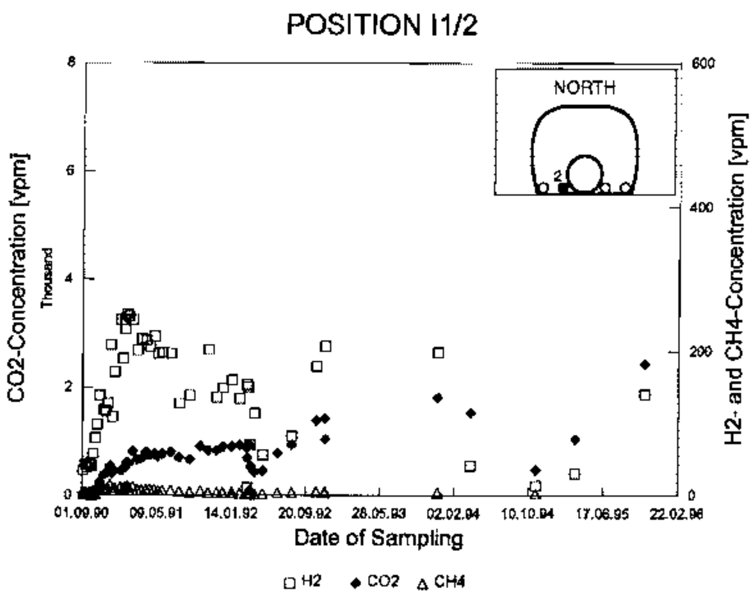

Fig. 6-26 Content of carbon dioxide, hydrogen and methane versus time at measuring point B / I2

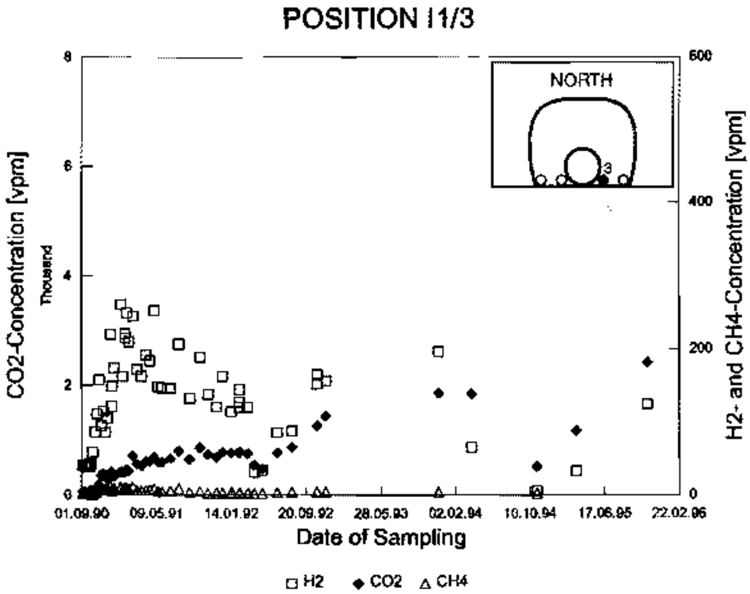

Fig. 6-27 Content of carbon dioxide, hydrogen and methane versus time at measuring point B / I3

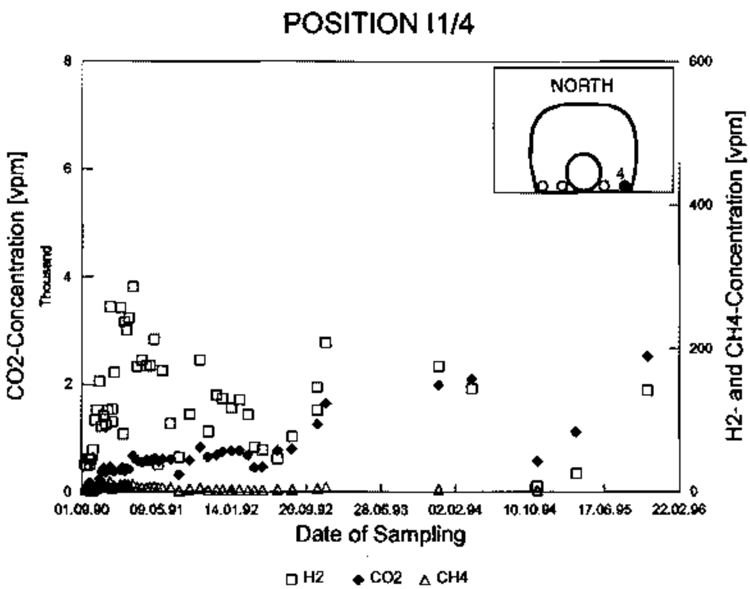

Fig. 6-28 Content of carbon dioxide, hydrogen and methane versus time at measuring point B / I4

The gas measurements had to be stopped due to financial cuts by the end of 1992. They were resumed in August 1994 with the support of the European Community.

The measurements in November 1994 indicate a drastic drop in concentration of the components CO_2 and CH_4. Further measurements are required in order to assess that behaviour.

In addition to the gases the humidity in the pore volume is determined. Prior to heating the values range between 15 to 20 g/m³. After three months of heating it increases up to 50 g/m³. For the following three months water condenses inside the teflon tube implying that humidity is not measurable any more. Later on the humidity increases to an amount larger than the saturation humidity of 50 g/m³ at 40 °C.

During laboratory investigations with the crushed salt used for backfilling, hydrochloric acid is released by heating above 80 °C. However, no hydrochloric acid is found in the test field. In the backfill all hydrochloric acid is reacting with the steel casks by generating hydrogen.

6.2 Determination of the Air Pressure

The gas concentration in the pore volume of the backfill correlates with the air pressure in the access drift of the test field. The air pressure is influenced by long term variations of about 50 mbar as a result of the meteorologic air pressure outside the mine and by the ventilation of the mine of about 10 mbar several times a day.

As the backfill in the drifts has a high porosity and permeability these pressure variations run through the backfill pumping out the gases in the pore volume with each pressure decrease. This permanent dilution may be calculated if the permeability and the variation of the air pressure is known.

The permeability can be calculated when the time delay of the pressure impulse running through the backfilled drift is known. For determining the total pressure variation and the time delay of the impulse within the backfill, barographs have been installed both in the access drift in front of the backfill and inside a perforated casing of a borehole running from the 750 m level into the backfill on the 800 m level. The distance between both measuring points is about 70 m. Between these points a gas flow can take place via the pore volume of the backfill as well as via the bypass which is caused by the cable duct near the roof of the drift. The long term variation of the air pressure in the access drift as a result of the meteorology is between 1064 and 1104 mbar that means a total of 40 mbar (result of six independent measurements). The variation by switching the mine ventilation on or off is 7 to 8 mbar two to three times a day.

The measurements of the pressure in the access drift and in different areas of the backfill via the gas sampling filter indicate no measurable time delay of the pressure impulse by switching the mine ventilation on and off. That means that the total permeability of the backfilled drift including the bypass of the cable duct is comparatively high. The gases within the pore volume which are generated and released by corrosion and elevated temperature are pumped out by each pressure decrease without any impediment. By every 10 mbar pressure decrease and increase about one percent of the air inside the backfill is extracted and renewed again by mine air.

To estimate the total amount of gas release since the beginning of heating in September 1990, the variation of the total air pressure in the access drift has to be compiled what will be done in the future.

6.3 Determination of the Diffusivity

Beside the migration as a result of the pressure gradient gases are also spreading due to the concentration gradient called diffusivity. For estimating the total amount of gas release out of the backfilled drift this parameter is also of importance.

For determining the diffusivity the teflon tubes and glass filters which are normally used for taking gas samples are applied. The tracer gas neon has been pumped via one of the teflon tubes and its glass filter into the backfill. By taking gas samples from the other sampling points at different times and analysing the content of neon with a gas chromatograph the spreading of the tracer gas within the pore volume of the backfill has been determined.

The result of a first estimation at measuring point B / C3 with a spherical model is that the gas diffusivity within the pore volume of the backfill is in the range of $1.4 \cdot 10^{-5}$ m^2/s to $4 \cdot 10^{-5}$ m^2/s.

In the future further injection tests with the relevant gases and the calculation with a geometrical model of the test field have to be made in order to get more accurate values of the diffusivity.

6.4 Determination of the Total Water Content

The corrosion of the steel casks and the generation of hydrogen is a direct result of the water content within the pore volume of the backfill. This water is released from the crystal surfaces and the hydrated minor minerals within the rock salt.

Prior to heating the water content is in the range of 20 g/m^3 air. As a result of the elevated temperature and the dehydration of the rock salt the humidity increases to values greater than 50 g water per m^3 air and water condenses inside the teflon tubes running from the gas sampling filters to the access drift.

After about one year no further condensation is been seen but nevertheless it is not possible to determine the humidity with electronic devices. Another technique using a cooling trap was already tested in other test fields. This technique does not set an upper limit to determine the humidity and furthermore enables a chemical analysis of the collected water to be made. By this means informations can be obtained on the values of pH and gases like HCl, H_2S and CO_2 which may be soluted in the water.

Several measurements by which about 1 m^3 air from the vicinity of the heated steel casks in the backfill is pumped via the glass filters and the teflon tube into the cooling trap indicate a water content of 20 to 25 g in 1 m^3 air. The value of pH (number that describes the degree of acidity or alkalinity) is 3.42.

By chemical analysis the following ions are determined in the water:

- Na^+ (detected by ICP-OES) 128.6 mg / l = 5.59 mmol / l
- Na^+ (detected by ICP-MS) 124.5 mg / l = 5.42 mmol / l
- Cl^- (detected by IC) 165.5 mg / l = 4.69 mmol / l

Obviously there is an excess of sodium which has to be attributed to the presence of other minerals than NaCl in the rock salt.

Measurements of the air in the access drifts indicate a humidity in the range between 5 and 6 g water per m^3 air. As the drifts are ventilated their humidity is directly influenced by the meteorology outside of the mine.

7 Data Acquisition and Data Processing

In the TSS test different measurements are registrated on-line by the data acquisition system. This system involves the following tasks:

- Data acquisition in the test field
- Data conversion into a standard format and data transfer both to archive and evaluation computer
- Monitoring of the test from above ground
- Archiving of the data
- Data processing for documentation and evaluation purposes

A synoptic view of the whole system is given in Fig. 7-1.

7.1 Data Acquisition

The data acquisition in the TSS test is carried out by a number of four local front end processors which are operating independently. The measurements both around the test drifts on the 800 m level and from the observation drifts on the 750 m level are registrated by two units respectively. While one of these units is recording the electrical readings on each level, the other one is required for the hydraulic measurements.

GSSE front end processor (FEP) on the 800 m level

A GSSE front end processor (FEP) is used for the registration of the electrical devices on the 800 m level. At the moment the following gauges are connected to the unit:

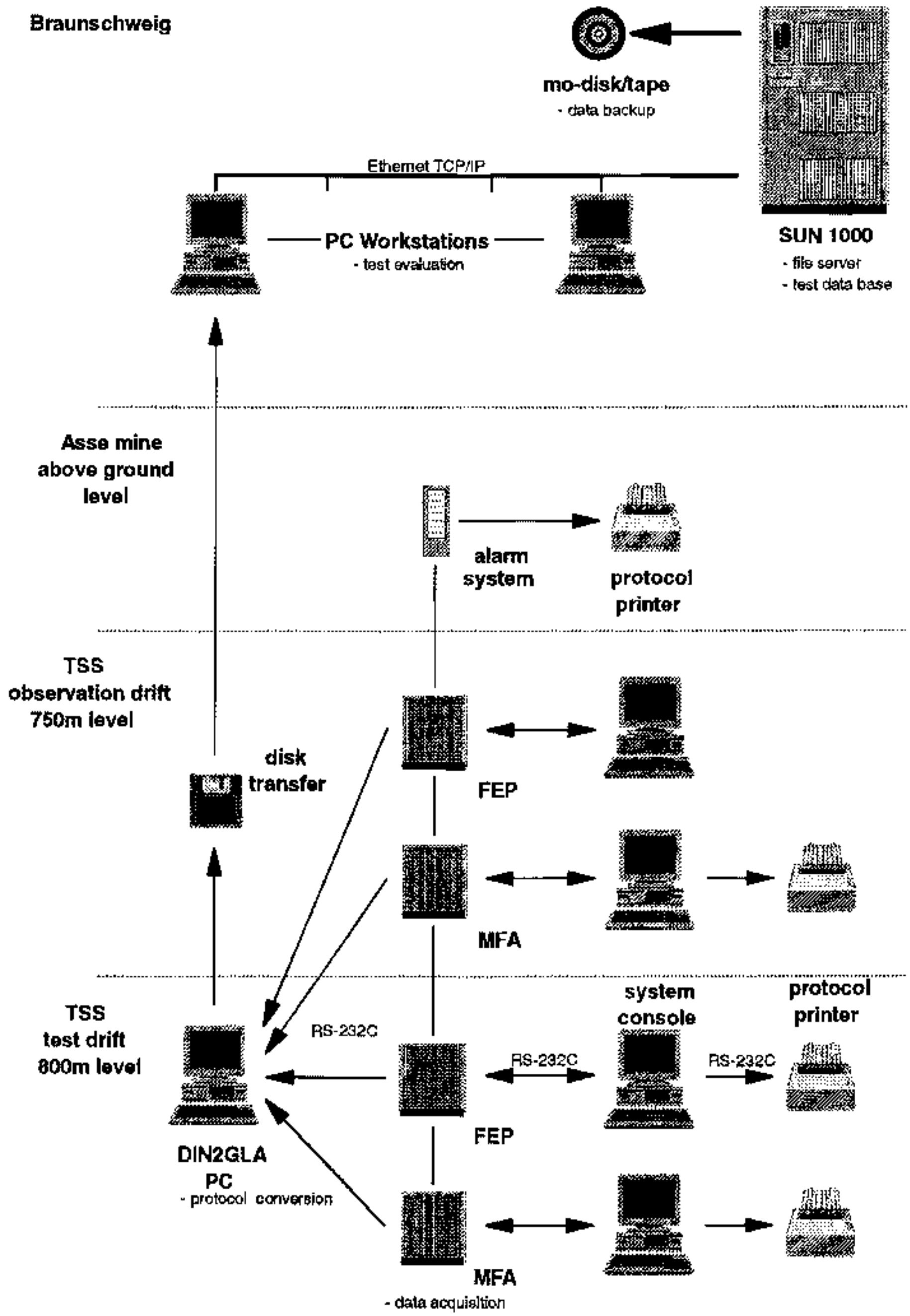

Fig. 7-1 Synoptic view of the TSS data acquisition system

- 660 temperature gauges (resistance thermometers of the PT100 type in four wire technique) and additionally 20 precision resistances for system control

- 152 deformation gauges (electric transducers of the potentiometer type in five wire technique) and additionally 18 precision resistances for system control

The FEP is able to carry out both the registration of the readings and their temporary storage as well as the identification and the signalling of faults.

The FEP is a modular designed Siemens SMP bus system with 12 bit AD converter, 8088 processor and 256 k main memory. At the input side the FEP is equipped with various interfaces for electric transducers which are isolated galvanically. The temporary data storage is realized by ring buffers via zero-power RAMs with a buffering time of approximately ten days. Mechanical memories like hard disks or tape drives are not existing.

The external communication is taking place via a RS-232C terminal and a protocol printer. The data transmission for further data processing is carried out via another RS-232C port and is supported by the DIN 66348 protocol. Digital outputs are available for fault messages.

The FEP is operated by an EPROM resident software without additional operating system. The individual electric transducers as well as the fault messages are directly accessible via the terminal by a menu system. Additionally, modifications of various parameters like transducer status, scan intervals, conversion functions or alarm limits are possible.

Glötzl front end processor (MFA) on the 800 m level

The measurements of the hydraulic pressure gauges on the 800 m level are registrated by an automatic Glötzl data acquisition unit (MFA). Furthermore, the MFA records both the power output and the status values of the heaters as well as the electrical measurements of the DBE test devices. The following gauges are connected to the unit:

- 66 hydraulic pressure gauges (Glötzl type hydraulic pressure cells) and additionally 5 hydraulic checkpoints for system control

- 27 electropneumatic pressure gauges (AWID type electropneumatic pressure cells) and additionally 2 pneumatic checkpoints for system control

- 12 deformation gauges (electric transducers of the potentiometer type in five wire technique) and additionally 8 precision resistances for system control

- 24 temperature gauges (resistance thermometers of the PT100 type in four wire technique) and additionally 6 precision resistances for system control

- 112 electric transducers of the heater control system

The MFA is operating stand-alone as well and is specially designed for a registration both of hydraulic and pneumatic signals. The unit is equipped with a 12 bit AD converter with V25 micro-controller and buffered RAMs. The buffering time for readings amounts to approximately seven days. Like the GSSE FEP the acquisition program is supplied by an EPROM firmware.

The MFA operation is supported by a keyboard panel and a LC display. A communication via PC is also provided. The data output is taking place via a thermal printer and a RS-232C interface. Additionally, a tape deck is available for an automatic back-up of the readings. Digital ports are used for the output of fault messages.

The MFA firmware includes all functions of a GSSE FEP but also provides numerous extended utilities like the implementation of hydraulic or pneumatic measurements.

GSSE front end processor (FEP) on the 750 m level

Another GSSE front end processor (FEP) is used for the registration of the electrical devices on the 750 m level. Currently, the following gauges are connected to the unit:

- 63 temperature gauges (resistance thermometers of the PT100 type in four wire technique) and additionally 10 precision resistances for system control

- 22 deformation gauges (electric transducers of the potentiometer type in five wire technique)

The FEP is of the same type as on the 800 m level but operates with a down-sized hardware.

Glötzl front end processor (MFA) on the 750 m level

Like on the 800 m level an automatic Glötzl data acquisition unit (MFA) is recording the measurements of the hydraulic pressure gauges on the 750 m level. The unit is operated in co-operation with BGR and registers additionally a number of electrical measurements of BGR. The following gauges are connected to the unit:

- 35 hydraulic pressure gauges (Glötzl type hydraulic pressure cells), respectively
  40 gauges after the replacement of the instrumentation in 1995 and additionally
  5 hydraulic checkpoints for system control

- 80 hydraulic pressure gauges of BGR (Glötzl type hydraulic pressure cells) and additionally 4 hydraulic checkpoints for system control

- 4 temperature gauges of BGR (resistance thermometers of the PT100 type in four wire technique)

7.2 Data Processing

DIN2GLA-PC

A central PC (DIN2GLA-PC) is installed on the 800 m level which receives all data of the FEPs and MFAs both on the 750 m level and the 800 m level via RS-232C interfaces. The data are converted into a standardized temporary format ("GLA-Lesespeicherformat").

The data conversion is necessary as all FEP data are transferred via a DIN 66348 transmission protocol. The data files are stored on hard disk. For safety reasons the files on this PC are saved temporarily for several months. Once a week the data of the DIN2GLA-PC are transferred by disks to the archiving and evaluation computer in Braunschweig.

The DIN2GLA-PC is operating since March 1994. The system is replacing the former ERMEDA and VEMEDA program on a VAX computer which was shut down due to a system change.

Alarm system

A simple alarm system is registrating different fault messages in the test field. It is based on a two wire transmission system in free topology with decentralized arbitration. The coded fault messages are transmitted above ground where they are shown on a display and recorded as a print-out.

At the moment the following 13 fault messages are registrated:

- 750 m level:
  - Main power failure in the data acquisition container
  - Temperature control in the data acquisition container
  - MFA fault
  - FEP fault

- 800 m level:
  - Main power failure in the data acquisition container of GRS
  - Main power failure in the data acquisition container of BGR
  - Temperature control in the data acquisition container of GRS
  - Temperature control in the data acquisition container of BGR
  - MFA fault of the GRS unit
  - MFA fault of the BGR unit
  - FEP fault
  - Failure of the compressed air supply for the AWID type pressure gauges
  - Fault at the heater control system

Data archiving and data protection

In Braunschwelg the data from the Asse DIN2GLA-PC are transferred by disks to another PC into the archiving and evaluation program Glötzl GLA. The archiving of the data is carried out by a local TCP/IP network on a hard disk of the central file server SUN 1000. In this way an access to the data can be restricted by passwords and file attributes. The hard disk is saved regularly on DAT-tapes or MO-disks.

All data are archived in a standardized format. Thereby a structuring in data groups is carried out combining measurements of the same kind respectively. In each data group the readings of different channels are saved in separate files. A set of readings comprises the following parameters:

- Channel number
- Sampling time
- Physical value
- Status value

Additionally, general administrative informations are existing like channel name, measuring point, physical unit or remarks.

Data evaluation

The data evaluation is carried out by the Glötzl GLA program. The hard disk of the file server is directly accessible via the network. For evaluation and presentation purposes several numerical and graphical outputs are available on screen or printer. Further mathematical and special functions like the compensation of readings or the setting of different flags are provided as well.

7.3 Data Protection

Precautions have been taken both against the loss of data and an unauthorized access.

As the data acquisition is distributed among several front end processors (decentralization), the failure of a single unit causes only a partial loss of data. Each fault message is signalled promptly by the alarm system enabling an immediate reaction to the failure. All front end systems are designed for elevated temperatures to improve their reliability.

In case of a failure of the central DIN2GLA-PC all front end processors are able to save their readings temporarily over more than a week without a loss of data.

Main power drops and spikes are compensated by an uninterruptable power supply unit both for the front end processors and the DIN2GLA-PC. Furthermore, the power supply is also monitored by the alarm system.

All data acquisition systems in the test field are housed in environmentally sealed cases inside of closed and air-conditioned containers. The temperature in these containers is controlled by the alarm system.

For the protection of the archived data on the server hard disk all utilities of a multi-user and multitasking operating system against an unauthorized access are available.

In case of an archiving failure the correct status of the archive can be restored easily due to the long-term buffering time of the DIN2GLA-PC and a regularly carried out backup of the SUN file server archive.

8 Conclusions

The phase of heating of the TSS demonstration test started in September 1990 and continued over more than five years up to now.

A maximum temperature of approximately 210 °C at the surface of the heater casks is reached after five months. Since the thermal conductivity of the backfill increases with its compaction the temperature at the surface of the casks decreases subsequently, reaching between 165 °C and 175 °C at the moment.

The temperature distribution in the heated area of the test drifts depends on the distance of the measuring position from the heaters. Temperatures in the warm backfill range up to 135 °C approaching quasi steady state conditions after three years of heating. With increasing distance from the heaters a steady state has not been reached yet.

The rock temperatures in the area next to the heated drifts and all over the heated pillar approach quasi steady state conditions after five years of heating. Farther away the rock temperatures are still increasing as well as the rock temperatures in the cold sections.

By the TSS test a large number of temperature data are available now for the validation of thermomechanical models. Measured temperatures in the test drifts fit quite well with theoretical calculations.

Gradual closure of the drifts causes an increasing compaction of the backfill. This process is accelerated considerably by heating. Convergence rates in the heated area rise by a factor of ten immediately after the start of heating. Three months later the rates are already decreasing indicating the beginning support by the backfill. Current rates are still twice as much as prior to heating.

As a result of drift closure the initial backfill porosity of about 35 % has been reduced to 26.5 % to 28 % in the heated area after five years of heating.

The measured drift convergences are considerably lower than calculated. Accordingly, the porosity of the backfill is decreasing slower than predicted.

The settling of the backfill due to gravity leads to the opening of a gap between the roof and the top of the backfill. In the heated area the acceleration of drift closure almost immediately induces the closing of the gap within a few weeks.

Backfill compaction starts not until the gap at the roof is closed. During the first months mainly the upper part of the heated backfill is compacted. Subsequently increasing portions of the lower part are involved. After two years of heating the vertical distribution is approximately balanced with hardly any change up to now.

The rock deformations around the test drifts are accelerated significantly by heating. The closer the measuring points are located to the heater casks the earlier the deformations start. Next to the heated drifts the deformations are accelerated by a factor of ten to twenty. After two to three months the deformation rates are decreasing again indicating the beginning support by the backfill. Unlike the deformations next to the heated drifts which are continuously decreasing since that time, the rates of the distant extensometers as well as the deformation rates in the non-heated sections are still constant.

Backfill pressure in the heated area starts to rise immediately after the beginning of heating. The pressure increases continuously reaching a maximum of 2.9 MPa at the roof after five years of heating. Currently, the average backfill pressure at the roof has reached 18 % to 20 % of the initial vertical stress, which has been estimated to about 12 MPa in the test field.

The rock pressure in the heated area rises significantly after the start of heating by up to 7 MPa. The thermally induced elastic stress changes, however, are only a short-term effect. Subsequently, the rock pressure decreases again to the original state of stress prior to heating due to relaxation of the induced stress by creeping of the rock salt.

Though the measuring equipment in the test field is exposed to extraordinary conditions, the designed measuring systems prove to be successful. However, the measuring lines ought to have been protected better against damages.

The backfill compaction is determined by different in-situ measurements.

A superconducting gravimeter proves to be not suited to monitor changes in the backfill density, as even its extraordinary low drift is not sufficient for this purpose.

The density determination with radiometric γ-γ-borehole devices is successfully applied. In the non-heated area the backfill density increases from 1200 - 1300 kg/m^3 at the bottom of the backfill to over 1500 kg/m^3 towards the top. This trend is caused by the slinger technique used for the backfilling which produces a separation of different grain fractions. The heterogeneous density distribution is being conserved during compaction. In the heated area the average density increases from 1400 kg/m^3 in the beginning to approximately 1540 kg/m^3 at the moment.

The backfill compaction is monitored by sonic measurements as well. These measurements are only feasible in the non-heated area because of the low temperature resistance of the equipment. Due to the high porosity of the cold backfill even after five years of compaction only qualitative estimations are possible.

Gas samples are taken from the backfill both in the northern and the southern drift and analyzed by gas chromatography in the underground laboratory. Already at the ambient temperature of approximately 36 °C on the 800 m level hydrogen, methane and carbon dioxide are detected in the backfill in concentrations of 28 to 44 vpm, $\leq$4 vpm and 35 to 75 vpm respectively.

Significant gas release starts immediately after the heaters are switched on. Within six months the concentration of the major gas components hydrogen, methane and carbon dioxide increases up to 550 vpm, 40 vpm and 3000 vpm respectively.

As the backfill is comparatively porous and permeable, the concentration of the released gases is constantly diluted by pressure changes due to variations in the mine ventilation and long-term changes in the atmospheric pressure. The concentration of hydrogen and carbon dioxide in the backfill decreases gradually implying that a larger amount of the gases is escaping than is generated and released.

In order to determine the total amount of gas generated, one of the test drifts will be sealed gastight at is entrance. Preliminary works are already done to seal the entrance using an appropriate polyethylene foil allowing an air pressure compensation in the pore volume of the backfill and the access drift.

First results of diffusivity measurements using a spherical model indicate a gas diffusivity within the pore volume of the backfill in the range of $1.4 \cdot 10^{-5}$ m^2/s to $4 \cdot 10^{-5}$ m^2/s.

A water content of 20 to 25 g in 1 m^3 air from the pore volume of the backfill is determined by using a liquid nitrogen cooling trap.

The in situ measurements will be continued in the next years to study the further thermomechanical reactions of backfill and surrounding rock salt to the heat input. For the necessary validation of thermal and thermomechanical models a more representative degree of backfill compaction is necessary to allow a reliable extrapolation of the measurements over a longer period of time.

9 References

/BEC 89/ Bechthold, W., Heusermann, S., Schrimpf, C. and Gommlich, G. (1989): Large scale test on in-situ backfill properties and behavior under reference repository conditions. - NEA/CEC Workshop on Sealing of Radioactive Waste Repositories, Braunschweig, Germany, May 22 - 25.

/KFK 89/ Kernforschungszentrum Karlsruhe (1989): Development status of direct disposal in the Federal Republic of Germany. - Projektgruppe Andere Entsorgungstechniken, Report AE No. 23 E, Karlsruhe, Germany.

/KOR 91/ Korthaus, E. (1991): Thermische und thermomechanische Prognoserechnungen zum TSS-Versuch (Thermische Simulation der Streckenlagerung). - Primärbericht 19.03.03P04A, Kernforschungszentrum Karlsruhe.

/SNE 93/ Schneefuß, J., Droste, J., Gommlich, G., Jockwer, N., Kunze, J., Mönig, J. et al. (1993): Testplan zum Demonstrationsversuch "Thermische Simulation der Streckenlagerung" im Salzbergwerk Asse (Revidierte Fassung). - Hauptband Direkte Endlagerung, Kernforschungszentrum Karlsruhe.

/SNE 94/ Schneefuß, J., Droste, J., Heusermann, S. and Sönnke, J. (1994): Recent results of geomechanical field measurements in the TSDE Test at the Asse Salt Mine. - Proc. Eurock '94, Rock Mechanics in Petroleum Engineering, p. 715 - 724, Rotterdam (Balkema).

/SNE 95/ Schneefuß, J., Feddersen, H.-K., Jockwer, N. and Droste, J. (1995): The TSS-Project: In-situ Research on Compaction of and Gas Release in Saliferous Backfill. - Final Report for the Period August 1994 - April 1995, GSF - Institut für Tieflagerung, Abteilung für Endlagertechnologie, Abteilungsbericht IfT 5/95.

Gesellschaft für Anlagen- und Reaktorsicherheit (GRS) mbH

Schwertnergasse 1
50667 Köln
Telefon (02 21) 20 68-0
Telefax (02 21) 20 68-888

Forschungsgelände
85748 Garching b. München
Telefon (0 89) 3 20 04-0
Telefax (0 89) 3 20 04-599

Kurfürstendamm 200
10719 Berlin
Telefon (0 30) 8 85 89-0
Telefax (0 30) 8 85 89-111

Theodor-Heuss-Straße 4
38122 Braunschweig
Telefon (0531) 80 12-0
Telefax (0531) 80 12-200